CORA Cork Open Research Archive
Cartlann Taighde Oscailte Chorcaí

Title	Multifaceted computational modelling in pharmaceutical research and development
Authors	Vinay Kumar Reddy, Cheemarla
Publication date	2023
Original Citation	Vinay Kumar Reddy, C. 2023. Multifaceted computational modelling in pharmaceutical research and development. PhD Thesis, University College Cork.
Type of publication	Doctoral thesis
Rights	© 2023, Cheemarla Vinay Kumar Reddy. - https://creativecommons.org/licenses/by-nc/4.0/
Download date	2026-11-01 13:22:13
Item downloaded from	https://hdl.handle.net/10468/16014



UCC
University College Cork, Ireland
Coláiste na hOllscoile Corcaigh

Ollscoil na hÉireann, Corcaigh

National University of Ireland, Cork



Multifaceted Computational Modelling in Pharmaceutical Research and Development

Thesis presented by

Cheemarla Vinay Kumar Reddy, B.Pharm, M.S

https://orcid.org/0000-0002-8781-6541

for the degree of

Doctor of Philosophy

University College Cork

School of Chemistry

Head of School/Department: Dr. Anita Maguire

Supervisor(s): Dr. Davide Tiana and Dr. Simon Lawrence

2023

Abstract

Drug development is a multi-step process and takes around 12 to 15 years for a new drug to get approved. In the current scenario, to accelerate the drug development process and to reduce the time frame, most pharmaceutical companies have in-house developed workflows comprised of a hybrid use of computational and experimental approaches. This thesis was focused on employing state-of-the-art molecular modelling methods in three significant areas of pharmaceutical research and development. This thesis comprises an introductory part (chapter 1) and a productive part (chapter 3 to chapter 5). The first chapter of this thesis is the literature review, outlining the foundational studies and research framework used in chapters 3 to 5. The second chapter describes the thesis structure and objectives of the other three chapters. The third chapter explores the hit identification process, utilising docking to screen a small database of phytopharmaceuticals against sclerostin protein followed by an investigation of the stability of the protein-ligand complexes through standard molecular dynamics and funnel meta dynamics. The fourth chapter involves the modelling of adsorption and diffusion of doxorubicin, paclitaxel, carboplatin, and gemcitabine anticancer drugs and also drug combinations such as doxorubicin with carboplatin, paclitaxel with gemcitabine and carboplatin employing NUIG-4 metal-organic framework as drug delivery agents. In this chapter, the comprehensive understanding of molecular interactions governing drug adsorption and diffusion was studied using Grand Canonical Monte Carlo (GCMC) and Molecular Dynamics (MD) simulations. The fifth chapter focuses on investigating the mechanism of chiral Bronsted acid catalysed asymmetric synthesis of homoallyl alcohols from ortho vinyl benzaldehydes and allyl boron pinacol ester using density functional theory methods (DFT), QTAIM, and NCI analysis. Furthermore, a comparative analysis of transition structures of Ortho vinyl and ortho alkynyl benzaldehyde substrates was studied.

Declaration

I hereby declare that the work reported in this thesis is my own and not submitted for any other degree at University College Cork or anywhere else. I acknowledged and cited external sources and references. I completely understand the regulations and intellectual property rights at University College Cork.

Cheemarla Vinay

Acknowledgments

I would like to express my heartfelt thanks to my PhD thesis supervisor Dr. Davide Tiana for providing me the opportunity to conduct the research and guiding me in every aspect throughout the four years of my PhD. I also consider this opportunity to thank my PhD thesis co-advisor Dr. Simon Lawrence, who talks endlessly about cricket, and Dr. Peter Byrne for acting as an internal examiner. The comments and reviews provided by both of you led me to finish my thesis in time. Next on the list to convey my thanks are William Daly and Amy with whom I spent most of the time in the lab having all the fun besides working seriously.

I am grateful to the collaborative spirit of Shan Huang, Naresh, and Bruno who generously shared their insights and engaged in constructive discussions which helped me to get an in-depth understanding of diverse topics.

I owe my thanks to Charlie Dolan, and Sharon Davin from APC, Dublin for providing me with the internship opportunity and giving me wonderful industrial experience. I am immensely thankful to UCC and SSPC staff members for their assistance during my PhD duration.

I would like to thank my friends, and family for their unwavering support throughout my journey.

List of Publications

1. In Silico Screening of Natural Bioactive Compounds Against Sclerostin Target in Osteoporosis And Application Of Funnel Metadynamics to Study the Binding Mechanism. (manuscript under preparation)
2. Computational Investigation Of NUIG-4 As Multi-Drug Delivery Agents For Ovarian Anticancer Agents (manuscript under preparation)
3. DFT Insights Into The Mechanism Of Enantioselective Synthesis Of Homoallylic Alcohols From Ortho-Vinyl And Ortho-Alkynyl Benzaldehydes Via Asymmetric Allylboration (manuscript under preparation)

Other publications not included in the thesis

1. **Experimental and Theoretical Investigation of Hydrogen-Bonding Interactions in Cocrystals of Sulfaguanidine**
   Shan Huang, Vinay K. R. Cheemarla, Davide Tiana, and Simon E. Lawrence
   Crystal Growth & Design 2023 23 (4), 2306-2320
   DOI: 10.1021/acs.cgd.2c01337
2. **Exploring the Crystal Structure Landscape of Sulfasalazine through Various Multicomponent Crystals**
   Shan Huang, Vinay K. R. Cheemarla, Davide Tiana, and Simon E. Lawrence
   Crystal Growth & Design 2023 23 (8), 5446-5461
   DOI: 10.1021/acs.cgd.2c01403

Index

List of Figures X

List of Tables XIII

Chapter 1: Introduction 15

Section 1. In-silico ligand screening of phytopharmaceuticals 16

1.1. Post-menopausal osteoporosis 16

1.2. Computational methods for screening of ligands 20

Section 2. Theoretical investigation of drug delivery applications of MOF. 25

2.1. Drug delivery 25

2.2. Metal-organic frameworks 26

2.3. MOFs as drug delivery agents..... 27

2.4. Computational modelling of adsorption and diffusion of drugs in MOFs. 28

Section 3. DFT study of transition states of Enantioselective synthesis of homoallyl alcohols. 30

3.1. Homoallyl alcohols 30

3.2. Chiral drugs..... 31

3.3. Asymmetric synthesis 32

3.4. Computational study of transition states. 34

4. Bibliography..... 36

Chapter 2: General Objectives 53

Thesis Structure 54

Objectives: 54

Chapter 3: In Silico Screening of Natural Bioactive Compounds Against Sclerostin Target in Osteoporosis and Application of Funnel Metadynamics to Study the Binding Mechanism. 56

Chapter 4: Computational Investigation of NUIG-4 as Multi-drug Delivery Agents for Ovarian Anticancer Agents 77

Chapter 5: DFT Insights into the Mechanism of Enantioselective Synthesis of Homoallylic Alcohols from *Ortho*-Vinyl and *Ortho*-Alkynyl Benzaldehydes via Asymmetric Allylboration 91

Chapter 6: Conclusions and future work: 113

Supplementary data for Chapter 3 115

Supplementary data for Chapter 4 122

Supplementary data for Chapter 5 143

List of Figures

Chapter 1

Figure 1.1: Bone remodelling **a)** oestrogen stimulates osteoblast differentiation and function and suppresses osteoclast differentiation and activity by down-regulating the production of nuclear factor- κB ligand (RANKL). **b)** In the case of oestrogen deficiency production of RANKL is upregulated which results in increased osteoclast number and activity. Simultaneously, the activity of sclerostin is increased leading to suppression of osteoblasts. Adapted from Eastell, R.; O'Neill, T. W.; Hofbauer, L. C.; Langdahl, B.; Reid, I. R.; Gold, D. T.; Cummings, S. R. Postmenopausal Osteoporosis. *Nature Reviews Disease Primers 2016 2:1* **2016**, *2* (1), 1–16.[1] 17

Figure 1.2: In the inactive state (OFF), Frizzled/LRP5/6 coreceptors are not bound to Wnt as a result β-catenin in the cytosol is phosphorylated by destruction complex and subsequently degraded by the proteasome. In the active state (ON), Wnt binding to Frizzled/LRP5/6 co-receptor attracts Dishevelled protein (DSH) to the intracellular tail of the Frizzled receptor resulting in the separation of the destruction complex preventing β-catenin from phosphorylation. This Unphosphorylated β-catenin translocates into the nucleus to regulate gene expression. Adapted from Marini, F.; Giusti, F.; Palmini, G.; Brandi, M. L. Role of Wnt Signaling and Sclerostin in Bone and as Therapeutic Targets in Skeletal Disorders. *Osteoporosis International 2022 34:2* **2022**, *34* (2), 213–238.[2] 18

Figure 1.3: Representation of sclerostin protein, disulfide bonds are highlighted in red. Blue-coloured residues are the β-sheet residues. Adapted from Veverka, V.; Henry, A. J.; Slocombe, P. M.; Ventom, A.; Mulloy, B.; Muskett, F. W.; Muzylak, M.; Greenslade, K.; Moore, A.; Zhang, L.; Gong, J.; Qian, X.; Paszty, C.; Taylor, R. J.; Robinson, M. K.; Carr, M. D. Characterization of the Structural Features and Interactions

of Sclerostin: MOLECULAR INSIGHT INTO A KEY REGULATOR OF Wnt-MEDIATED BONE FORMATION*S. *J Biol Chem* **2009**, *284* (16), 10890.[3] 20

Figure 1.4: Schematic diagram showing the ligand binding to protein and the funnel restraint potential used in funnel metadynamic. *Z* in the figure is the axis of the binding path of the ligand. z_{cc} represents the distance where the restraint potential changes from cone to cylinder. α-angle represents the cone amplitude and R_{cyl} is the radius of the cylindrical section. The funnel`s shape is adjusted by the parameters mentioned above. Adapted from Kou, L. F.; Huang, H. E.; Lin, X. L.; Jiang, X. Y.; Wang, Y.; Luo, Q. H.; Sun, J.; Yao, Q.; Ganapathy, V.; Chen, R. J. Endocytosis of ATB(0,+)(SLC6A14)-Targeted Liposomes for Drug Delivery and Its Therapeutic Application for Pancreatic Cancer. *Expert Opin Drug Deliv* **2020**, *17* (3), 395–405.[31] 25

Figure 1.5: MOF-5 structure representation a) metal ion (Zn) and organic linker (Terephthalic acid) b) Secondary Building Unit (SBU) c) MOF-framework formed by coordination of SBUs to organic linker d) Final morphology of MOF-5. Adapted from Inoue, M.; Suzuki, T.; Nakada, M. Asymmetric Catalysis of Nozaki-Hiyama Allylation and Methallylation with a New Tridentate Bis(Oxazolinyl)Carbazole Ligand. *J Am Chem Soc* **2003**, *125* (5), 1140–1141.[74] 27

Chapter 3

Figure 3.1: Hydrophobic, hydrogen bonding, and salt bridge interactions of top six docking poses. Hydrogen bonds are represented as blue lines, and hydrophobic interactions, and salt bridges are represented as orange and yellow dashes respectively. 63

Figure 3.2: **A)** Radius of gyration of Salvanoic Acid (SAL) and Verbascoside (VER). The average radius of gyration is in green and blue for Salvanoic Acid and Verbascoside protein complex respectively. **(B)** Root Mean

Square Deviation (RMSD) of two ligands. Blue and green lines represents running averages of Verbascoside and Salvanoic acid.....64

Figure 3.3: Snapshots of MD simulation. The snapshots are taken from 100 ns to 500 ns with an interval of 100 ns to show the binding poses of SAL. 66

Figure 3.4: Snapshots of MD simulation. The snapshots are taken from 100 ns to 500 ns with an interval of 100 ns to show the binding poses of VER. 67

Figure 3.5: Hydrogen bond occupancy percentage calculated during 500 ns molecular dynamics simulation of **A)** Verbascoside and **B)** Salvanoic acid protein complexes 68

Figure 3.6: Representation of funnel restraint potential used in funnel meta-dynamics of sclerostin protein and ligands (Verbascoside and Salvanoic Acid). The collective variable (CV) d1 is the distance between the C15 of the ligand to the HN atom of ILE95(green dot). The Z-axis originates from the LYS142 residue and is limited to 100 Å from the origin (red sphere). The cone-shaped funnel was defined by α-angle (0.6 rad) and Zcc (65 Å)is the distance from the origin to the vertex where the cone changes to the cylinder. Rcyl (1 Å) is the radius of the cylinder.....69

Figure 3.7: Active site residues of three binding poses. Residues and labels are color-coded with respect to the free energy surface plot of the sclerostin and verbascoside complex 70

Figure 3.8: **A)** Free energy surface plot and snapshots of different binding poses identified in funnel meta-dynamics of sclerostin protein and Verbascoside complex 72

Figure 3.9: A) Free energy surface plot and B) residues within 5Å of ligand and C) snapshot of binding pose identified in funnel meta-dynamics of sclerostin protein and Salvanoic Acid 72

Supplementary data for chapter 3

Figure S 3. 1: Residue interactions of Fluticasone and Valproic acid..... 121

Chapter 4

Figure 4.1: Images showing the site of adsorption in NUIG-4. A) DOX; B) DOX-CAR; C) NUIG-4 framework; D) PAL; E) PAL+CAR; F)PAL+GEM. The NUIG-4 atoms are in grey its metal cluster is represented as a blue-coloured polyhedron. DOX, PAL, CAR, and GEM are in the ball and stick representation coloured in sky blue, brown, yellow, and violet respectively. Hydrogens are not shown for clarity. 83

Chapter 5

Figure 5.1: Allylboration of alkenes and alkynes catalyzed by BINOL phosphoric acid 94

Figure 5.2: Mechanism of the asymmetric allylboration and Ring-Closing Metathesis (RCM) 96

Figure 5.3: Quadrant projection of Chiral phosphoric acid ((R)-3,3'-Bis(2,4,6-triisopropylphenyl)-1,1'-binapthyl-2,2'-diyl hydrogen phosphate)catalyst down the C2 symmetry axis. 98

Figure 5.4: TS conformations of the major and minor pathways with hydrogen bond lengths located through QTAIM analysis. The estimated Hydrogen Binding Energies (HBE) of both conformers are in kJ/mol. and distances are in Angstroms. 99

Figure 5.5: Quadrant projections of the TS conformers leading to the major product. The allyl boronic acid pinacol ester is coloured blue to distinguish it from the catalyst. II and III are empty quadrants and I and IV are filled quadrants 100

Figure 5.6: Quadrant projections of TS conformers leading to the minor product. Allyl boronic acid pinacol ester is coloured blue to distinguish it from the catalyst. II and III are empty quadrants and I and IV are filled quadrants..... 101

Figure 5.7: 2D and 3D NCI plots of TS-1-ene-major (right) and TS-1-ene-minor (left) conformers. Peaks towards negative s(ρ) represent strong hydrogen bond (blue) interactions, vdW interactions peaks are around 0 (green), and steric interactions peaks are towards positive. 102

Figure 5.8: Hydrogen bond interactions in ortho-alkynyl benzaldehyde TS (a) and 3D and 2D NCI plots in Ortho alkynyl (b) and ortho-vinyl (c) benzaldehyde transition states achieving higher ee. Estimated hydrogen binding energies are in kJ/mol. 104

Figure 5.9: Low energy TS structures of ortho-alkynyl benzaldehyde (A and B) and Ortho-vinyl benzaldehyde (C and D). CPA catalyst atoms are coloured grey and allyl boron pinacol ester atoms are coloured blue. Red and blue planes are drawn to show quadrants (I, II, III, IV) of the TS catalyst. I and IV are filled quadrants and the presence of bulky substituents in these quadrants results in low enantioselectivity. II and III are empty quadrants 106

Figure 5.10: Quadrant projection of phenyl substituted ortho alkynyl benzaldehyde 107

List of Tables

Chapter 3

Table 3.1: List of the top 6 hit molecules and their residue interactions with sclerostin loop 2 active site region. 62

Supplementary data for chapter 3

Table S 3.1: List of drugs and residue interactions of top 33 of GOLD docking 115

Table S 3.2: Docking score and list of ligand interaction residues reported experimentally 121

Chapter 4

Table 4.1: Average adsorption predicted from GCMC simulations of single and co-adsorbed drugs in mg/gm of NUIG-4 MOF 81

Table 4.2: Intermolecular interaction energies in kcal/mol calculated from pseudo plane wave DFT method in Quantum espresso..... 82

Table 4. 3: Drug diffusion coefficient in $Å2/ps$ calculated during 200 ns molecular dynamics trajectory..... 84

Supplementary data for chapter 4

Table S 4.1: Cartesian coordinates of NUIG-4 and drugs to prepare input files and calculate the binding energy 122

Chapter 5

Supplementary data for chapter 5

Table S 5.1: List of structures with details of major conformers identified in cluster analysis. Structures are selected based on the presence of benzaldehydehyde substituents in quadrants. 143

Table S 5.2: List of structures with details of minor conformers identified in cluster analysis. Structures are selected based on the presence of benzaldehydehyde substituents in quadrants 143

Table S 5.3: Cartesian co-ordinates of major and minor conformers included in the study 144

Chapter 1: Introduction

Section 1. In-silico ligand screening of phytopharmaceuticals

1.1. Post-menopausal osteoporosis

Osteoporosis is the disease condition where bone becomes fragile and is likely to get fractured due to low bone mass. This condition arises due to an imbalance between two processes of bone remodelling, the first one is the resorption of old or matured bone and the other is the formation of new bone. Three types of bone cells are involved in bone formation, bone resorption, and bone growth, they are osteoblasts, osteoclasts, and osteocytes respectively. The function of osteoblasts depends mainly on the activation of the Wnt (Wingless related integration site) signalling pathway, bone morphogenetic protein, and transforming growth factor beta (TGFβ). Wnt inhibitors such as sclerostin inhibit the signalling pathway and decrease the activity of osteoblasts, resulting in low bone mass and further, leading to osteoporosis. The prevalence of osteoporosis is higher in women than men due to Oestrogen, a female sex hormone that regulates bone formation. This hormone suppresses the apoptosis of osteoblasts and promotes the apoptosis of osteoclasts by increased production of TGFβ. Naturally, bone formation slows down after a certain age but in some cases especially in older women during menopause, oestrogen hormone levels are decreased as a result osteoclast activity increases leading to an increase in bone resorption rate, which makes bone brittle and causes the bone fractures.

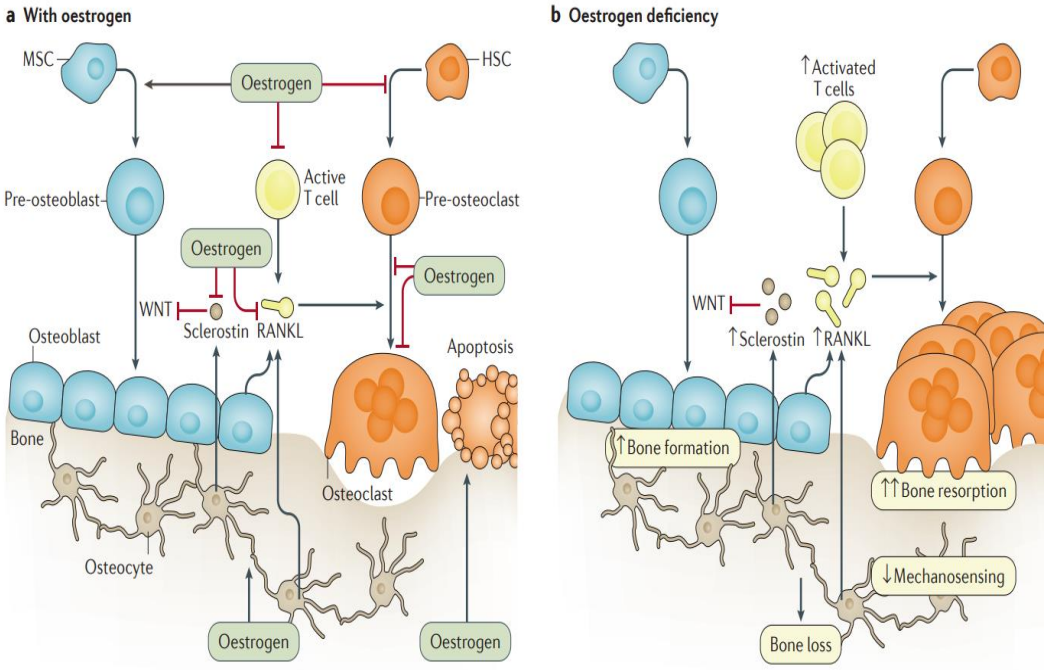


Figure 1.1: Bone remodelling **a)** oestrogen stimulates osteoblast differentiation and function and suppresses osteoclast differentiation and activity by down-regulating the production of nuclear factor- κB ligand (RANKL). **b)** In the case of oestrogen deficiency production of RANKL is upregulated which results in increased osteoclast number and activity. Simultaneously, the activity of sclerostin is increased leading to suppression of osteoblasts. Adapted from Eastell, R.; O'Neill, T. W.; Hofbauer, L. C.; Langdahl, B.; Reid, I. R.; Gold, D. T.; Cummings, S. R. Postmenopausal Osteoporosis. *Nature Reviews Disease Primers 2016 2:1* **2016**, *2* (1), 1–16.[1]

1.1.1. Canonical Wnt/β-catenin signalling system.

The Canonical Wnt/β-catenin pathway is essential to regulate bone homeostasis and remodelling. Wnt binding to the LRP5/6 co-receptor and frizzle receptor inhibits the axin protein complex, the main function of this complex is phosphorylation of β-catenin. Inhibition of this complex results in the accumulation of unphosphorylated β-catenin which translocate to the nucleus and bind to the T cell factor/lymphatic enhancement factor complex. This leads to the activation of genes that promote the bone formation.

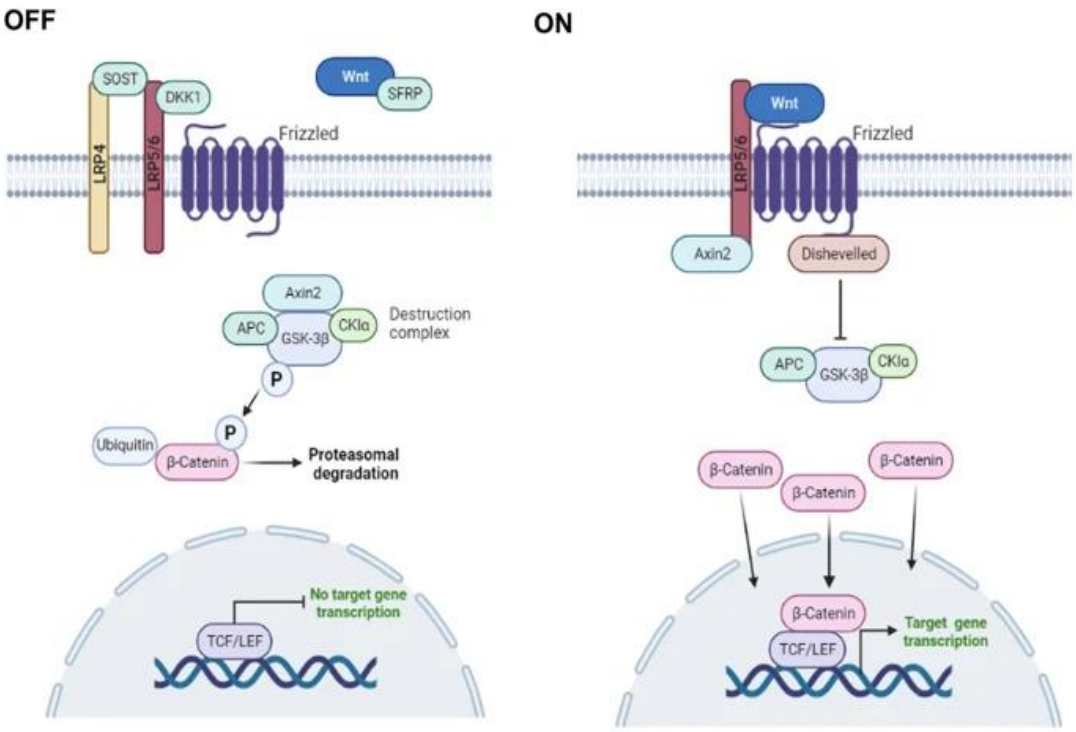


Figure 1.2: In the inactive state (OFF), Frizzled/LRP5/6 coreceptors are not bound to Wnt as a result β-catenin in the cytosol is phosphorylated by destruction complex and subsequently degraded by the proteasome. In the active state (ON), Wnt binding to Frizzled/LRP5/6 co-receptor attracts Dishevelled protein (DSH) to the intracellular tail of the Frizzled receptor resulting in the separation of the destruction complex preventing β-catenin from phosphorylation. This Unphosphorylated β-catenin translocates into the nucleus to regulate gene expression. Adapted from Marini, F.; Giusti, F.; Palmini, G.; Brandi, M. L. Role of Wnt Signaling and Sclerostin in Bone and as Therapeutic Targets in Skeletal Disorders. *Osteoporosis International 2022 34:2* **2022**, *34* (2), 213–238.[2]

When Sclerostin binds to LRP5/6 co-receptors, the interaction between the WNT and LRP5/6 is inhibited, leading to the phosphorylation of β-catenin and further degradation by the proteasome. As sclerostin protein plays a crucial role in the Wnt signalling pathway, inhibition of this protein from binding to LRP5/6 co-receptors results in an increased bone formation rate. Several

experimental studies show that ligands that inhibit the sclerostin exhibited positive outcomes in postmenopausal osteoporosis.[66-70] Hence, this protein was selected to perform in-silico screening of phytopharmaceuticals.

1.1.2. Sclerostin structural characteristics

Sclerostin is a 190-residue-long glycoprotein with an observed mass of 21.57 kDa. The NMR data of sclerostin shows it has three loops, cysteine-knot motif, long N- (1-55), and C- (145-189) terminal regions.[3] The loop 1 residues are from Arg-57 to Val-80, loop 2 residues are from Gly-86 to Arg-109 and loop 3 residues are from Ile-111 to Ser-140. Loop 1 and 3 residues form twisted anti-parallel β-strands with the tips joined by a disulfide bond, shown in Fig. 1.3. The N- terminal, C- terminal, and loop 2 regions of protein show high flexibility and adopt a wide range of conformations. Experimental studies show that the loop 2 region of sclerostin binds to LRP5/6 co-receptors inhibiting the Wnt signalling.[3] The ligands binding to this loop 2 region inhibit the sclerostin from binding to LRP5/6 co-receptors thereby bone formation is increased. Hence, sclerostin is considered a therapeutic target and Romosozumab was the first approved monoclonal antibody(mAb) by FDA[4,5] which acts as a sclerostin inhibitor to treat post-menopausal osteoporosis. Some other monoclonal antibodies in various stages of drug development are Blosozumab,[6] Setrusumab,[7] SHAR-1222, and AMG167. Though these mAbs act as potential inhibitors, several adverse effects are associated with them.[8] So, alternative chemical molecules have to be explored to identify the potential molecules that are binding to sclerostin.

Phytopharmaceuticals are the natural bioactive compounds derived from plants. They possess pharmacological activity and are used to treat viruses,[9] parasites[10], bacterial infections,[11] used as anticancer agents[12] and also in treating central nervous system(CNS) related diseases.[13] Due to low toxicity and being more cost-effective compared to mAbs, phytochemicals were selected to perform in-silico screening. The following section briefs the methods used in screening the molecules.

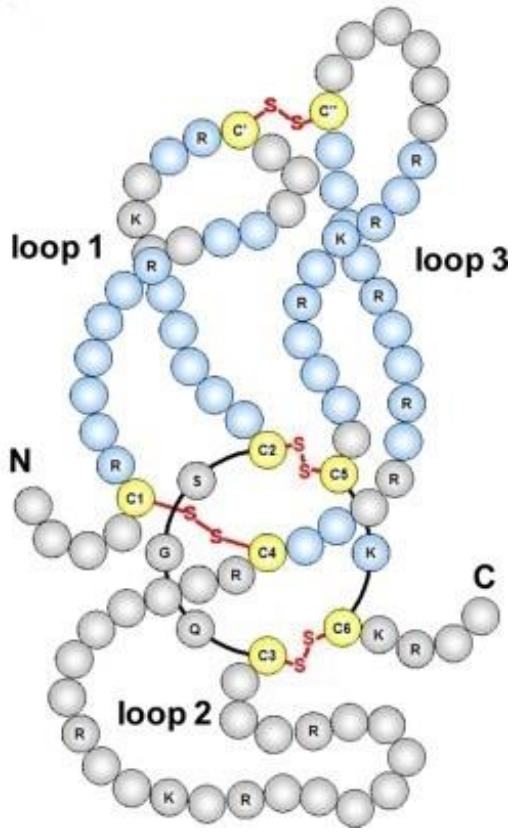


Figure 1.3: Representation of sclerostin protein, disulfide bonds are highlighted in red. Blue-coloured residues are the β-sheet residues. Adapted from Veverka, V.; Henry, A. J.; Slocombe, P. M.; Ventom, A.; Mulloy, B.; Muskett, F. W.; Muzylak, M.; Greenslade, K.; Moore, A.; Zhang, L.; Gong, J.; Qian, X.; Paszty, C.; Taylor, R. J.; Robinson, M. K.; Carr, M. D. Characterization of the Structural Features and Interactions of Sclerostin: MOLECULAR INSIGHT INTO A KEY REGULATOR OF Wnt-MEDIATED BONE FORMATION*S. *J Biol Chem* **2009**, *284* (16), 10890.[3]

1.2. Computational methods for screening of ligands

1.2.1. Molecular Docking

There are a plethora of virtual screening methods to filter ligands for a particular biological target which are discussed in detail by Tiago *et al.* [14] In this thesis we focus particularly on docking-based selection of potential ligands for sclerostin protein. The docking methods are well established to predict the

binding affinity and best binding pose of a ligand, these methods are proven to be successful in drug discovery. The first docking algorithm was developed by Kuntz *et al.* [15] Since then several docking algorithms such as AutoDock,[16] GOLD,[17] DOCK,[18] Glide,[19] have come into existence. GOLD[17] is one of the docking programs that stands on top in predicting ligand-binding interactions. All the docking programs have two components through which they differ from each other, they are conformational sampling which enables these programs to search the conformational space and the other is the scoring function that calculates the energy of protein-ligand complex and differentiates the correct binding modes generated by the conformation sampling.

1.2.1.1. Conformational sampling

Based on the degree of flexibility during conformational sampling, docking methods are classified into rigid docking where protein and ligand are rigid, semi-flexible docking in which only ligand is considered flexible and flexible docking where both protein and ligand are flexible. The ligand flexibility in semiflexible docking is implemented through systemic search and stochastic methods. The flexibility in systemic search is achieved through three approaches: a) in the first approach, all rotatable bonds of ligand are rotated in a systemic way to generate the conformers; b) in the second approach, one fragment of ligand is docked into the protein's active site and followed by attaching the other fragments incrementally; c) in the final approach, an ensemble of generated conformers are docked into the protein.

On the other hand, stochastic methods introduce randomness through: a) Monte Carlo methods where the ligand degrees of freedom are modified randomly in each step and the energy is calculated for the modified binding pose, if the energy is improved, the modification is accepted or it moves to the next step; b) in Tabu search methods, random modifications are made similar to Monte Carlo but the new pose is accepted only if it is not similar to any other previously explored binding poses; c) in the third approach, evolutionary algorithms are used which work similarly to biological evolution. Here, the

ligand degrees of freedom are explored and only the best-fit ones are selected through mutation and crossover; d) the final approach is the particle swarm optimisation method that explores multiple conformations at each iteration, stores the best solutions of individual conformer search and continues till the best conformer is found or after finishing all the iterations.

In semi-flexible docking, only ligand flexibility is taken into consideration but in flexible docking, protein flexibility should also be taken into consideration. In reality, this is difficult to achieve, so different approaches are used in the flexible docking technique: a) in the first approach, vdW repulsion terms of single protein conformation are modified to allow small clashes to simulate the induced fit or to explore alternative conformations of side chains;[20] b) in the second approach, the ensemble of protein conformations is taken to consider the flexibility of a protein structure.[21]

1.2.1.2. Scoring functions

Scoring functions are mathematical functions that distinguish the correct binding modes generated from the conformational sampling. These are categorised into four types: a) force-field based scoring functions like AutoDock[22] and Dock[18] etc., that calculate the energy as the sum of bonded and non-bonded interactions, the energy equation is shown in section 3.2.2 b) empirical scoring functions like LUDI[23] score and ChemScore[24] etc., consist of various energy terms accompanied with the weighted coefficients obtained from experimental data through regression analysis, and c) the final one is knowledge-based scoring functions like penalized matrix factorisation (IPMF),[25] these scoring functions are developed using the structural information of protein-ligand complexes determined by experiments to transform the atom pair into pairwise potentials. We have employed ChemPLP scoring function[17] for docking the molecules into sclerostin protein. An empirical scoring function with four components, the first two are hydrogen bond and van der Waals energy of protein-ligand complex, and the next two components are ligand internal energy that arises due to van der Waals forces and internal torsional strain.

Molecular docking aids in predicting the best-fit ligand in the protein active site, this technique alone cannot address the protein-ligand interactions and dynamic behaviour of the docking complex. So, molecular dynamics simulations help in assessing the stability of binding pose by simulating the dynamic behaviour of the protein-ligand complex over time.

1.2.2. Molecular Dynamics

This technique applies the classical laws of motion to study the behaviour of atoms and molecules. The position and velocities of atoms are calculated by integration of Newton`s second law ($F = ma$) over time, updated in each time step, and stored in trajectory. The analysis of this trajectory gives an insight into the interactions and dynamic behaviour of the system under study. The forces are computed from the forcefield by using the following equation. This is the general equation of forcefield and there may be the introduction of other terms into the equation that leads to different types of forcefields, some common forcefields used are CHARMM[26], AMBER[27], GROMOS[28], OPLS.[29]

$$E_{tot} = \sum_{bonds} K_b(b - b_0)^2 + \sum_{angles} K_\theta(\theta - \theta_0)^2 + \sum_{dihedrals} K_{\emptyset,n}[1 + \cos(n\emptyset - \delta_n)] + \sum_{improper} K_\emptyset(\emptyset - \emptyset_0) + \sum_{i \neq j} \left(\frac{q_i q_j}{r_{ij}}\right) + 4\varepsilon[-\left(\frac{r_0}{r_{ij}}\right)^6 + \left(\frac{r_0}{r_{ij}}\right)^{12}]$$

Equation 1: Mathematical representation of forcefield

In the above equation, the first four terms represent the bonded terms, and the last two are non-bonded terms that represent Coulomb and van der Waals interactions. $K_b, K_\theta, K_\emptyset, K_{\emptyset,n}, \varepsilon$ are force field constants derived from experimental data or quantum mechanics calculations. b, θ, b_0, θ_0 are bond length, bond angle, equilibrium bond length, and equilibrium bond angle

respectively. $\emptyset, \emptyset_0$ are improper dihedral angles and equilibrium dihedral angles. $q_i q_j$ are partial charges on atoms i and j. r_0 is a constant whose value depends upon the atom type and r_{ij} is the interatomic distance.

The simulation of the binding and unbinding process needs efficient exploration of the energy landscape. Classical molecular dynamics simulations are inefficient in conformational exploration as they are time-consuming and computationally intensive. To overcome these limitations, several new methods were proposed, they are coarse-grained molecular dynamics (CGMD)[30] and enhanced sampling methods. In CGMD, a group of heavy atoms are defined as beads to reduce the degrees of freedom and fine interaction details thereby resources are reduced to run the longer simulations. These simulations are particularly useful for studying biological phenomena such as protein folding, and self-assembly of proteins but all-atom details are lost in this method which makes them insignificant for characterising ligand interactions with protein residues. The other methods such as umbrella sampling and metadynamics conformational sampling are accelerated by facilitating the system to escape from local minima by adding the bias force or potential (more details of enhanced sampling are provided in Appendix). Funnel meta-dynamics[31] is an enhanced sampling approach primarily introduced to sample multiple binding and unbinding events. This is achieved by applying funnel restraint potential where the binding site is defined as a cone and the direction to the solvent is defined as a cylinder. The molecule movement inside the funnel is controlled by a repulsive bias which restricts the molecule movement if it reaches the edge of the funnel. This helps in achieving multiple binding and unbinding of ligands to protein inside the funnel. The funnel boundaries are carefully chosen to properly explore the binding sites of the protein.

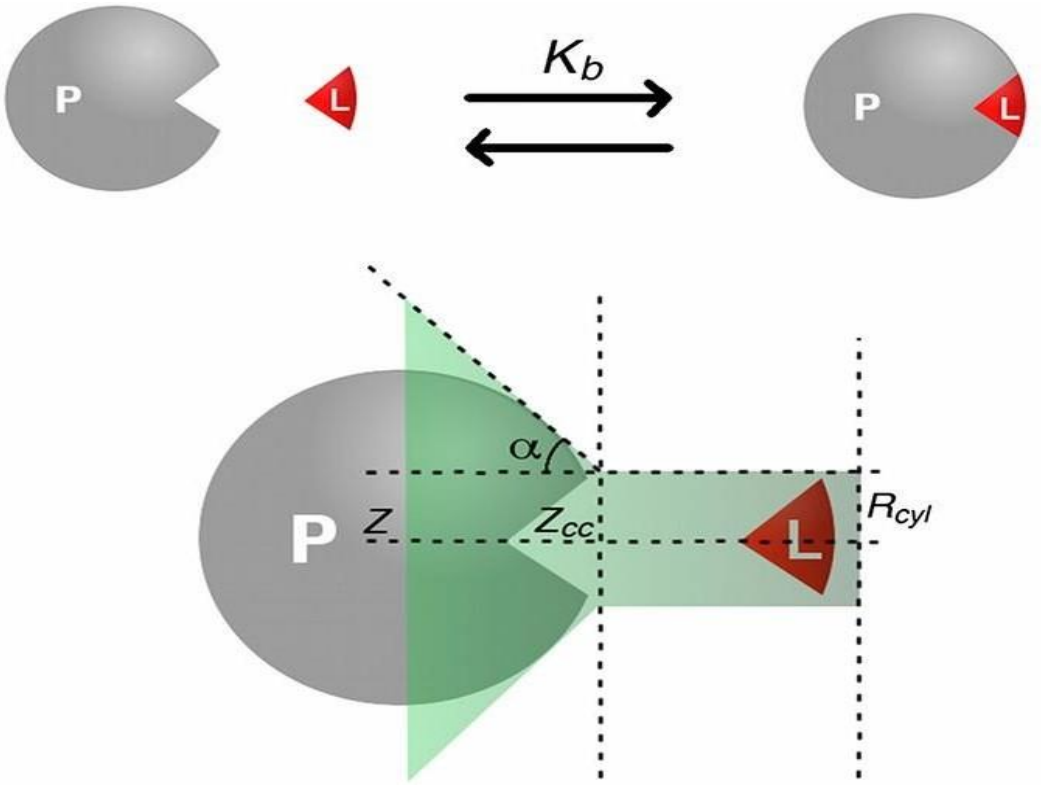


Figure 1.4: Schematic diagram showing the ligand binding to protein and the funnel restraint potential used in funnel metadynamic. *Z* in the figure is the axis of the binding path of the ligand. z_{cc} represents the distance where the restraint potential changes from cone to cylinder. α-angle represents the cone amplitude and R_{cyl} is the radius of the cylindrical section. The funnel`s shape is adjusted by the parameters mentioned above. Adapted from Kou, L. F.; Huang, H. E.; Lin, X. L.; Jiang, X. Y.; Wang, Y.; Luo, Q. H.; Sun, J.; Yao, Q.; Ganapathy, V.; Chen, R. J. Endocytosis of ATB(0,+)(SLC6A14)-Targeted Liposomes for Drug Delivery and Its Therapeutic Application for Pancreatic Cancer. *Expert Opin Drug Deliv* **2020**, *17* (3), 395–405.[31]

Section 2. Theoretical investigation of drug delivery applications of MOF.

2.1. Drug delivery

Drugs are substances ingested or introduced into the body to show therapeutic effect. The amount of drug available in systemic circulation depends on the solubility of a drug. Poorly soluble drugs are slowly absorbed through the

gastrointestinal tract which results in low bioavailability thereby the desired therapeutic effect is hindered. To overcome the solubility problems and to improve bioavailability, some common approaches used are i) modification of the drug itself by reducing the particle size to increase the surface area, ii) preparation of nanosized colloidal dispersion to facilitate better dissolution iii) changing the drug environment by the use of surfactant,[32] iv) converting drugs into salt forms,[33] v) adjusting the pH[34] and vi) preparing the solid dispersions involving the dispersions of active pharmaceutical ingredients within a matrix. The other most common and predominantly used approach is utilising nanomaterials as drug delivery agents. This is the most preferable method if one aims for prolonged drug release or controlled release at the target site. Nanomaterials are the particles present as single units or agglomerates with sizes generally between 1 nm to 100 nm.[35] However, not all the particles used in the pharmaceutical industry comply with the present definition of nanoparticles. Being smaller in size they offer greater surface area and increased cell uptake. Nanoparticles can be manufactured in different shapes and sizes and also its surfaces can be modified through which they can be engineered as the most efficient drug delivery agents.[36] Several nanoparticles currently used in drug delivery are biopolymers,[37–39] liposomes,[40–44] polymeric micelles,[45–48] dendrimers,[49–52] inorganic materials,[53–55] nanocrystals,[53,54,56] metallic nanoparticles,[57–60] quantum dots,[61–64] protein and polysaccharides.[65,66] Recently, metal organic frameworks (MOFs) have been studied as drug delivery agents due to their structural characteristics and superior properties which will be discussed below. [67–71]

2.2. Metal-organic frameworks

Extensive research on MOFs was started in the early 2000s after Omar Yaghi and his group reported the preparation and crystallisation of MOFs.[72] They exist in one-, two- or three-dimensional porous structures formed by the coordination of metal clusters (also called secondary building units) to organic linkers, see Fig 1.5. MOFs can be synthesized with varied pore sizes by careful selection of organic linkers. A classic example of this is the synthesis of 16

MOFs with the same framework topology using different organic linkers.[73] Further, post-synthetic modification of MOFs enables the functionalisation and fine-tuning of other properties such as pore size, surface chemistry, and chemical and thermal stabilities through which host-guest interactions can be altered to show the desired effect. Due to the above-mentioned advantages, MOFs are used for gas storage and transportation, reaction catalysts and drug delivery dosage forms. We are focusing only on the drug delivery aspect of MOFs in this thesis.

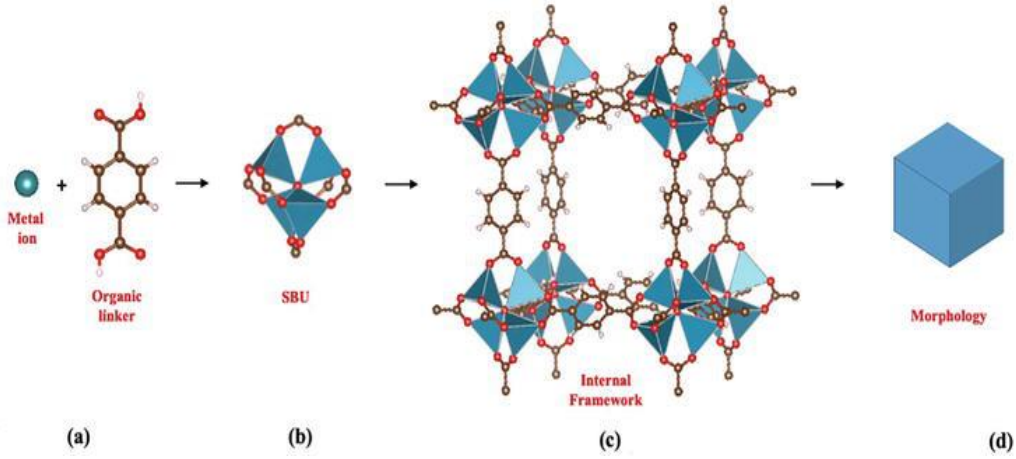


Figure 1.5: MOF-5 structure representation a) metal ion (Zn) and organic linker (Terephthalic acid) b) Secondary Building Unit (SBU) c) MOF- framework formed by coordination of SBUs to organic linker d) Final morphology of MOF-5. Adapted from Inoue, M.; Suzuki, T.; Nakada, M. Asymmetric Catalysis of Nozaki-Hiyama Allylation and Methallylation with a New Tridentate Bis(Oxazolinyl)Carbazole Ligand. *J Am Chem Soc* **2003**, *125* (5), 1140–1141.[74]

2.3. MOFs as drug delivery agents

Drug loading capacity in MOFs is higher in comparison to other delivery agents. Drug loading depends on MOF composition and loading method. The methods of drug loading are mainly classified into one-step and two-step methods.

2.3.1. One-step methods

During the one-step method, drug molecules are incorporated into MOF synthesis either by co-crystallisation, one-pot method, or by using drugs as organic linkers. Co-crystallisation is the process of crystal engineering where two or more different molecules co-exist. This method was employed for poorly soluble drugs to co-crystallize with MOFs to form a lattice structure. The second method is one-pot synthesis, this method is used when MOF pores are too small to adsorb the bulky molecules like nucleic acids or proteins. Here, the molecules are loaded by insertion or coating onto the surface. The last method is the incorporation of drugs as organic molecules which co-ordinate with metal clusters to form MOFs. Upon disintegration of MOFs, the drug molecules are released.

2.3.2. Two-step methods

During the two-step method, drugs are loaded into the MOFs either by grinding the drug molecules and MOFs together or by immersing the MOF in the drug solution. As this is carried out after MOF synthesis they are also called post-synthetic methods. Impregnation is the most used method where the drugs and MOFs are immersed in solution allowing the diffusion of drug molecules into MOFs. This method has a leaching problem, to overcome this the MOF's surface-active groups are used to form covalent bonding with drugs and biomolecules. This method of loading avoids leaching and also promotes the binding affinity to protein targets.

2.4. Computational modelling of adsorption and diffusion of drugs in MOFs

Drug loading and release from MOFs are treated as adsorption and diffusion phenomena respectively. While the experimental methods discussed above offer valuable insights, computational modelling of adsorption and diffusion helps in the understanding of the interactions of MOF-drug complexes and aids in tailoring MOFs to achieve the desired effect. Further, it serves as a

predictive tool to facilitate the screening and selection of MOFs for drug delivery before the experimental synthesis. In general, molecular modelling techniques such as Grand Canonical Monte Carlo (GCMC) simulations are extensively used to study drug adsorption in porous materials[75–77] and equilibrium or non-equilibrium molecular dynamics simulations serve as a tool to investigate the diffusion of drugs from MOFs at a molecular level.[78,79]

2.4.1. Grand Canonical Monte Carlo (GCMC) simulations

During adsorption, the number of adsorbate molecules (drugs) on a surface or in pores changes. The grand canonical ensemble is an ideal choice to simulate the adsorption in a system with varying particle numbers under constant temperature, pressure and chemical potential.[80] In GCMC, adsorption is replicated by simulating the reversible exchange of particles between the reservoir and MOFs. This is implemented by Monte Carlo sampling which performs trial insertions and deletions of drug molecules into the MOF pore and calculates the free energy change. Acceptance or rejection of the step is based on the Metropolis criterion change in energy. If $\Delta E < 0$, the move is accepted and if $\Delta E > 0$, the move is accepted with probability which is given by.

$$P = e^{-\Delta E/kT}$$

Where P is the acceptance probability, ΔE is the energy difference between the current state and the proposed date, *k is the* Boltzmann constant, and T is the temperature.

These simulations provide information such as drug loading capacity, and adsorption isotherms and aid in characterising the adsorption behaviour at various conditions. However, the accuracy of the results relies on the forcefield parameters so careful selection of the parameters results in accurate results.

2.4.2. Equilibrium Molecular Dynamics (EMD) or Non- Equilibrium Molecular Dynamics (NEMD)

Drug diffusion from pores of MOFs is investigated by employing EMD or NEMD simulations. EMD simulations are conducted to investigate the diffusion under equilibrium conditions.[81] In NEMD, external forces are applied to induce a non-equilibrium state in the system to study the non-equilibrium diffusion phenomenon.[82] In this thesis, the motion of a drug molecule over time is simulated using equilibrium molecular dynamics simulation to capture the drug interactions with MOFs. The diffusion from the pores is computed from the mean square displacement equation shown below, where $r^i(t)$ and $r^i(t)$ are the reference position and position of i^{th} drug at time t respectively and N is the number of drug molecules.

$$\mathrm{MSD}(t) = \frac{1}{N}\sum_{i=1}^{N}\left|r^i(t) - r^i(0)\right|^2$$

Equation 2: Formula to calculate mean square displacement

Section 3. DFT study of transition states of Enantioselective synthesis of homoallyl alcohols.

3.1. Homoallyl alcohols

Three carbon atoms forming a chain with alternating single and double bonds is known as an allyl group. If all the carbon atoms in a chain are homologous and the alcohol group is attached to one of the atoms in the allyl group then it is called homoallyl alcohol. CH_2CH_2CHOH is the general formula of homoallyl alcohols. The multiple functional groups can be used as substituents in homoallyl alcohols, hence they serve as intermediates in the synthesis of natural products, chiral drug compounds,[83] agrochemicals[84,] and polymers.[85] Due to the versatility of homoallyl alcohols, they are mostly used as starting materials for the synthesis of chiral drugs.

3.2. Chiral drugs

The term chiral came from "*ceir"* (a Greek word) that refers to hands as they possess similar characteristics because they look like mirror images but cannot be superimposed. A molecule is termed chiral if it contains more than one chiral center. If two molecules have the same bonding and molecular formula but differ in spatial arrangement, they are termed as stereoisomers. Among the stereoisomers, enantiomers are pair of molecules that are mirror images of each other but cannot be superimposable. These enantiomers are further classified as dextrorotatory or laevorotatory, if they rotate the plane polarised light into right or left, respectively.

The significance of chirality resonates within the components of the human body starting from small molecules such as amino acids and sugars to large molecules such as proteins, all these molecules possess chirality. As these molecules are chiral, they only have binding affinity to selective drug enantiomers to show pharmacological action. Due to this selective binding of chiral drugs, the drug delivery to the specific target[86] can be achieved and additionally, elimination of undesired side effects would be possible by using one enantiomer over the other; a critical lesson observed in the case of thalidomide.[87] Since they have positive outcomes in managing the disease more research focusing on synthetic routes of chiral drugs was put forward recently.[88] As previously stated, a homoallyl alcohol serves as an essential unit and the efficient synthesis of these moieties facilitates the production of chiral drug compounds. Some commonly named reactions for the synthesis of homoallyl alcohols that exist in literature are allylation of aldehydes or ketones, Pd-catalysed allylic substitution,[89,90] Grignard reaction,[91] Wittig reaction,[92] hydroboration-oxidation,[93] Reformatsky reaction,[94] and cross-coupling reactions.[95] These reactions are successfully employed in asymmetric synthesis and considered valuable to achieve high stereoselectivity in producing one enantiomer over the other.

3.3. Asymmetric synthesis

Asymmetric synthesis or enantioselective synthesis is defined as the production of unequal amounts of stereoisomeric products from a substrate molecule through chemical reactions. This term was first introduced by Emil Fischer in 1894. There are three approaches to asymmetric synthesis which are outlined below.

3.3.1. Chiral pool synthesis

The stock of readily available chiral molecules is used as starting materials to transform the prochiral substrate into a chiral product. The main advantage of this method is its cost-effectiveness if and only if the desired molecule has structural similarity to naturally occurring chiral compounds such as amino acids and sugar. This method needs stoichiometric amounts of starting material and if the desired molecule lacks similarity to the readily available chiral molecules, the synthesis will become expensive to procure the chiral starting materials.[96,97]

3.3.2. Asymmetric Induction

The process of chiral synthesis under the influence of chiral features of a substrate, reagent, or catalyst is termed asymmetric induction.[98,99] The induction mainly occurs in three ways. In the first approach, the chiral center covalently binds to the reactive center and continues to remain bound throughout the reaction, this phenomenon is called internal asymmetric induction. The second approach uses the chiral auxiliaries to introduce chirality. These auxiliaries are added in one step and subsequently removed in another step. This whole process is termed as relayed asymmetric induction. In the last approach, the chiral information is induced through the chiral catalyst ligand, as this approach employs an external catalyst, it is called external asymmetric induction. The main disadvantage of these approaches is adding or removing substrate or reagent during synthesis can introduce additional complexity.

3.3.3. Asymmetric catalysis

Asymmetric catalysis uses a chiral catalyst in small amounts to promote the formation of a selected enantiomer in large amounts. This approach of chiral synthesis garnered attention in the 1970s after L-DOPA, an anti-Parkinson's drug was synthesized by employing the first rhodium-based asymmetric catalyst prepared by Willaim Knowles. After three decades of this groundbreaking research, Knowles received the Nobel prize in association with Ryoji Noyori and K.Barry Sharpless in 2001.[100] The catalysts employed in enantiocontrol reactions can be categorised into three types. Organocatalysts, biocatalysts, and chiral metal-ligand complexes. Biological molecules and living cells can act as biocatalysts for enantioselective reactions. They are non-toxic and possess a high reaction rate and specificity but suffer from stability issues. The second class of catalysts is developed using chiral or achiral ligands that chelate around the metal to form chiral metal complexes and act as an asymmetric catalyst. They are used in small amounts and the ligands around the metal form non-covalent reactions with the substrates to achieve high enantiocontrol. For this reason, they are mostly used in reactions such as Bronsted/acid-base catalysis,[101] phase transfer catalysis,[102] nucleophilic reactions[103,] and photocatalysis[104]. However, these catalysts are difficult to separate from products, sensitive to temperature and moisture and the metals used in developing catalysts are toxic and harmful to the environment. The last class of catalysts are organocatalysts. Organic molecules with chiral centers are used as organocatalysts to accelerate the stereoselectivity in the asymmetric synthesis. They are simple, readily available, low cost, and less sensitive to air and moisture. Hence mostly they are used in comparison to the other classes of catalysts.

Though organocatalysis was discovered in the 1970s,[105] the development and use of organocatalysts in asymmetric catalysis was started after Benjamen List and David McMillan explored small organic molecules to catalyse the enantioselective reactions in the early 21st century.[106,107] This led to the extensive research and development of organocatalysts and they both received the Nobel Prize in chemistry in 2021 for their groundbreaking research.

Organocatalysts initiate the reactions by the addition or removal of electrons or protons from the substrate, based on this they are classified into Lewis acids, Lewis bases, Bronsted acids, and Bronsted bases.

Chiral phosphoric acid (CPA), a type of Bronsted acid catalyst gained popularity among the organic catalysts for its high enantioselectivity and wide substrate scope. As stated before, allylation of aldehydes and ketones is one of the most common approaches to synthesise homoallyl alcohols. The scope and mechanism of these reactions catalysed by CPA are discussed in Chapter 5. Understanding the mechanism aspects of allylboration and the origin of enantioselectivity by CPA catalyst uncovers the interactions and reveals the factors responsible for high enantioselectivity.

Transition states are the high-energy configurations along the reaction coordinate. The arrangement of atoms in transition states influences the orientation and interactions between the reacting species that directly determine the activation energy and reaction pathway. This can also lead to different stereoisomers. In asymmetric synthesis, the arrangement of atoms in a transition state is studied to understand the electronic and steric effects influencing the stereochemistry of the reaction. Therefore, a theoretical investigation of these noncovalent interactions in the transition state is carried out to explore the enantiocontrol mechanism, enabling the design of highly effective synthetic methodologies.

3.4. Computational study of transition states.

DFT methods are well known for studying the mechanism of reactions by locating transition states or saddle points along the reaction coordinates. Some common methods that locate the transition states are potential energy scans,[108] nudged elastic bands (NEB)[109,] and dimer methods.[110] In chapter 5, an initial guess of transition state conformers was generated using conformer generator algorithms and subjected to energy minimisation and studied further.

In terms of atomic perspective, the chemical reaction is a rearrangement of nuclei and there could be many possible paths of rearrangement of reactants to form products. Searching all these paths on the potential energy surface (PES) is a daunting task. Transition state theory was proposed in the 1930`s to address this problem. It states that the saddle point (also termed a transition state) is a high-energy configuration of a molecule along the minimum energy path of a reaction in the PES connecting reactants and products, where bond breaking, and formation occurs. On the other hand, minima are the stable points in the PES. Eigenvalues of the Hessian matrix computed from the DFT calculations distinguish the transition state from the local minima. This method requires an initial estimated structure that is close to the expected transition state of a reaction followed by constrained optimisation during which the bond length of bonds relevant to the reaction are fixed and all others are allowed to relax. Thereafter vibrational frequencies are calculated to verify the imaginary frequency corresponds to the movement of bond formed during the reaction. Complete details of the computational methodology adopted in this section are discussed in Chapter 5.

4. Bibliography

(1) Eastell, R.; O'Neill, T. W.; Hofbauer, L. C.; Langdahl, B.; Reid, I. R.; Gold, D. T.; Cummings, S. R. Postmenopausal Osteoporosis. *Nature Reviews Disease Primers 2016 2:1* **2016**, *2* (1), 1–16. https://doi.org/10.1038/nrdp.2016.69.

(2) Marini, F.; Giusti, F.; Palmini, G.; Brandi, M. L. Role of Wnt Signaling and Sclerostin in Bone and as Therapeutic Targets in Skeletal Disorders. *Osteoporosis International 2022 34:2* **2022**, *34* (2), 213–238. https://doi.org/10.1007/S00198-022-06523-7.

(3) Veverka, V.; Henry, A. J.; Slocombe, P. M.; Ventom, A.; Mulloy, B.; Muskett, F. W.; Muzylak, M.; Greenslade, K.; Moore, A.; Zhang, L.; Gong, J.; Qian, X.; Paszty, C.; Taylor, R. J.; Robinson, M. K.; Carr, M. D. Characterization of the Structural Features and Interactions of Sclerostin: MOLECULAR INSIGHT INTO A KEY REGULATOR OF Wnt-MEDIATED BONE FORMATION*S. *J Biol Chem* **2009**, *284* (16), 10890. https://doi.org/10.1074/JBC.M807994200.

(4) Miller, S. A.; St. Onge, E. L.; Whalen, K. L. Romosozumab: A Novel Agent in the Treatment for Postmenopausal Osteoporosis. *J Pharm Technol* **2021**, *37* (1), 45. https://doi.org/10.1177/8755122520967632.

(5) Miller, S. A.; St. Onge, E. L.; Whalen, K. L. Romosozumab: A Novel Agent in the Treatment for Postmenopausal Osteoporosis. *J Pharm Technol* **2021**, *37* (1), 45. https://doi.org/10.1177/8755122520967632.

(6) Recker, R. R.; Benson, C. T.; Matsumoto, T.; Bolognese, M. A.; Robins, D. A.; Alam, J.; Chiang, A. Y.; Hu, L.; Krege, J. H.; Sowa, H.; Mitlak, B. H.; Myers, S. L. A Randomized, Double-Blind Phase 2 Clinical Trial of Blosozumab, a Sclerostin Antibody, in Postmenopausal Women with Low Bone Mineral Density. *Journal of Bone and Mineral Research* **2015**, *30* (2), 216–224. https://doi.org/10.1002/JBMR.2351.

(7) Glorieux, F. H.; Devogelaer, J. P.; Durigova, M.; Goemaere, S.; Hemsley, S.; Jakob, F.; Junker, U.; Ruckle, J.; Seefried, L.; Winkle, P. J. BPS804 Anti-Sclerostin Antibody in Adults With Moderate Osteogenesis Imperfecta: Results of a Randomized Phase 2a Trial. *J Bone Miner Res* **2017**, *32* (7), 1496–1504. https://doi.org/10.1002/JBMR.3143.

(8) Hansel, T. T.; Kropshofer, H.; Singer, T.; Mitchell, J. A.; George, A. J. T. The Safety and Side Effects of Monoclonal Antibodies. *Nature Reviews Drug Discovery 2010 9:4* **2010**, *9* (4), 325–338. https://doi.org/10.1038/nrd3003.

(9) Españo, E.; Kim, J.; Lee, K.; Kim, J. K. Phytochemicals for the Treatment of COVID-19. *J Microbiol* **2021**, *59* (11), 959. https://doi.org/10.1007/S12275-021-1467-Z.

(10) Tse, E. G.; Korsik, M.; Todd, M. H. The Past, Present and Future of Anti-Malarial Medicines. *Malaria Journal 2019 18:1* **2019**, *18* (1), 1–21. https://doi.org/10.1186/S12936-019-2724-Z.

(11) Khameneh, B.; Eskin, N. A. M.; Iranshahy, M.; Fazly Bazzaz, B. S. Antibiotics Phytochemicals: A Promising Weapon in the Arsenal against Antibiotic-Resistant Bacteria. **2021**. https://doi.org/10.3390/antibiotics10091044.

(12) Rudzińska, A.; Juchaniuk, P.; Oberda, J.; Wiśniewska, J.; Wojdan, W.; Szklener, K.; Mańdziuk, S. Phytochemicals in Cancer Treatment and Cancer Prevention—Review on Epidemiological Data and Clinical Trials. *Nutrients* **2023**, *15* (8), 1896. https://doi.org/10.3390/NU15081896.

(13) Bhattacharjee, A.; Purohit, P.; Roy, P. K. Neuroprotective Drug Discovery From Phytochemicals and Metabolites for CNS Viral Infection: A Systems Biology Approach With Clinical and Imaging Validation. *Front Neurosci* **2022**, *16*, 917867. https://doi.org/10.3389/FNINS.2022.917867/FULL.

(14) Nitulescu, M.; Alves de Oliveira, T.; Pires da Silva, M.; Habib Bechelane Maia, E.; Marques da Silva, A.; Gutterres Taranto, A. Virtual Screening Algorithms in Drug Discovery: A Review Focused on Machine and Deep Learning Methods. *Drugs and Drug Candidates 2023, Vol. 2, Pages 311-334* **2023**, *2* (2), 311–334. https://doi.org/10.3390/DDC2020017.

(15) Meng, E. C.; Shoichet, B. K.; Kuntz, I. D. Automated Docking with Grid-Based Energy Evaluation. *J Comput Chem* **1992**, *13* (4), 505–524. https://doi.org/10.1002/JCC.540130412.

(16) Jones, G.; Willett, P.; Glen, R. C.; Leach, A. R.; Taylor, R. *Development and Validation of a Genetic Algorithm for Flexible Docking*; 1997.

(17) Verdonk, M. L.; Cole, J. C.; Hartshorn, M. J.; Murray, C. W.; Taylor, R. D. Improved Protein–Ligand Docking Using GOLD. *Proteins: Structure, Function, and Bioinformatics* **2003**, *52* (4), 609–623. https://doi.org/10.1002/PROT.10465.

(18) Meng, E. C.; Shoichet, B. K.; Kuntz, I. D. Automated Docking with Grid-based Energy Evaluation. *J Comput Chem* **1992**, *13* (4), 505–524. https://doi.org/10.1002/JCC.540130412.

(19) Friesner, R. A.; Banks, J. L.; Murphy, R. B.; Halgren, T. A.; Klicic, J. J.; Mainz, D. T.; Repasky, M. P.; Knoll, E. H.; Shelley, M.; Perry, J. K.; Shaw, D. E.; Francis, P.; Shenkin, P. S. Glide: A New Approach for Rapid, Accurate Docking and Scoring. 1. Method and Assessment of Docking Accuracy. *J Med Chem* **2004**, *47* (7), 1739–1749. https://doi.org/10.1021/JM0306430/SUPPL_FILE/JM0306430_S.PDF.

(20) Kalid, O.; Toledo Warshaviak, D.; Shechter, S.; Sherman, W.; Shacham, S. Consensus Induced Fit Docking (CIFD): Methodology, Validation, and Application to the Discovery of Novel Crm1 Inhibitors. https://doi.org/10.1007/s10822-012-9611-9.

(21) Carlson, H.; … K. M.-T. J. of P.; 1999, undefined. Method for Including the Dynamic Fluctuations of a Protein in Computer-Aided Drug Design. *ACS Publications* **1999**, *103* (49), 10213–10219. https://doi.org/10.1021/jp991997z.

(22) Forli, S.; Olson, A. J. A Force Field with Discrete Displaceable Waters and Desolvation Entropy for Hydrated Ligand Docking. *J Med Chem* **2012**, *55* (2), 623–638. https://doi.org/10.1021/JM2005145.

(23) Böhm, H. J. The Development of a Simple Empirical Scoring Function to Estimate the Binding Constant for a Protein-Ligand Complex of Known Three-Dimensional Structure. *J Comput Aided Mol Des* **1994**, *8* (3), 243–256. https://doi.org/10.1007/BF00126743.

(24) Eldridge, M. D.; Murray, C. W.; Auton, T. R.; Paolini, G. V.; Mee, R. P. Empirical Scoring Functions: I. The Development of a Fast Empirical Scoring Function to Estimate the Binding Affinity of Ligands in Receptor Complexes. *J Comput Aided Mol Des* **1997**, *11* (5), 425–445. https://doi.org/10.1023/A:1007996124545.

(25) Shen, Q.; Xiong, B.; Zheng, M.; Luo, X.; Luo, C.; Liu, X.; Du, Y.; Li, J.; Zhu, W.; Shen, J.; Jiang, H. Knowledge-Based Scoring Functions in Drug Design: 2. Can the Knowledge Base Be Enriched? *J Chem Inf Model* **2011**, *51* (2), 386–397. https://doi.org/10.1021/CI100343J/SUPPL_FILE/CI100343J_SI_003.TXT.

(26) Vanommeslaeghe, K.; Hatcher, E.; Acharya, C.; Kundu, S.; Zhong, S.; Shim, J.; Darian, E.; Guvench, O.; Lopes, P.; Vorobyov, I.; Mackerell, A. D. CHARMM General Force Field: A Force Field for Drug-like Molecules Compatible with the CHARMM All-Atom Additive Biological Force Fields. *J Comput Chem* **2010**, *31* (4), 671–690. https://doi.org/10.1002/JCC.21367.

(27) Ponder, J. W.; Case, D. A. FORCE FIELDS FOR PROTEIN SIMULATIONS. **2003**.

(28) Scott, W. R. P.; Hünenberger, P. H.; Tironi, I. G.; Mark, A. E.; Billeter, S. R.; Fennen, J.; Torda, A. E.; Huber, T.; Krüger, P.; Van Gunsteren, W. F. The GROMOS Biomolecular Simulation Program Package. *Journal of Physical Chemistry A* **1999**, *103* (19), 3596–3607. https://doi.org/10.1021/JP984217F.

(29) Jorgensen, W. L.; Maxwell, D. S.; Tirado-Rives, J. Development and Testing of the OPLS All-Atom Force Field on Conformational Energetics and Properties of Organic Liquids. *J Am Chem Soc* **1996**, *118* (45), 11225–11236. https://doi.org/10.1021/JA9621760.

(30) Rudd, R. E.; Broughton, J. Q. Coarse-Grained Molecular Dynamics: Nonlinear Finite Elements and Finite Temperature. *Phys Rev B Condens Matter Mater Phys* **2005**, *72* (14). https://doi.org/10.1103/PHYSREVB.72.144104.

(31) Limongelli, V.; Bonomi, M.; Parrinello, M. Funnel Metadynamics as Accurate Binding Free-Energy Method. *Proc Natl Acad Sci U S A* **2013**, *110* (16), 6358–6363. https://doi.org/10.1073/PNAS.1303186110/SUPPL_FILE/SM01.MOV.

(32) Parikh, V.; Gumaste, S. G.; Phadke, S. Effect of the Interaction Between an Ionic Surfactant and Polymer on the Dissolution of a Poorly Soluble Drug. *AAPS PharmSciTech* **2018**, *19* (7), 3040–3047. https://doi.org/10.1208/s12249-018-1125-x.

(33) Putra, O. D.; Umeda, D.; Fujita, E.; Haraguchi, T.; Uchida, T.; Yonemochi, E.; Uekusa, H. Solubility Improvement of Benexate through Salt Formation Using Artificial Sweetener. *Pharmaceutics* **2018**, *10* (2). https://doi.org/10.3390/pharmaceutics10020064.

(34) Almotairy, A.; Almutairi, M.; Althobaiti, A.; Alyahya, M.; Sarabu, S.; Alzahrani, A.; Zhang, F.; Bandari, S.; Repka, M. A. Effect of PH Modifiers on the Solubility, Dissolution Rate, and Stability of Telmisartan Solid Dispersions Produced by Hot-Melt Extrusion Technology. *J Drug Deliv Sci Technol* **2021**, *65*. https://doi.org/10.1016/j.jddst.2021.102674.

(35) *Chemicals policy - Library*. https://circabc.europa.eu/ui/group/8ee3c69a-bccb-4f22-89ca-277e35de7c63/library/a40b7f19-2eec-40c0-b905-08e74efe7747 (accessed 2023-09-29).

(36) Yagublu, V.; Karimova, A.; Hajibabazadeh, J.; Reissfelder, C.; Muradov, M.; Bellucci, S.; Allahverdiyev, A. Overview of Physicochemical Properties of Nanoparticles as Drug Carriers for Targeted Cancer Therapy. *Journal of Functional Biomaterials 2022, Vol. 13, Page 196* **2022**, *13* (4), 196. https://doi.org/10.3390/JFB13040196.

(37) Chronopoulou, L.; Nocca, G.; Castagnola, M.; Paludetti, G.; Ortaggi, G.; Sciubba, F.; Bevilacqua, M.; Lupi, A.; Gambarini, G.; Palocci, C. Chitosan Based Nanoparticles Functionalized with Peptidomimetic Derivatives for Oral Drug Delivery. *N Biotechnol* **2016**, *33* (1), 23–31. https://doi.org/10.1016/J.NBT.2015.07.005.

(38) Grumezescu, V.; Gherasim, O.; Negut, I.; Banita, S.; Holban, A. M.; Florian, P.; Icriverzi, M.; Socol, G. Nanomagnetite-Embedded PLGA Spheres for Multipurpose Medical Applications. *Materials (Basel)* **2019**, *12* (16). https://doi.org/10.3390/MA12162521.

(39) Kim, D.; Le, Q. V.; Kim, Y. B.; Oh, Y. K. Safety and Photochemotherapeutic Application of Poly(γ-Glutamic Acid)-Based Biopolymeric Nanoparticle. *Acta Pharm Sin B* **2019**, *9* (3), 565–574. https://doi.org/10.1016/j.apsb.2019.01.005.

(40) Zhang, L. N.; Zhang, Q.; Wang, X.; Zhang, W. J.; Lin, C. C.; Chen, F.; Yang, X. G.; Pan, W. S. Drug-in-Cyclodextrin-in-Liposomes: A Novel Drug Delivery System for Flurbiprofen. *Int J Pharm* **2015**, *492* (1–2), 40–45. https://doi.org/10.1016/j.ijpharm.2015.07.011.

(41) Kou, L. F.; Huang, H. E.; Lin, X. L.; Jiang, X. Y.; Wang, Y.; Luo, Q. H.; Sun, J.; Yao, Q.; Ganapathy, V.; Chen, R. J. Endocytosis of

ATB(0,+)(SLC6A14)-Targeted Liposomes for Drug Delivery and Its Therapeutic Application for Pancreatic Cancer. *Expert Opin Drug Deliv* **2020**, *17* (3), 395–405. https://doi.org/10.1080/17425247.2020.1723544.

(42) Li, W. Z.; Hao, X. L.; Zhao, N.; Han, W. X.; Zhai, X. F.; Zhao, Q.; Wang, Y. E.; Zhou, Y. Q.; Cheng, Y. C.; Yue, Y. H.; Fu, L. N.; Zhou, J. L.; Wu, H. Y.; Dong, C. J. Propylene Glycol-Embodying Deformable Liposomes as a Novel Drug Delivery Carrier for Vaginal Fibrauretine Delivery Applications. *JOURNAL OF CONTROLLED RELEASE* **2016**, *226*, 107–114. https://doi.org/10.1016/j.jconrel.2016.02.024.

(43) Long, M. M.; Lu, A. L.; Lu, M.; Weng, L. Y.; Chen, Q. P.; Zhu, L.; Chen, Z. P. Azo-Inserted Responsive Hybrid Liposomes for Hypoxia-Specific Drug Delivery. *Acta Biomater* **2020**, *115*, 343–357. https://doi.org/10.1016/j.actbio.2020.07.061.

(44) Lankalapalli, S.; Tenneti, V. Formulation and Evaluation of Rifampicin Liposomes for Buccal Drug Delivery. *Curr Drug Deliv* **2016**, *13* (7), 1084–1099. https://doi.org/10.2174/1567201813666151221145617.

(45) Jiang, L. T.; Liang, Y.; Huo, Q. Q.; Pu, Y. J.; Lu, W.; Han, S. C.; Cao, J.; He, B.; Sun, Y. Viral Capsids Mimicking Based on PH-Sensitive Biodegradable Polymeric Micelles for Efficient Anticancer Drug Delivery. *J Biomed Nanotechnol* **2018**, *14* (8D), 1409–1419. https://doi.org/10.1166/jbn.2018.2587.

(46) Bae, Y.; Alani, A. W. G.; Rockich, N. C.; Lai, T.; Kwon, G. S. Mixed PH-Sensitive Polymeric Micelles for Combination Drug Delivery. *Pharm Res* **2010**, *27* (11), 2421–2432. https://doi.org/10.1007/s11095-010-0234-3.

(47) Smejkalova, D.; Muthny, T.; Nesporova, K.; Hermannova, M.; Achbergerova, E.; Huerta-Angeles, G.; Svoboda, M.; Cepa, M.; Machalova, V.; Luptakova, D.; Velebny, V. Hyaluronan Polymeric Micelles for Topical Drug

Delivery. *Carbohydr Polym* **2017**, *156*, 86–96. https://doi.org/10.1016/j.carbpol.2016.09.013.

(48) Li, Y. M.; Zhang, H.; Zhai, G. X. Intelligent Polymeric Micelles: Development and Application as Drug Delivery for Docetaxel. *J Drug Target* **2017**, *25* (4), 285–295. https://doi.org/10.1080/1061186X.2016.1245309.

(49) Sweet, D. M.; Kolhatkar, R. B.; Ray, A.; Swaan, P.; Ghandehari, H. Transepithelial Transport of PEGylated Anionic Poly(Amidoamine) Dendrimers: Implications for Oral Drug Delivery. *JOURNAL OF CONTROLLED RELEASE* **2009**, *138* (1), 78–85. https://doi.org/10.1016/j.jconrel.2009.04.022.

(50) Parham, N.; Panahi, H. A.; Feizbakhsh, A.; Moniri, E. Synthesis of PEGylated Superparamagnetic Dendrimers and Their Applications as a Drug Delivery System. *Polym Adv Technol* **2021**, *32* (4), 1568–1578. https://doi.org/10.1002/pat.5194.

(51) Gokce, B. B.; Boran, T.; Calik, F. E.; Ozhan, G.; Sanyal, R.; Gungor, S. Dermal Delivery and Follicular Targeting of Adapalene Using PAMAM Dendrimers. *Drug Deliv Transl Res* **2021**, *11* (2), 626–646. https://doi.org/10.1007/s13346-021-00933-6.

(52) Pan, J. Z.; Wen, M.; Yin, D. Q.; Jiang, B.; He, D. S.; Guo, L. Design and Synthesis of Novel Amphiphilic Janus Dendrimers for Bone-Targeted Drug Delivery. *Tetrahedron* **2012**, *68* (14), 2943–2949. https://doi.org/10.1016/j.tet.2012.02.040.

(53) Bernik, D. L. Silicon Based Materials for Drug Delivery Devices and Implants. *Recent Pat Nanotechnol* **2007**, *1* (3), 186–192. https://doi.org/10.2174/187221007782360402.

(54) Carazo, E.; Borrego-Sanchez, A.; Garcia-Villen, F.; Sanchez-Espejo, R.; Cerezo, P.; Aguzzi, C.; Viseras, C. Advanced Inorganic Nanosystems for

Skin Drug Delivery. *CHEMICAL RECORD* **2018**, *18* (7–8), 891–899. https://doi.org/10.1002/tcr.201700061.

(55) Alshehri, M. H. Adsorption of Cisplatin Molecules in Nanoporous Inorganic Materials as Drug Delivery Vehicles. *MATHEMATICS* **2022**, *10* (7). https://doi.org/10.3390/math10071018.

(56) Spillmann, C. M.; Naciri, J.; Algar, W. R.; Medintz, I. L.; Delehanty, J. B. Multifunctional Liquid Crystal Nanoparticles for Intracellular Fluorescent Imaging and Drug Delivery. *ACS Nano* **2014**, *8* (7), 6986–6997. https://doi.org/10.1021/nn501816z.

(57) Coelho, S. C.; Reis, D. P.; Pereira, M. C.; Coelho, M. A. N. Doxorubicin and Varlitinib Delivery by Functionalized Gold Nanoparticles Against Human Pancreatic Adenocarcinoma. *Pharmaceutics* **2019**, *11* (11). https://doi.org/10.3390/pharmaceutics11110551.

(58) Mendes, C.; Thirupathi, A.; Correa, M.; Gu, Y. D.; Silveira, P. C. L. The Use of Metallic Nanoparticles in Wound Healing: New Perspectives. *Int J Mol Sci* **2022**, *23* (23). https://doi.org/10.3390/ijms232315376.

(59) Li, Y.; Song, K.; Cao, Y.; Peng, C.; Yang, G. Keratin-Templated Synthesis of Metallic Oxide Nanoparticles as MRI Contrast Agents and Drug Carriers. *ACS Appl Mater Interfaces* **2018**, *10* (31), 26039–26045. https://doi.org/10.1021/acsami.8b08555.

(60) Menagen, B.; Avnir, D. Entrapment of Drugs within Metallic Platinum and Their Delivery. *ACS Biomater Sci Eng* **2019**, *5* (5), 2355-+. https://doi.org/10.1021/acsbiomaterials.9b00379.

(61) Choi, Y.; Kim, S.; Choi, M. H.; Ryoo, S. R.; Park, J.; Min, D. H.; Kim, B. S. Highly Biocompatible Carbon Nanodots for Simultaneous Bioimaging and Targeted Photodynamic Therapy In Vitro and In Vivo. *Adv Funct Mater* **2014**, *24* (37), 5781–5789. https://doi.org/10.1002/adfm.201400961.

(62) Tang, J.; Kong, B.; Wu, H.; Xu, M.; Wang, Y. C.; Wang, Y. L.; Zhao, D. Y.; Zheng, G. F. Carbon Nanodots Featuring Efficient FRET for Real-Time Monitoring of Drug Delivery and Two-Photon Imaging. *ADVANCED MATERIALS* **2013**, *25* (45), 6569–6574. https://doi.org/10.1002/adma.201303124.

(63) Yadav, H.; Rout, D.; Upadhyaya, A. K.; Agarwala, P.; Sharma, A.; Sasmal, D. K. Carbon Quantum Dots for Efficient Delivery of Curcumin in Live Cell. *CHEMICAL PHYSICS IMPACT* **2023**, *7*. https://doi.org/10.1016/j.chphi.2023.100279.

(64) Chen, S. C.; Lin, C. Y.; Cheng, T. L.; Tseng, W. L. 6-Mercaptopurine-Induced Fluorescence Quenching of Monolayer MoS2 Nanodots: Applications to Glutathione Sensing, Cellular Imaging, and Glutathione-Stimulated Drug Delivery. *Adv Funct Mater* **2017**, *27* (41). https://doi.org/10.1002/adfm.201702452.

(65) Shimoda, A.; Sawada, S.; Akiyoshi, K. Intracellular Protein Delivery Using Self-Assembled Amphiphilic Polysaccharide Nanogels. In *INTRACELLULAR DELIVERY II: FUNDAMENTALS AND APPLICATIONS*; Prokop, A., Iwasaki, Y., Harada, A., Eds.; 2014; Vol. 7, pp 265–274. https://doi.org/10.1007/978-94-017-8896-0_14.

(66) Wang, Y. P.; Yan, L. S.; He, S. S.; Zhou, D. F.; Cheng, Y. X.; Chen, X. S.; Jing, X. B.; Huang, Y. B. A Versatile Method to Prepare Protein Nanoclusters for Drug Delivery. *Macromol Biosci* **2018**, *18* (2). https://doi.org/10.1002/mabi.201700282.

(67) Wang, Z.; Hu, S.; Yang, J.; Liang, A.; Li, Y.; Zhuang, Q.; Gu, J.; Wang, Z.; Yang, J.; Li, Y. S.; Zhuang, Q. X.; Gu, L.; Hu, S.; Liang, A. Nanoscale Zr-Based MOFs with Tailorable Size and Introduced Mesopore for Protein Delivery. *Adv Funct Mater* **2018**, *28* (16), 1707356. https://doi.org/10.1002/ADFM.201707356.

(68) Bendre, A.; Hegde, V.; Ajeya, K. V.; Thagare Manjunatha, S.; Somasekhara, D.; Nadumane, V. K.; Kant, K.; Jung, H. Y.; Hung, W. S.; Kurkuri, M. D. Microfluidic-Assisted Synthesis of Metal—Organic Framework — Alginate Micro-Particles for Sustained Drug Delivery. *Biosensors (Basel)* **2023**, *13* (737), 737. https://doi.org/10.3390/BIOS13070737.

(69) Lei, B.; Wang, M.; Jiang, Z.; Qi, W.; Su, R.; He, Z. Constructing Redox-Responsive Metal-Organic Framework Nanocarriers for Anticancer Drug Delivery. *ACS Appl Mater Interfaces* **2018**, *10* (19), 16698–16706. https://doi.org/10.1021/ACSAMI.7B19693/ASSET/IMAGES/MEDIUM/AM-2017-19693R_M002.GIF.

(70) Du, J.; Chen, G.; Yuan, X.; Yuan, J.; Li, L. Multi-Stimuli Responsive Cu-MOFs@Keratin Drug Delivery System for Chemodynamic Therapy. *Front Bioeng Biotechnol* **2023**, *11*. https://doi.org/10.3389/FBIOE.2023.1125348/FULL.

(71) Zhao, X.; He, S.; Li, B.; Liu, B.; Shi, Y.; Cong, W.; Gao, F.; Li, J.; Wang, F.; Liu, K.; Sheng, C.; Su, J.; Hu, H. G. DUCNP@Mn-MOF/FOE as a Highly Selective and Bioavailable Drug Delivery System for Synergistic Combination Cancer Therapy. *Nano Lett* **2023**, *23* (3), 863–871. https://doi.org/10.1021/ACS.NANOLETT.2C04042/ASSET/IMAGES/LARGE/NL2C04042_0004.JPEG.

(72) Li, H.; Eddaoudi, M.; O'Keeffe, M.; Yaghi, O. M. Design and Synthesis of an Exceptionally Stable and Highly Porous Metal-Organic Framework. *Nature 1999 402:6759* **1999**, *402* (6759), 276–279. https://doi.org/10.1038/46248.

(73) Eddaoudi, M.; Kim, J.; Rosi, N.; Vodak, D.; Wachter, J.; O'Keeffe, M.; Yaghi, O. M. Systematic Design of Pore Size and Functionality in Isoreticular MOFs and Their Application in Methane Storage. *Science (1979)* **2002**, *295* (5554), 469–472. https://doi.org/10.1126/SCIENCE.1067208.

(74) Mittal, A.; Roy, I.; Gandhi, S.; Mittal, A.; Roy, I.; Gandhi, S. Drug Delivery Applications of Metal-Organic Frameworks (MOFs). *Drug Carriers* **2022**. https://doi.org/10.5772/INTECHOPEN.103684.

(75) Liu, J.; Yang, Z.; Che, Y.; Zhang, Y.; Zhang, Z.; Zhao, C. X. Computational Investigation of Metal Organic Frameworks as Potential Drug Carriers for Antihypertensive Amlodipine. *AIChE Journal* **2022**, *68* (1). https://doi.org/10.1002/AIC.17474.

(76) Bernini, M. C.; Fairen-Jimenez, D.; Pasinetti, M.; Ramirez-Pastor, A. J.; Snurr, R. Q. Screening of Bio-Compatible Metal–Organic Frameworks as Potential Drug Carriers Using Monte Carlo Simulations. *J Mater Chem B* **2014**, *2* (7), 766–774. https://doi.org/10.1039/C3TB21328E.

(77) Sose, A. T.; Cornell, H. D.; Gibbons, B. J.; Burris, A. A.; Morris, A. J.; Deshmukh, S. A. Modelling Drug Adsorption in Metal–Organic Frameworks: The Role of Solvent. *RSC Adv* **2021**, *11* (28), 17064–17071. https://doi.org/10.1039/D1RA01746B.

(78) Erucar, I.; Keskin, S. Efficient Storage of Drug and Cosmetic Molecules in Biocompatible Metal Organic Frameworks: A Molecular Simulation Study. *Ind Eng Chem Res* **2016**, *55* (7), 1929–1939. https://doi.org/10.1021/ACS.IECR.5B04556/SUPPL_FILE/IE5B04556_SI_001.PDF.

(79) Amirjalayer, S.; Schmid, R. Mechanism of Benzene Diffusion in MOF-5: A Molecular Dynamics Investigation. *Microporous and Mesoporous Materials* **2009**, *125* (1–2), 90–96. https://doi.org/10.1016/J.MICROMESO.2009.02.006.

(80) Allen, M. P.; Tildesley, D. J.; Banavar, J. R. Computer Simulation of Liquids. *Phys Today* **1989**, *42* (3), 105–106. https://doi.org/10.1063/1.2810937.

(81) Rice, B. M.; Sewell, T. D. Equilibrium Molecular Dynamics Simulations. *Static Compression of Energetic Materials* **2009**, 255–290. https://doi.org/10.1007/978-3-540-68151-9_7.

(82) Ciccotti, G.; Kapral, R.; Sergi, A. Non-Equilibrium Molecular Dynamics. *Handbook of Materials Modeling* **2005**, 745–761. https://doi.org/10.1007/978-1-4020-3286-8_38.

(83) Tauber, J.; Schwartz, L. A.; Krische, M. J. Catalytic Enantioselective Synthesis of Chiral Organofluorine Compounds: Alcohol-Mediated Hydrogen Transfer for Catalytic Carbonyl Reductive Coupling. *Org Process Res Dev* **2019**, *23* (5), 730. https://doi.org/10.1021/ACS.OPRD.9B00035.

(84) Rossiter, B. E.; Barry Sharpless, K. Asymmetric Epoxidation of Homoallylic Alcohols. Synthesis of (-)-Γ-Amino-β(R)-Hydroxybutyric Acid (GABOB). *Journal of Organic Chemistry* **1984**, *49* (20), 3707–3711. https://doi.org/10.1021/JO00194A007/ASSET/JO00194A007.FP.PNG_V03.

(85) Larsen, M. B.; Wang, S. J.; Hillmyer, M. A. Poly(Allyl Alcohol) Homo- and Block Polymers by Postpolymerization Reduction of an Activated Polyacrylamide. *J Am Chem Soc* **2018**, *140* (38), 11911–11915. https://doi.org/10.1021/JACS.8B07542/SUPPL_FILE/JA8B07542_SI_001.PDF.

(86) Chu, X.; Bu, Y.; Yang, X. Recent Research Progress of Chiral Small Molecular Antitumor-Targeted Drugs Approved by the FDA From 2011 to 2019. *Frontiers in Oncology*. Frontiers Media S.A. December 17, 2021. https://doi.org/10.3389/fonc.2021.785855.

(87) Kim, J. H.; Scialli, A. R. Thalidomide: The Tragedy of Birth Defects and the Effective Treatment of Disease. *Toxicological Sciences* **2011**, *122* (1), 1–6. https://doi.org/10.1093/toxsci/kfr088.

(88) Tamatam, R.; Shin, D. Asymmetric Synthesis of US-FDA Approved Drugs over Five Years (2016–2020): A Recapitulation of Chirality. *Pharmaceuticals*. MDPI March 1, 2023. https://doi.org/10.3390/ph16030339.

(89) de la Cruz-Sánchez, P.; Biosca, M.; Magre, M.; Faiges, J.; Margalef, J.; Pàmies, O.; Diéguez, M. Enantioselective Pd-Catalyzed Allylic Substitution Using Phosphite-Oxazoline PHOX-Based Ligands Containing a Methylene Linker. *Eur J Inorg Chem* **2022**, *2022* (10), e202100988. https://doi.org/10.1002/EJIC.202100988.

(90) Yao, K.; Yuan, Q.; Qu, X.; Liu, Y.; Liu, D.; Zhang, W. Pd-Catalyzed Asymmetric Allylic Substitution Cascade Using α-(Pyridin-1-Yl)-Acetamides Formed in Situ as Nucleophiles. *Chem Sci* **2019**, *10* (6), 1767. https://doi.org/10.1039/C8SC04626C.

(91) Sormunen, G. J.; Lewis, D. E. A Rapid and Convenient Synthesis of Homoallylic Alcohols by the Barbier-Grignard Reaction. *Synth Commun* **2004**, *34* (19), 3473–3480. https://doi.org/10.1081/SCC-200030967.

(92) NakaI, T.; MikamI, K. The [2,3]-Wittig Rearrangement. *Organic Reactions* **1994**, 105–209. https://doi.org/10.1002/0471264180.OR046.02.

(93) Allred, E. L.; Sonnenberg, J.; Winstein, S. Preparation of Homobenzyl and Homoallyl Alcohols by the Hydroboration Method. *Journal of Organic Chemistry* **1960**, *25* (1), 26–29. https://doi.org/10.1021/JO01071A007/ASSET/JO01071A007.FP.PNG_V03.

(94) Saeed, S.; Zahoor, A. F.; Ahmad, S.; Akhtar, R.; Sikandar, S. Reformatsky Reaction as a Key Step in the Synthesis of Natural Products: A Review. *Synth Commun* **2022**, *52* (3), 317–345. https://doi.org/10.1080/00397911.2021.2008447.

(95) Inoue, M.; Suzuki, T.; Nakada, M. Asymmetric Catalysis of Nozaki-Hiyama Allylation and Methallylation with a New Tridentate

Bis(Oxazolinyl)Carbazole Ligand. *J Am Chem Soc* **2003**, *125* (5), 1140–1141. https://doi.org/10.1021/JA021243P/SUPPL_FILE/JA021243P_S.PDF.

(96) Chu, X.; Bu, Y.; Yang, X. Recent Research Progress of Chiral Small Molecular Antitumor-Targeted Drugs Approved by the FDA From 2011 to 2019. *Frontiers in Oncology*. Frontiers Media S.A. December 17, 2021. https://doi.org/10.3389/fonc.2021.785855.

(97) Klar, U.; Röhr, B.; Kuczynski, F.; Schwede, W.; Berger, M.; Skuballa, W.; Buchmann, B. Efficient Chiral Pool Synthesis of the C1-C6 Fragment of Epothilones. *Synthesis (Stuttg)* **2005**, No. 2, 301–305. https://doi.org/10.1055/s-2004-834936.

(98) Lang, K.; Torker, S.; Wojtas, L.; Zhang, X. P. Asymmetric Induction and Enantiodivergence in Catalytic Radical C-H Amination via Enantiodifferentiative H-Atom Abstraction and Stereoretentive Radical Substitution. *J Am Chem Soc* **2019**, *141* (31), 12388–12396. https://doi.org/10.1021/JACS.9B05850/SUPPL_FILE/JA9B05850_SI_005.ZIP .

(99) Garrido-Castro, A. F.; Maestro, M. C.; Alemán, J. Asymmetric Induction in Photocatalysis – Discovering a New Side to Light-Driven Chemistry. *Tetrahedron Lett* **2018**, *59* (14), 1286–1294. https://doi.org/10.1016/J.TETLET.2018.02.040.

(100) Halpern J; Trost BM. Asymmetric Catalysis. *Proc Natl Acad Sci U S A.* **2004**, *101* (15), 5347. https://doi.org/10.1073/pnas.0401811101.

(101) Rulev, Y. A.; Larionov, V. A.; Lokutova, A. V.; Moskalenko, M. A.; Lependina, O. L.; Maleev, V. I.; North, M.; Belokon, Y. N. Chiral Cobalt(III) Complexes as Bifunctional Brønsted Acid-Lewis Base Catalysts for the Preparation of Cyclic Organic Carbonates. *ChemSusChem* **2016**, *9* (2), 216–222. https://doi.org/10.1002/cssc.201501365.

(102) Maruoka, K. Design of High-Performance Chiral Phase-Transfer Catalysts with Privileged Structures. *Proceedings of the Japan Academy Series B: Physical and Biological Sciences*. Japan Academy 2018, pp 1–16. https://doi.org/10.2183/pjab.95.001.

(103) Nguyen, T. T. T.; Guyon, H.; Nguyen, K. P. P.; Boussonnière, A.; Mortier, J.; Castanet, A. S. Chiral Ligand-Mediated Nucleophilic Aromatic Substitution of Naphthoic Acids: A Fast and Efficient Access to Axially Chiral Biaryls. *European J Org Chem* **2020**, *2020* (25), 3829–3833. https://doi.org/10.1002/ejoc.202000317.

(104) Dey, P.; Rai, P.; Maji, B. Recent Development of Bis-Cyclometalated Chiral-at-Iridium and Rhodium Complexes for Asymmetric Catalysis. *ACS Organic and Inorganic Au*. American Chemical Society April 6, 2022, pp 99–125. https://doi.org/10.1021/acsorginorgau.1c00032.

(105) Hajos, Z. G.; Parrish, D. R. Asymmetric Synthesis of Bicyclic Intermediates of Natural Product Chemistry. *Journal of Organic Chemistry* **1974**, *39* (12), 1615–1621. https://doi.org/10.1021/JO00925A003/ASSET/JO00925A003.FP.PNG_V03.

(106) List, B.; Lerner, R. A.; Barbas, C. F. Proline-Catalyzed Direct Asymmetric Aldol Reactions [13]. *J Am Chem Soc* **2000**, *122* (10), 2395–2396. https://doi.org/10.1021/JA994280Y/ASSET/IMAGES/LARGE/JA994280YH00001.JPEG.

(107) Ahrendt, K. A.; Borths, C. J.; MacMillan, D. W. C. New Strategies for Organic Catalysis: The First Highly Enantioselective Organocatalytic Diels - Alder Reaction [16]. *J Am Chem Soc* **2000**, *122* (17), 4243–4244. https://doi.org/10.1021/JA000092S/SUPPL_FILE/JA000092S_S.PDF.

(108) Hoffmann, M. R.; Dyall, K. G. Low-Lying Potential Energy Surfaces. **2002**, *828*. https://doi.org/10.1021/BK-2002-0828.

(109) Sheppard, D.; Xiao, P.; Chemelewski, W.; Johnson, D. D.; Henkelman, G. A Generalized Solid-State Nudged Elastic Band Method. *J Chem Phys* **2012**, *136*, 74103. https://doi.org/10.1063/1.3684549.

(110) Xiao, P.; Sheppard, D.; Rogal, J.; Henkelman, G. Solid-State Dimer Method for Calculating Solid-Solid Phase Transitions. *J Chem Phys* **2014**, *140*, 174104. https://doi.org/10.1063/1.4873437.

Chapter 2: General Objectives

Thesis Structure

The main objective of the thesis is to apply molecular modelling techniques to research computational methodologies and establish a synergy between experiments and molecular modelling. This thesis revolves around the goal of elucidating the mechanisms and developing a pre-experiment screening tool to reduce the experimental workload, efforts to bridge a gap between theory and experiments were made. The thesis outlines four research projects among them three projects materialised into publications (manuscripts are ready to submit for journals) and the final project attached in this as an appendix at the end doesn't have concrete results to get published. Following are the objectives from Chapters 3 to 5

Objectives:

Chapter 3: This project arose from a collaboration with Naresh Kothuri working under Dr. Manish Kumar in CDRI, Lucknow, India. The main aim was to perform silicon screening of a small database of phytopharmaceutical molecules collected by them to identify a potential hit that acts as an inhibitor of sclerostin protein. As mentioned before in Section 1 of this chapter this protein inhibition can treat postmenopausal osteoporosis. Docking of molecules was performed on the crystal structure of sclerostin protein downloaded from the PDB database and protein-ligand interactions of the top 30 molecules were analysed and the top 2 protein-ligand complexes were subjected to 100 ns standard molecular dynamics and 50 ns funnel metadynamics to explore the stability of protein-ligand complex and to explore the ligand binding mechanism. Further, experimental studies have to be performed.

Chapter 4: This project is designed to screen metal-organic frameworks for drug loading and unloading. NUIG-4 metal-organic framework synthesised by materials lab group based in the University of Galway was considered to study the loading and unloading of individual and combination of drugs. We

employed periodic pseudopotential DFT calculations to optimise the structures and to calculate the binding energy of drugs.

Chapter 5: This chapter aims to explore the mechanism of allylboration by investigating the intermediate structures of two substrates ortho-vinyl benzaldehyde and ortho-alkynyl benzaldehyde. Geometry optimisation, single point, and frequency calculations are performed using DFT calculations. QTAIM and NCI analysis were performed.

.

Chapter 3: In Silico Screening of Natural Bioactive Compounds Against Sclerostin Target in Osteoporosis and Application of Funnel Metadynamics to Study the Binding Mechanism.

Data generated from the study is planned to be submitted to the *Journal of Biomolecular Structure and Dynamics*

Abstract:

Sclerostin is a negative regulator of the WNT signalling that binds to low-density lipoprotein receptor-related protein 5/6 (LRP5/6) co-receptors and inhibits bone formation and subsequently promotes bone resorption. In this study, 362 diverse sets of molecules collected from existing literature representing different phytopharmaceutical drug classes were docked in the loop 2 active site region of the sclerostin protein crystal structure (PDB ID: 2K8P). Further, the top two scored ligands verbascoside and salvianolic acid from docking were subjected to unbiased molecular dynamics and funnel meta-dynamics simulations to monitor the stability of the protein-ligand complex. The results from both simulations suggest that verbascoside binds to the sclerostin protein residues of ALA88, ALA94, PRO87, SER55, ARG145, and CYS143. Particularly ALA88 and ALA94 residues show higher hydrogen binding occupancy in the verbascoside protein complex than the salvanoic acid. In addition to that, funnel metadynamics simulations suggest that verbascoside has higher binding affinity as it shows interactions with multiple binding sites which are reported experimentally.

Reproduced with permission from:

Naresh Kothuri, Vinay K R Cheemarla, Aarti Abhishek Shah, Davide Tiana, Manish Kumar Chourasia

1. Introduction

Osteoporosis is a disease characterized by low bone mass and deterioration in the microarchitecture of bone tissue, leading to an increased risk of fracture. Worldwide, osteoporosis causes more than 8.9 million fractures annually, resulting in an osteoporosis fracture every 3 seconds. As per the WHO definition of osteoporosis, the disease affects approximately 6.3% of men over the age of 50 and 21.2% of women over the same age range globally.[1] Osteoporosis prevalence is higher in women and elderly patients.[2] Initial management of osteoporosis includes selective oestrogen receptor modulators, oestrogen replacement therapy, bisphosphonates, and denosumab. Anabolic therapy may also be used in patients with high fracture risk, usually consisting of teriparatide, a parathyroid hormone (PTH) synthetic analog. Nevertheless, most patients will need more than one anti-osteoporotic agent during their lifetime. Despite the well-documented efficacy of the above therapies, unmet needs for a more effective anti-fracture strategy still exist. From this perspective, a better understanding of biological pathways of bone metabolism and osteoblastic differentiation, such as the Wnt pathway, has led to the advent of new compounds that induce bone formation without coupling or even suppressing bone resorption.[3]

Sclerostin is a monomeric glycoprotein with a cysteine knot-like domain that has homology to the Cerebrus/DAN family of bone morphogenetic protein antagonists. It is a SOST gene product expressed by osteocytes and articular chondrocytes. Because of its high conservation across vertebrate species (the amino acid sequences in the vervet, rat, and mouse are 98%, 89%, and 88% identical respectively to the human sequence, animal models are potentially useful for studying sclerostin.[4] When sclerostin binds to the LRP5/6 and Frizzled coreceptors on the cell surface of osteoblasts, Wnt/β-catenin signalling is inhibited, thereby inhibiting osteoblast differentiation, proliferation, and activity, resulting in reduced osteoblastic bone formation.[5,6] As the Wnt pathway stimulates bone formation, the discovery of only one FDA-approved sclerostin natural antagonist, Romosozumab, (Evenity®) a human monoclonal antibody

injected subcutaneously directed against sclerostin.[7] The USFDA acknowledged the label of Evenity® but limited its approval to postmenopausal women at high risk for fractures and even recommended that the prescription duration should not exceed 12 months. The dosage regimen for romosozumab is 210 mg subcutaneously once every month for 12 doses in the abdomen, thigh, or upper arm.[8] A cohort study conducted in 2019 reported a total of 64 adverse events associated with the clinical use of romosozumab. The most common is a subcutaneous injection site reaction associated with pain, swelling, and redness lasting 2 days or longer. While other serious events involve cerebral infarction and osteonecrosis of the jaws.[9] Women at high risk of cardiovascular disease like myocardial infarction or stroke should not be considered for romosozumab treatment.[3] Aside from romosozumab some other monoclonal antibodies are being studied as sclerostin inhibitors and they are in various stages of drug development. Though they serve as promising agents the adverse events reported remain a concern. [4] Therefore, there is a need for natural alternative therapy for the inhibition of sclerostin in the treatment of osteoporosis. The toxicological limitations and the treatment cost associated with romosozumab can be resolved with alternate natural drug therapy.

In this work, we have collected natural bioactive compounds and performed docking against sclerostin protein to identify potential hits, and further molecular dynamics simulations were done to study the stability of the protein-ligand complex.

2. Methodology

2.1 Molecular Docking*:*

In this work, we have selected the library of 362 commercially available natural bioactive compounds containing a series of alkaloids, steroids, terpenoids, phenylpropanoids, stilbenes, flavonoids, polyphenol, and isoflavonoids. These compounds were screened against sclerostin protein and evaluated for its inhibition in the treatment of skeletal diseases. GOLD (Genetic

Optimisation for Ligand Docking) program [10] was used to perform docking. Loop 2 of the Sclerostin protein crystal structure (PDB ID: 2K8P) was used for docking the ligands. The grid enclosing box was centered over the active site amino acids (Proline (Pro)92, Asparagine (Asp)93, Alanine (Ala)94, Isoleucine (Ile)95 and glycine (Gly)96), represented as PNAIG, in the loop-2 region of sclerostin. In particular, we used the loop-2 region of sclerostin because LRP5/6 binds to amino acids in the loop2 region of sclerostin, known as the PNAIG motif, thus, inhibiting LRP5/6 activity. LRP5/6 activity is required for the activation of WNT signalling and subsequent bone formation. Additionally, a report has shown that a peptide derived from the loop2 region of sclerostin blocked the interaction of sclerostin with LRP5/6.[11] The binding site grid was generated by defining the 10 Å area around Pro92, Asn93, Ala94, Ile95, Gly96 active residues. The ligands were energy minimized initially using GAFF forcefield[12] incorporated in Antechamber tools. The optimized ligands were then docked onto the defined grid of protein. CHEMSCORE fitness function[13] was used for scoring and ranking the ligands. High fitness-scored ligands were selected from each class of molecules and the protein-ligand interaction profile was generated from the PLIP (Protein-Ligand Interaction Profiler) tool.[14]

2.2 Molecular Dynamics

Standard molecular dynamics simulations were carried out in Gromacs 2022.5 software.[15] CHARMM36 forcefield was used for protein and ligand parameterization.[16] The ligand forcefield parameters were obtained using the CGenff server and converted to Gromacs forcefield files using the Python script.[17] The protein-ligand complexes were placed in a unit cell of cubic shape with 1.0 nm length. The complex was solvated with the SPC/E water model neutralized with CL^- ions and then subjected to energy minimization.[18] The temperature and pressure equilibration of the system was carried out using a Berendsen thermostat and Parrinello-Rahman barostat with position restraints on protein and ligand.[19,20] The 500ns production run was carried out on these equilibrated systems releasing the position restraints using the same thermostat and barostat as in equilibration at 300 K and 1 atm pressure. During 500 ns

unbiased Molecular Dynamics (MD) simulations, the protein-ligand interactions were monitored using Root Mean Square Deviation (RMSD), hydrogen bond plots and Radius of gyration (Rg) of protein.

2.3 Funnel Meta-dynamics

The protein-ligand binding process involves several intermediate states before reaching the stable state. Though unbiased MD simulations reproduce the natural dynamics of a protein, all the conformations in the energy landscape cannot be explored due to time scale constraints. Funnel meta-dynamics overcomes this issue by adding history-dependent potential to the system, thereby exploring the conformational space in the energy landscape of a protein. Funnel meta-dynamics were carried out for a duration of 50 ns using plumed 2.9.0 metadynamics software patched with Gromacs [21,22] The binding pocket of protein is a flexible loop, so unbiased simulations suffer from a sampling of ligand binding in different loop conformations; to address this issue, protein-ligand binding and unbinding events were sampled using funnel meta-dynamics. It employs the funnel bias potential to sample the binding process and explore multiple binding pathways. The stability of protein-ligand complexes was assessed from the free-energy profiles of funnel metadynamics. The details of funnel restraint potential are provided in Fig. 3.5.

3. Results and discussion

3.1. Molecular Docking:

Due to the potential side effects and cost of the currently marketed sclerostin inhibitors, efforts were made to screen small molecules using virtual screening and in vitro studies, limited attention was given to phytopharmaceuticals. To bridge this gap, we performed docking of 362 molecules, and the top 33 molecules representing chemical diversity from each class were selected to investigate the ligand interactions with sclerostin, the ligand interactions and docking scores are in Table S 3.1. Most of the hits in the top 33 are forming hydrophobic interactions with LEU91, ILE95, TRP100, and

TRP101. In addition, ASN 93 and ILE95 are the other two residues most frequently involved in hydrogen bonding interactions with ligands. Furthermore, ARG102 forms a salt bridge with many ligands. The residue interactions list of the top 6 ligands and images of the top 6 hits are present in Table 3.1 and Fig. 3.1 respectively showing the binding orientations and key interactions contributing to high binding affinity. Generally, docking methods are validated by redocking the co-crystal ligand within the protein structure. However, there are no experimental co-crystal ligands with sclerostin which leads us to adopt an alternative way to validate our simulations using the invitro data of ligands.[23] These in vitro studies on the top-scored hits of virtual screening of drugs have shown valproic acid and fluticasone as good candidates for sclerostin inhibition. We performed docking on these two ligands and the scores were 30.12 and 41.80 respectively (details of interactions and images are provided in Table S 3.2 and Fig. S 3.1 respectively) which are comparatively less than our top-scored hits confirming the better performance of our new ligands, see Table 3.1.

Particularly, our docking analysis identified verbascoside and salvanoic acid forming strong interactions with a wide range of loop2 sclerostin residues. For this reason, the stability of these complexes was studied using MD simulations.

Table 3.1: List of the top 6 hit molecules and their residue interactions with sclerostin loop 2 active site region.

Compound name	Salt bridges	Hydrogen bond interactions Residues	Hydrophobic interactions Residues	PLP.Fitness score
Verbascoside	ARG102	LEU91, ASN93, ILE95, TRP101, ARG102	LEU91, ILE95, ARG97, LYS99	73.75
Salvianolic acid	ARG102	LEU91, ILE95, GLY96, ARG97, LYS99, TRP101, ARG102	LEU91, ASN93, ILE95, LYS99	63.77
Chicoric Acid	ARG89, ARG102	ARG89, ASN93, ALA94, ILE95	ARG89, LEU90, LEU91, ALA94, ILE95	60.3
Diosmin	ARG102	ARG89, ASN93, ILE95	LEU91, PRO92, ILE95, ARG97	58
Epimedin C	ARG89	ARG89, ASN93, ILE95, GLY96, SER104	TRP100, ARG102	55.24
Hesperidin	ARG89	ASN93, ILE95, GLY96	LEU91, ALA94	54.91

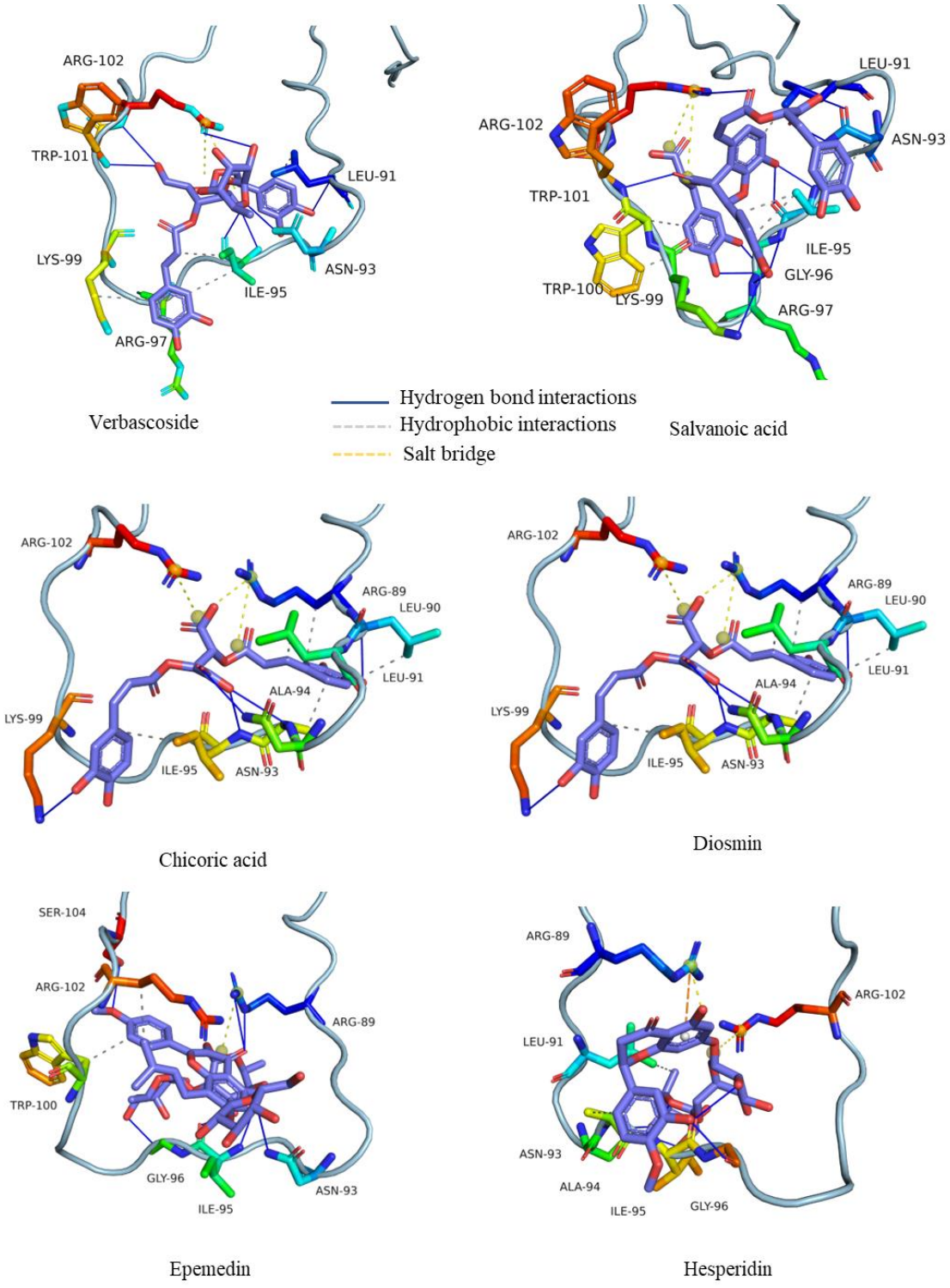


Figure 3.1: Hydrophobic, hydrogen bonding, and salt bridge interactions of top six docking poses. Hydrogen bonds are represented as blue lines, and

hydrophobic interactions, and salt bridges are represented as orange and yellow dashes respectively.

3.2. Molecular Dynamics

3.2.1. Unbiased MD simulations:

Root Mean Square Deviation (RMSD) measures the similarity between the starting structure and sampled structures during the simulation. The RMSD values calculated for the verbascoside and salvanoic acid (Fig. 3.2) during the 500ns simulation show verbascoside binding pose is stable till the duration of 250 ns and a significant jump observed after that indicates that the change in the binding pose of a ligand. This observation was justified by the snapshot captured after 200 ns in Fig. 3.4, the ligand dissociates from the protein and binds at C-terminal and loop3 regions of sclerostin which corresponds to snapshots 4 and 5 respectively. Hence, the RMSD of verbascoside was reduced thereafter.

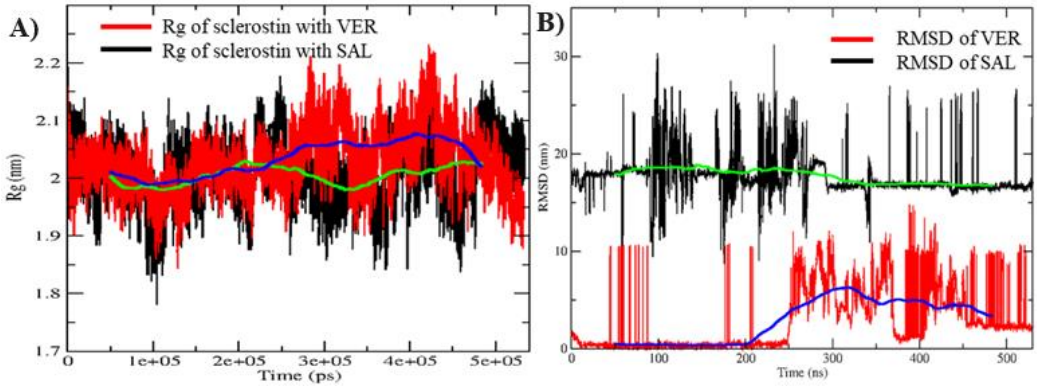


Figure 3.2: **A)** Radius of gyration of Salvanoic Acid (SAL) and Verbascoside (VER). The average radius of gyration is green and blue for the Salvanoic Acid and Verbascoside protein complex respectively. **(B)** Root Mean Square Deviation (RMSD) of two ligands. Blue and green lines represent running averages of Verbascoside and Salvanoic acid

On the other hand, salvanoic acid shows RMSD around 20 nm which is high when compared to verbascoside which shows that the binding pose of salvanoic acid is unstable. The RMSD of the ligand was slightly increased after

100 ns as the ligand disassociated from the protein (see Fig. 3.3) and tend to interact with loop after 200 ns and to the N-terminal of sclerostin after 300 ns and continued to bind till 500 ns, as a result, slight decrease in RMSD of salvanoic acid was observed after 200 ns. The Radius of Gyration (Rg) is another measure of compactness of protein structure. Rg values in Fig. 3.2A of the verbascoside system show a similar trend as observed in the RMSD plot. The average Rg of sclerostin was less till 100ns (see Fig. 3.2 A) and increased slightly thereafter due to the protein destabilization after the salvanoic acid dissociation from the sclerostin as shown in Fig. 3.3 and again after 200 ns the average Rg is reduced highlighting that the sclerostin trying to reach stable state when salvanoic acid is binding to loop2 and a slight increase in average Rg was observed after 300 ns after it started binding to N-terminal region of sclerostin as seen from the third snapshot of Fig. 3.3.

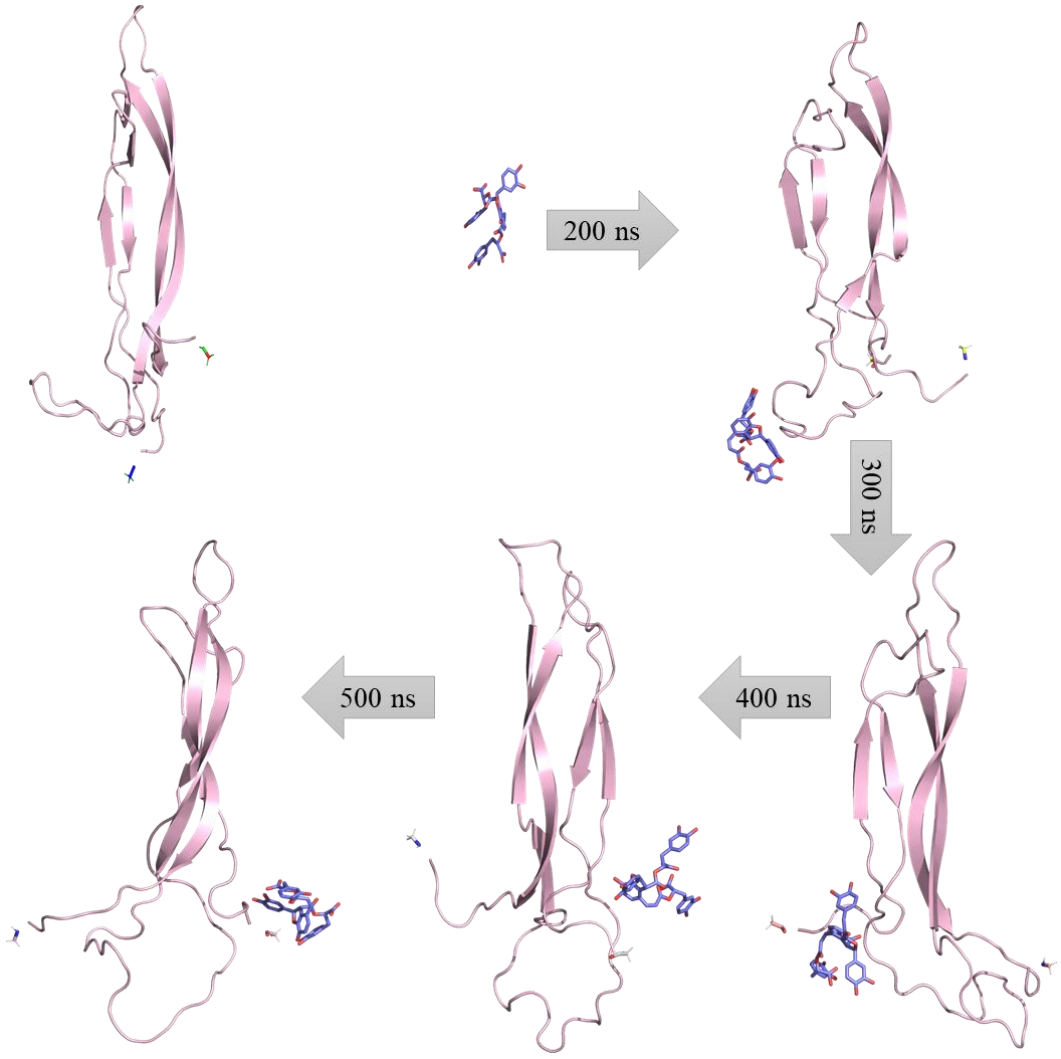


Figure 3.3: Snapshots of MD simulation. The snapshots are taken from 100 ns to 500 ns with an interval of 100 ns to show the binding poses of SAL. The protein is represented as a pink ribbon and the ligand is represented as purple in sticks

The average Rg of sclerostin was stable till 200 ns as the verbascoside binds to loop2 residues during this period. A significant increase in average Rg was observed after 200 ns that indicate sclerostin is unstable as verbascoside disassociates from sclerostin as shown in the third snapshot of Fig. 3.4. The average Rg decreased after the ligand binds to loop2 and loop3 of sclerostin protein which corresponds to the fourth and fifth snapshots of Fig. 3.4. The

analysis of average Rg provides relation between the binding site and protein stability.

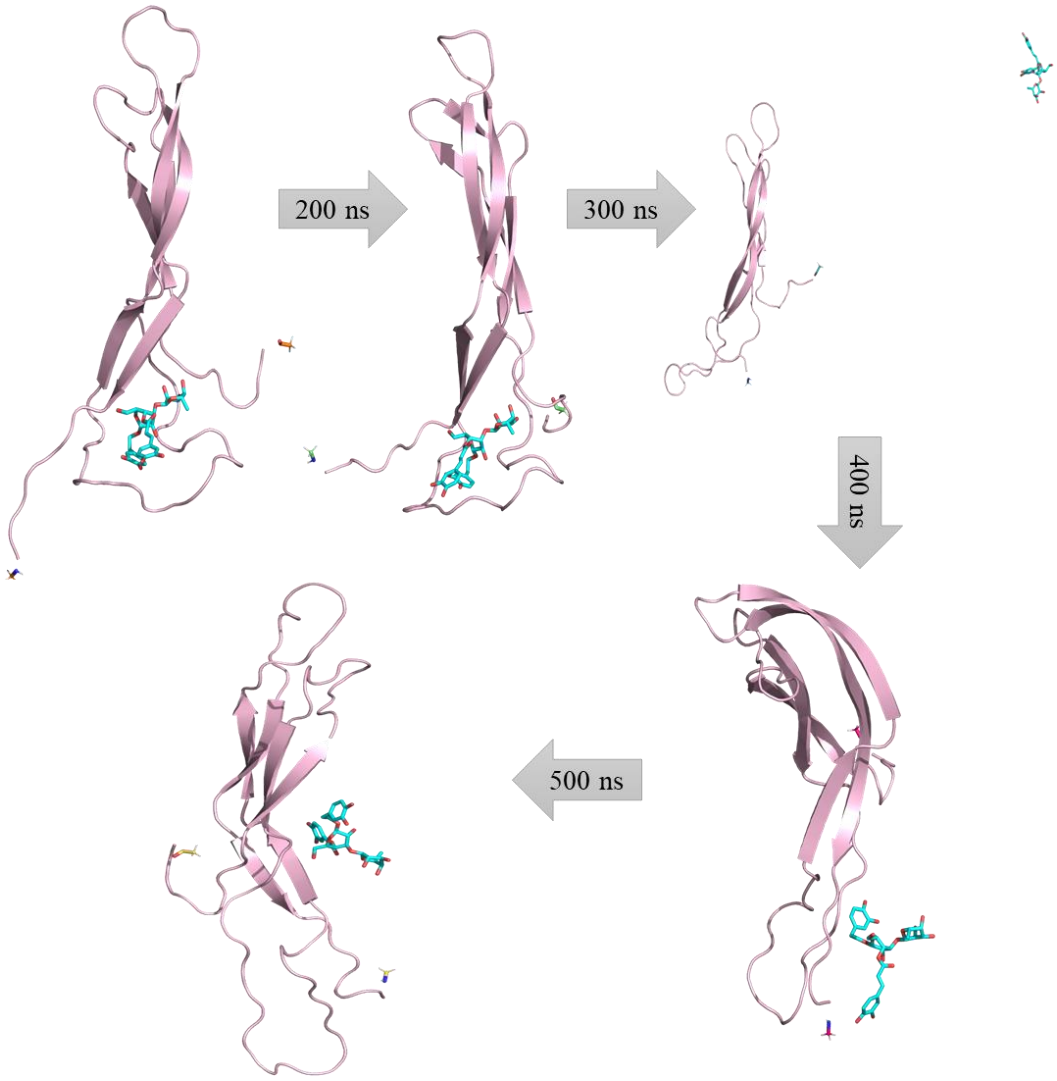


Figure 3.4: Snapshots of MD simulation. The snapshots are taken from 100 ns to 500 ns with an interval of 100 ns to show the binding poses of VER. The protein is represented as a pink ribbon and the ligand is represented as blue in sticks

The above two types of analysis provide information about the stability, dynamics, and compactness of protein when it binds with the ligands. Analysis of hydrogen bonding was also performed to provide insights into the

characteristics of interactions between protein and ligand. The fraction of the time a protein residue is forming hydrogen bonds with ligands during the total 500 ns simulation is defined as percentage occupancy and is shown in Fig. 3.3. Verbascoscide shows high hydrogen bonding occupancy with ALA88, ALA94, SER55, PRO87, ARG145 and GLU78 residues where in salvanoic acid the similar residues show less hydrogen bonding occupancy. The salvanoic acid shows higher hydrogen occupancy with ASP50 (N-terminal residue) as it resides mostly at the N-terminal after 300 ns (see Fig. 3.3). On the other hand, verbascoside shows more prominent and strong hydrogen bonds with ALA88, PRO87, ARG102 loop2 residues of sclerostin. This suggests that verbascoside forms a more stable complex with the sclerostin loop2 region compared to salvanoic acid. Aside from binding to the loops in the protein these two ligands also show affinity to N (SER55) and C (ARG 145 and ARG 148) terminal residues highlighting the two ligands' dynamic nature to bind to multiple sites of protein.

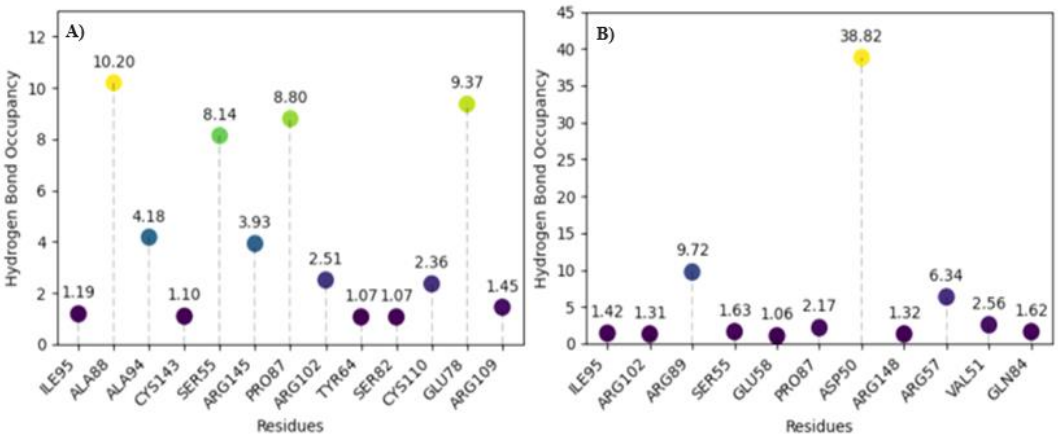


Figure 3.5: Hydrogen bond occupancy percentage calculated during 500 ns molecular dynamics simulation of **A)** Verbascoside and **B)** Salvanoic acid protein complexes

3.2.2 Funnel Meta-dynamics

We employed the distance between ligand and active site residue (d1) as a collective variable shown in Fig. 3.5. During the simulation, the bias potential

is added at different distances facilitating the transitions and exploring diverse binding routes of ligand. During the 50 ns funnel meta-dynamics the two ligands explored different binding modes. The free energy surface of both ligands was constructed with respect to the distance (d1) as shown in Fig. 3.8 and 3.9.

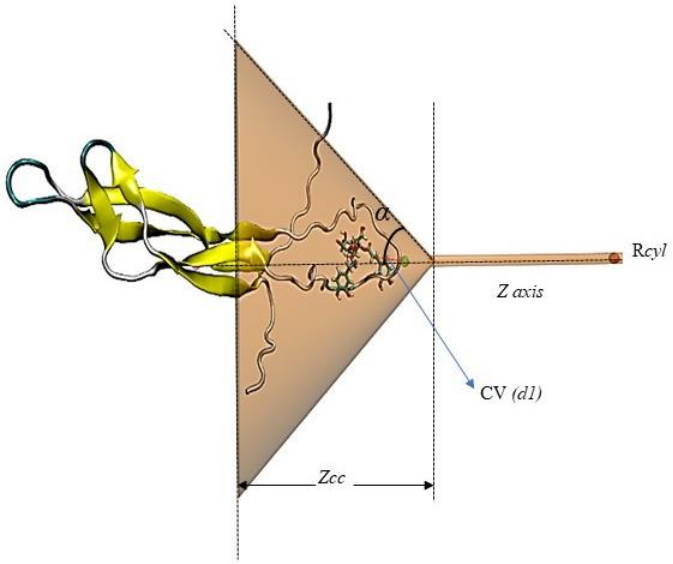


Figure 3.6: Representation of funnel restraint potential used in funnel meta-dynamics of sclerostin protein and ligands (Verbascoside and Salvanoic Acid). The collective variable (CV) d1 is the distance between the C15 of the ligand to the HN atom of ILE95(green dot). The Z-axis originates from the LYS142 residue and is limited to 100 Å from the origin (red sphere). The cone-shaped funnel was defined by α-angle (0.6 rad) and Zcc (65 Å)is the distance from the origin to the vertex where the cone changes to the cylinder. Rcyl (1 Å) is the radius of the cylinder

There were three low-energy minima in verbascoside and one low-energy minima in salvanoic Acid. Cluster analysis was carried out to cluster similar binding modes, and the average representation of the structure representing the minima in the free energy surface plot was considered for studying the ligand and protein residue interactions for each binding pose. The free energy surface along with the three binding modes of verbascoside are shown in Fig. 3.8. SER82, TRP100, CYS110, TYR115, VAL135, LEU146, and

CYS141 in loop 2 and loop 3 are some of the binding site residues found in the binding pose analysis that closely match the heparin-binding site residues of sclerostin found in experimental NMR studies[24]. Another experimental study revealed a new binding site between the C-terminus of mutant sclerostin and the LRP6 E2 domain.[25] Our funnel metadynamics results of verbascoside in binding mode 2 also showed interactions with C-terminus residues Leu 146, THR 147, ASP 107, ARG 148, and PHE149 corroborating the validity of our predictions. In another study, the cysteine knot residues of sclerostin were found to play a crucial role in flexible loop folding which influences the binding of residues in this loop with LRP6 protein .[26] The binding mode 1 of verbascoside shows interactions with cysteine-knot residues CYS 141, CYS81, and CYS110 further proving that sclerostin can be also inhibited by interacting with these residues.

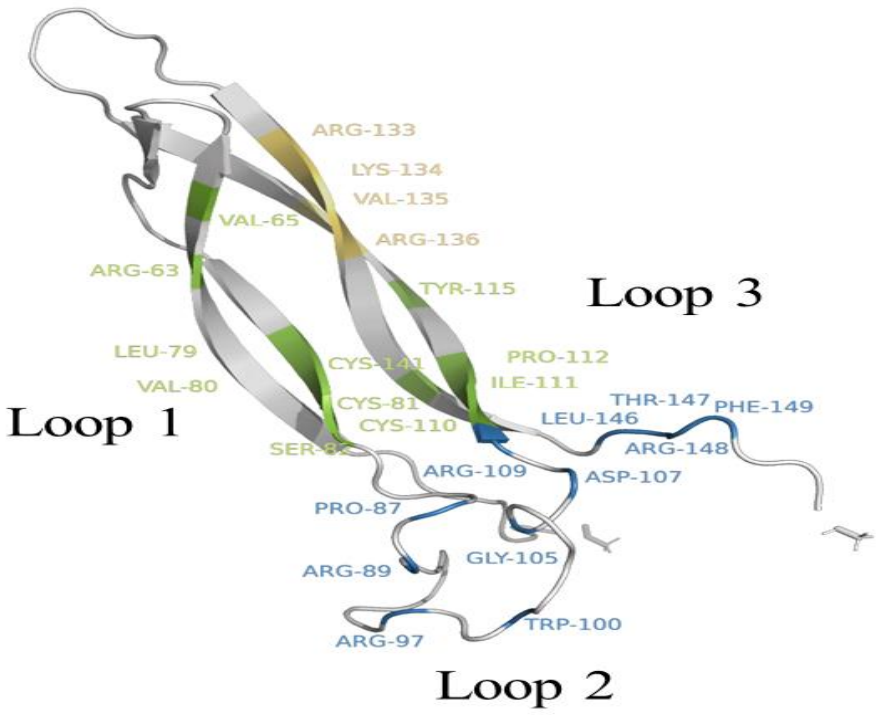


Figure 3.7: Active site residues of three binding poses. Residues and labels are color-coded with respect to the free energy surface plot of the sclerostin and verbascoside complex

The multiple ways of sclerostin inhibition are possible by ligand which shows affinity to all these three binding sites. Most of the binding site residues located in these three binding modes are present in loop 2, loop 3, and the C-terminus of protein (**residues are highlighted in Fig. 3.7**), and verbascoside shows affinity to these three binding sites. Contrastingly, salvanoic acid has only one binding mode which corresponds to the energy minima as shown in **Fig. 3.9A,** and the ligand confines mostly in the loop 2 region. Further, the results of unbiased MD simulations also support these observations, the radius of gyration and RMSD of salvanoic acid was high compared to verbascoside because the flexibility of the loop poses a challenge to bind for a prolonged duration. However, the ability of verbascoside to bind at multiple sites of protein increases the ligand-protein inhibition activity and our findings shed light on the stability and binding mechanisms of ligands to sclerostin protein. This study also highlights the enhanced sampling capabilities of funnel metadynamics where multiple binding sites of sclerostin are sampled in short duration compared to unbiased simulations which required 500 ns to uncover similar binding sites.

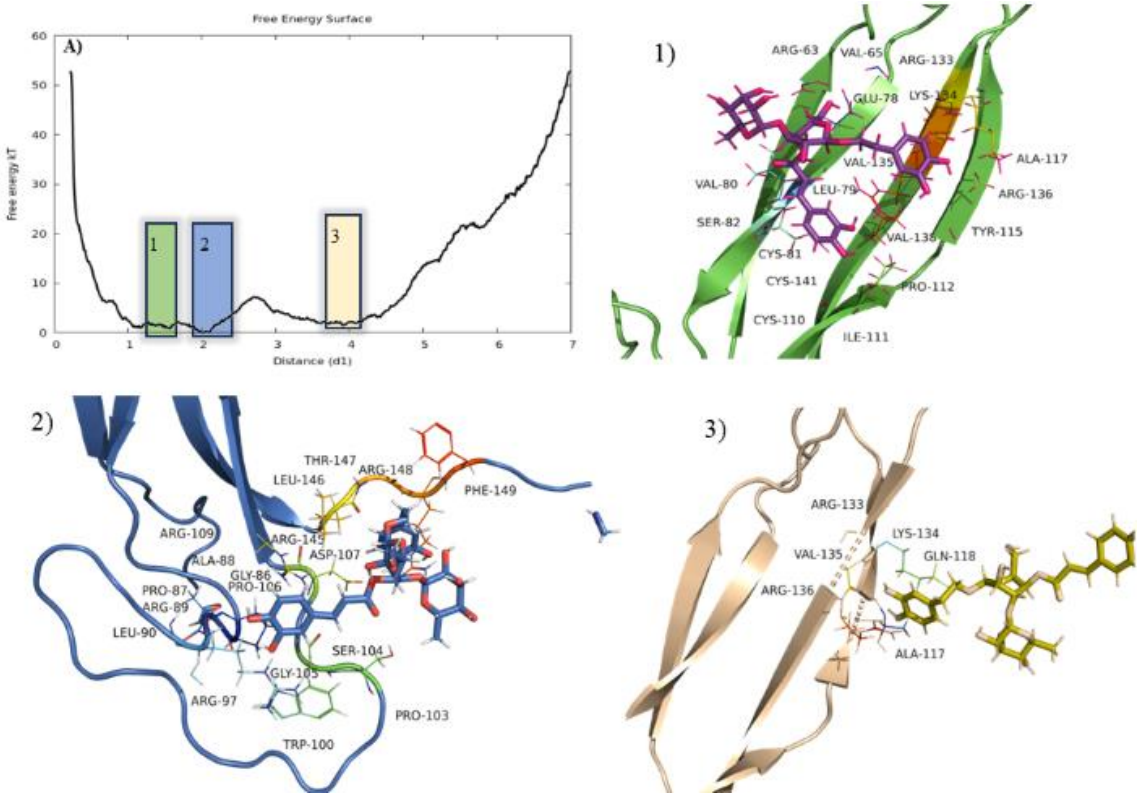


Figure 3.8: **A)** Free energy surface plot and snapshots of different binding poses identified in funnel meta-dynamics of sclerostin protein and Verbascoside complex

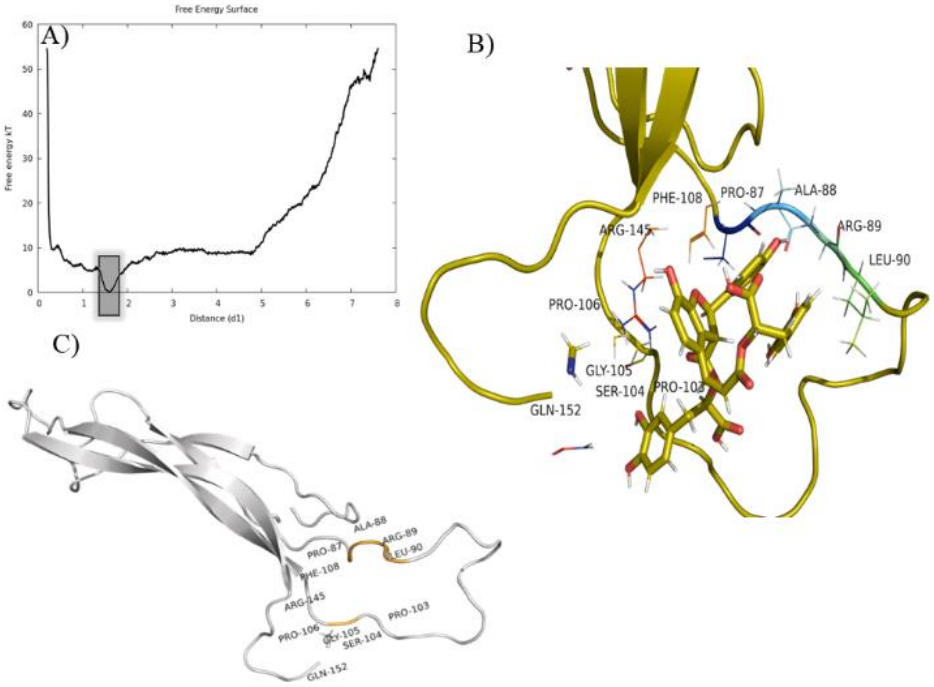


Figure 3.9: A) Free energy surface plot and B) residues within 5Å of ligand and C) snapshot of binding pose identified in funnel meta-dynamics of sclerostin protein and Salvanoic Acid

4. Conclusion

In summary, the virtual screening of 362 phytopharmaceutical molecules was conducted against sclerostin protein using a GOLD docking module. Unbiased molecular dynamics simulations highlighted the stability of the top-ranked verbascoside-sclerostin complex obtained from docking. Furthermore, with the aid of funnel meta-dynamics simulations different binding sites of sclerostin protein were explored and the free energy plots from metadynamics provided the energy landscape of the ligand binding process. The three binding

modes identified showcase the versatility of verbascoside when interacting with the sclerostin protein.

5. Bibliography

(1) *Epidemiology of Osteoporosis and Fragility Fractures*. https://www.osteoporosis.foundation/facts-statistics/epidemiology-of-osteoporosis-and-fragility-fractures.

(2) Babhulkar, S.; Seth, S. Prevalence of Osteoporosis in India: An Observation of 31238 Adults. *Int J Res Orthop* **2021**, *7* (2), 362. https://doi.org/10.18203/issn.2455-4510.IntJResOrthop20210630.

(3) Shoback, D.; Rosen, C. J.; Black, D. M.; Cheung, A. M.; Murad, M. H.; Eastell, R. Pharmacological Management of Osteoporosis in Postmenopausal Women: An Endocrine Society Guideline Update. *J Clin Endocrinol Metab* **2020**, *105* (3), 587–594. https://doi.org/10.1210/clinem/dgaa048.

(4) Lewiecki, E. M. Role of Sclerostin in Bone and Cartilage and Its Potential as a Therapeutic Target in Bone Diseases. *Ther Adv Musculoskelet Dis* **2014**, *6* (2), 48–57. https://doi.org/10.1177/1759720X13510479.

(5) Yu, S.; Li, D.; Zhang, N.; Ni, S.; Sun, M.; Wang, L.; Xiao, H.; Liu, D.; Liu, J.; Yu, Y.; Zhang, Z.; Yeung, S. T. Y.; Zhang, S.; Lu, A.; Zhang, Z.; Zhang, B.; Zhang, G. Drug Discovery of Sclerostin Inhibitors. *Acta Pharm Sin B* **2022**, *12* (5), 2150–2170. https://doi.org/10.1016/j.apsb.2022.01.012.

(6) Holdsworth, G.; Roberts, S. J.; Ke, H. Z. Novel Actions of Sclerostin on Bone. *J Mol Endocrinol* **2019**, *62* (2), R167–R185. https://doi.org/10.1530/JME-18-0176.

(7) Fabre, S.; Funck-Brentano, T.; Cohen-Solal, M. Anti-Sclerostin Antibodies in Osteoporosis and Other Bone Diseases. *J Clin Med* **2020**, *9* (11), 3439. https://doi.org/10.3390/jcm9113439.

(8) US Food and Drug Administration (FDA). EVENITY™ (Romosozumab-Aqqg) Injection, for Subcutaneous Use [Bula]. **2019**, 20.

(9) Kobayakawa, T.; Suzuki, T.; Nakano, M.; Saito, M.; Miyazaki, A.; Takahashi, J.; Nakamura, Y. Real-World Effects and Adverse Events of Romosozumab in Japanese Osteoporotic Patients: A Prospective Cohort Study. *Bone Rep* **2021**, *14*, 101068. https://doi.org/10.1016/J.BONR.2021.101068.

(10) Jones, G.; Willett, P.; Glen, R. C.; Leach, A. R.; Taylor, R. Development and Validation of a Genetic Algorithm for Flexible Docking 1 1Edited by F. E. Cohen. *J Mol Biol* **1997**, *267* (3), 727–748. https://doi.org/10.1006/jmbi.1996.0897.

(11) Muthusamy, K.; Mohan, S.; Nagamani, S.; Kesavan, C. Identification of Novel Small Molecules That Bind to the Loop2 Region of Sclerostin – an in Silico Computational Analysis. *Physiol Res* **2016**, *65* (5), 871–878. https://doi.org/10.33549/physiolres.933267.

(12) Wang, J.; Wolf, R. M.; Caldwell, J. W.; Kollman, P. A.; Case, D. A. Development and Testing of a General Amber Force Field. *J Comput Chem* **2004**, *25* (9), 1157–1174. https://doi.org/10.1002/jcc.20035.

(13) Verdonk, M. L.; Cole, J. C.; Hartshorn, M. J.; Murray, C. W.; Taylor, R. D. Improved Protein-Ligand Docking Using GOLD. *Proteins: Structure, Function, and Bioinformatics* **2003**, *52* (4), 609–623. https://doi.org/10.1002/prot.10465.

(14) Adasme, M. F.; Linnemann, K. L.; Bolz, S. N.; Kaiser, F.; Salentin, S.; Haupt, V. J.; Schroeder, M. PLIP 2021: Expanding the Scope of the Protein–Ligand Interaction Profiler to DNA and RNA. *Nucleic Acids Res* **2021**, *49* (W1), W530–W534. https://doi.org/10.1093/nar/gkab294.

(15) Lindahl; Abraham; Hess; Spoel, van der. GROMACS Documentation. *GROMACS 2021.3 Manual* **2021**, 1–623. https://doi.org/10.5281/zenodo.7586765.

(16) Huang, J.; MacKerell, A. D. CHARMM36 All-Atom Additive Protein Force Field: Validation Based on Comparison to NMR Data. *J Comput Chem* **2013**, *34* (25), 2135–2145. https://doi.org/10.1002/jcc.23354.

(17) Vanommeslaeghe, K.; MacKerell, A. D. Automation of the CHARMM General Force Field (CGenFF) I: Bond Perception and Atom Typing. *J Chem Inf Model* **2012**, *52* (12), 3144–3154. https://doi.org/10.1021/ci300363c.

(18) Gereben, O.; Pusztai, L. On the Accurate Calculation of the Dielectric Constant from Molecular Dynamics Simulations: The Case of SPC/E and SWM4-DP Water. *Chem Phys Lett* **2011**, *507* (1–3), 80–83. https://doi.org/10.1016/j.cplett.2011.02.064.

(19) Parrinello, M.; Rahman, A. Polymorphic Transitions in Single Crystals: A New Molecular Dynamics Method. *J Appl Phys* **1981**, *52* (12), 7182–7190. https://doi.org/10.1063/1.328693.

(20) Berendsen, H. J. C.; Postma, J. P. M.; van Gunsteren, W. F.; DiNola, A.; Haak, J. R. Molecular Dynamics with Coupling to an External Bath. *J Chem Phys* **1984**, *81* (8), 3684–3690. https://doi.org/10.1063/1.448118.

(21) Tribello, G. A.; Bonomi, M.; Branduardi, D.; Camilloni, C.; Bussi, G. PLUMED 2: New Feathers for an Old Bird. *Comput Phys Commun* **2014**, *185* (2), 604–613. https://doi.org/10.1016/j.cpc.2013.09.018.

(22) Limongelli, V.; Bonomi, M.; Parrinello, M. Funnel Metadynamics as Accurate Binding Free-Energy Method. *Proceedings of the National Academy of Sciences* **2013**, *110* (16), 6358–6363. https://doi.org/10.1073/pnas.1303186110.

(23) Sangadala, S.; Kim, C. H.; Fernandes, L. M.; Makkar, P.; Beck, G. R.; Boden, S. D.; Drissi, H.; Presciutti, S. M. Sclerostin Small-Molecule Inhibitors Promote Osteogenesis by Activating Canonical Wnt and BMP Pathways. *Elife* **2023**, *12*, 63402. https://doi.org/10.7554/ELIFE.63402.

(24) Veverka, V.; Henry, A. J.; Slocombe, P. M.; Ventom, A.; Mulloy, B.; Muskett, F. W.; Muzylak, M.; Greenslade, K.; Moore, A.; Zhang, L.; Gong, J.; Qian, X.; Paszty, C.; Taylor, R. J.; Robinson, M. K.; Carr, M. D. Characterization of the Structural Features and Interactions of Sclerostin. *Journal of Biological Chemistry* **2009**, *284* (16), 10890–10900. https://doi.org/10.1074/jbc.M807994200.

(25) Kim, J.; Han, W.; Park, T.; Kim, E. J.; Bang, I.; Lee, H. S.; Jeong, Y.; Roh, K.; Kim, J.; Kim, J. S.; Kang, C.; Seok, C.; Han, J. K.; Choi, H. J. Sclerostin Inhibits Wnt Signaling through Tandem Interaction with Two LRP6 Ectodomains. *Nat Commun* **2020**, *11* (1). https://doi.org/10.1038/S41467-020-19155-4.

(26) Boschert, V.; Van Dinther, M.; Weidauer, S.; Van Pee, K.; Muth, E. M.; Ten Dijke, P.; Mueller, T. D. Mutational Analysis of Sclerostin Shows Importance of the Flexible Loop and the Cystine-Knot for Wnt-Signaling Inhibition. *PLoS One* **2013**, *8* (11), 81710. https://doi.org/10.1371/JOURNAL.PONE.0081710.

Chapter 4: Computational Investigation of NUIG-4 as Multi-drug Delivery Agents for Ovarian Anticancer Agents

Data generated from this study will be submitted to the *Journal of Chemical theory and Computation.*

Abstract:

Metal-organic frameworks (MOFs) are hybrid materials renowned for their tunable properties, making them promising candidates for drug delivery applications. The porous nature of MOFs enables them to function as nanocarriers with high drug-loading capacity, addressing the poor solubility of anticancer drugs and facilitating targeted drug delivery. In the current study, we utilized Grand Canonical Monte Carlo (GCMC) simulations to model the drug adsorption in NUIG-4 employing Bader atomic charges and validated Lennard Jones potential parameters were used to explore the adsorption behaviour of paclitaxel (PAL), doxorubicin (DOX), gemcitabine (GEM) and carboplatin (CAR) onto NUIG-4. We found that DOX and PAL drugs were loaded into NUIG-4 while GEM and CAR remain unabsorbed as single components although both drugs are co-adsorbed if loaded with GEM and PAL. Drug diffusion from pores of NUIG-4 was investigated with Molecular Dynamics (MD) simulations. Difuusion coeffecients were calculated from mean square displacement using Einstein mathematical expression. Adsorption simulation with a multidrug combination was done to explore the potential of NUIG-4 as a multi-drug delivery agent. Our discoveries reveal that NUIG-4 displays a high drug loading capacity and slow diffusion rates, indicating its potential as an effective drug carrier.

Reproduced with permission from:

Vinay K R Cheemarla, Davide Tiana

1. Introduction

In ovarian cancer, ovary cells grow abnormally in an uncontrolled way and it's the seventh most common occurring cancer in women. Annually 0.3 million women are diagnosed with ovarian cancer and among them, 0.2 million die.[1] Globocons projections forecasted that the number of women with ovarian cancer will rise to 37 % by 2040. Though the prevalence of ovarian cancer is less, the mortality rate is high as its diagnosis is delayed.[2] Ongoing advanced research in cancer therapy led to design the of efficient chemotherapy agents and diagnostic methods to treat ovarian cancer. The standard treatment regimen of ovarian cancer includes debulking surgery and chemotherapy treatment with a combination of platinum-based DNA alkylating agents (carboplatin) and plant alkaloids (Taxanes).[3] Carboplatin induces cell death by inhibiting the synthesis of DNA through an intercalation mechanism. Taxanes like paclitaxel bind to microtubules and stabilize them which leads to mitotic arrest and cell death. Targeting the cancer cells through multiple pathways enhances the treatment effectiveness hence, the idea of combining these drugs to create a synergistic effect led to the development of drug combination therapies such as Paclitaxel/Carboplatin,[4] Doxorubicin/Carboplatin,[5] which proved to have synergetic effect in the treatment of cancer and also the other combinations like Gemcitabine/Carboplatin[6], Paclitaxel/Gemcitabine[7] are used for treating chemotherapy resistant cancer.

Many anticancer drugs due to their chemical nature show poor solubility in water and tend to get slowly absorbed into the blood circulation. This results in low bioavailability which limits their efficacy. To mitigate this problem, drug delivery agents have been uncovered to increase the solubility and control the release of drugs, e.g. dendrimers, biopolymers, endosomes, liposomes, carbon nanotubes, and many more yet to come.[8] Though they serve as excellent drug delivery agents they possess some disadvantages like poor solubility, toxicity, not being biodegradable, agglomeration, less stable, and poor drug release profiles. These limitations present a big challenge and efforts have been made to engineer better drug delivery systems. In recent years the research on using

Metal Organic Frameworks (MOF) as drug carriers has increased because of their porous nature and biocompatibility.[9,10] They offer high surface area and high loading capacities this is why they are used for storage and separation of gas, catalysis, and encapsulating macromolecules like enzymes[10,11], vitamins[12], drugs[13] etc., MOFs also exhibit varied responses to external stimuli such as alterations in pH, temperature, and magnetic fields, this versatile functionality of MOFs sparked interest in several research groups. Horcajada et al. were the first to explore MOFs for drug delivery applications,[14] further studies were conducted to investigate MOFs for targeted pH-responsive drug release and alongside applications in imaging techniques. Subsequently, computational studies on MOFs were performed to complement experimental studies and to establish the correlation between the molecular properties of MOFs and drug adsorption and release.

The recent experimental study on NUIG-4 MOF revealed it has a high DOX loading capacity.[15] This work uses Gran Canonical Monte Carlo (GCMC) and Molecular Dynamic (MD) simulations to explore the adsorption and diffusion behaviour of NUIG-4 with single-component anticancer drugs DOX PAL, CAR, and GEM and the drug combinations that proved to show synergistic effects in cancer treatment.[4–6]

2. Methodology

Adsorption of drugs onto NUIG-4 was explored using grand canonical Monte Carlo (GCMC) simulations using RASPA[16] at 298 K temperature and 1atm pressure with 12-6 Lennard Jones (LJ) shift potentials with 14 A distance cutoff. Atomic charges were calculated using the Quantum Theory of Atoms in Molecules (QTAIM)[17] from periodic density functional theory (DFT) following this procedure; the NUIG-4 crystal structure was downloaded from the Cambridge crystallographic data center (CCDC) database.[15] The optimization of crystal structure was performed by only relaxing the atomic positions of MOF through hybrid use of PAW[18] and norm-conservating[19] pseudopotentials using 95 Ry electron density cut-off in Quantum Espresso.[20] The code CRITIC2[21] was

used to calculate the BADER charges.[22] All the drugs studied here for adsorption were downloaded from the drug bank and optimised followed by charge derivation using the similar protocol followed in NUIG-4. LJ parameters of both NUIG-4 and drugs were derived from Universal Force Field (UFF) and Drieding forcefield.[23] Ewald precision was set to 10^{-6} and 1x1x1 unit cell was used. The simulation was conducted with 10^4 initiation steps and 15 x 10^4 steps of production with a time step of 0.0005. The final snapshots extracted from GCMC simulations were subjected to single-point calculations to calculate the binding energy of MOF and drugs and to assess the intermolecular interaction energies between co-adsorbed drugs.

Diffusion of drugs from pores was investigated employing Molecular Dynamics (MD) simulations using Gromacs.[24] The input geometry for MD simulations was taken from GCMC snapshots. Bonded parameters of NUIG-4 and drugs were calculated from the OBGMX tool.[25] The atomic charges and LJ parameters used in MD are those used in GCMC simulations. The MOF drug complex is subjected to energy minimization and then temperature is equilibrated to 310 K using NVT ensemble with Berendsen thermostat[26] over 200 Pico seconds of simulation. The equilibrated system was then subjected to an 80 ns production run. The drug diffusion was computed from the mean square displacement (MSD) of drug molecules.

4. Results and Discussions

4.1. Monte Carlo simulations of MOFs

DOX is one of the most common chemotherapy drugs used in anticancer treatment and it suffers from low solubility and high toxicity hence DOX is most widely used in studying MOFs as drug delivery agents.[27–29] NUIG-4 is a biocompatible cubic MOF with well-defined pores. The experimental studies of adsorption and controlled release of DOX using NUIG-4 have shown excellent results, assuring NUIG-4 is an effective drug delivery agent. We used NUIG-4 experimental data to validate the goodness of our parameters. Initially, through

our computational methodology, we explored UFF LJ parameters to simulate the DOX adsorption, and the average amount of drug adsorbed was found to be 920.96 mg/gm of NUIG-4 which is less than experimentally reported adsorption (1955 mg/gm). Subsequently, utilizing Drieding LJ parameters the average adsorption was found to be 2014 mg/gm and the predicted packing of DOX was similar to the experimental packing arrangement in NUIG-4 as shown in Fig. 4.1A. While the predicted loading capacity exceeds the experimental loading, such variations in results are expected due to crystal defects and are not uncommon in adsorption modelling.[30–32] After the validation of LJ parameters, we studied the single-component adsorption of paclitaxel (PAL), gemcitabine (GEM), and carboplatin (CAR), see Table 4.1. It was found that PAL could be loaded into NUIG-4 (1394 mg/mg) while GEM and CAR were not adsorbed. While DOX average adsorption is higher, binding energy calculations revealed PAL has higher binding energy (18.29 kcal/mol) compared to DOX (14.33 kcal/mol) with NUIG-4. it is possibly because PAL shows interactions with open metal sites in the NUIG-4 in addition to the organic linker as shown in Fig.4.1D, while doxorubicin was showing interactions only with the organic linker (see Fig. 4.1A). Additionally, the pore size of NUIG-4 also plays a crucial role, PAL being bulkier and bigger than DOX saturation of metal sites with PAL results in low average adsorption.

Table 4.1: Average adsorption predicted from GCMC simulations of single and co-adsorbed drugs in mg/gm of NUIG-4 MOF

Single component drugs	Average loading	Drug Combinations (Drug 1+Drug 2)	Average loading	
			Drug 1	Drug 2
DOX	2014.68	PAL+GEM	1582.55	758.26
PAL	1394.25	DOX+CAR	1427.61	1684.55
CAR	0	PAL+CAR	1582.55	1376.14
GEM	0	GEM+CAR	0	0

Co-adsorption of paclitaxel with gemcitabine (PAL-GEM) and carboplatin (PAL-CAR), doxorubicin with carboplatin (DOX-CAR), and gemcitabine with carboplatin (GEM-CAR) were also studied as these drug combinations were found to show synergistic effects in treating ovarian cancer as discussed earlier in the introduction.[4–7] As mentioned before, CAR and GEM were not adsorbed as single components but when combined with DOX and PAL they were adsorbed into NUIG-4 revealing a cooperative effect between the drugs as shown in Fig. 4.1

Our binding energy analysis revealed that the intermolecular interaction energy between the drug components increases the affinity to NUIG-4 and promotes the co-adsorption of components, see Table 4.2.

Table 4.2: Intermolecular interaction energies in kcal/mol calculated from pseudo plane wave DFT method in Quantum espresso

Drug combinations	Intermolecular energy
PAL+GEM	11.98
DOX+CAR	46.27
PAL+CAR	33.22

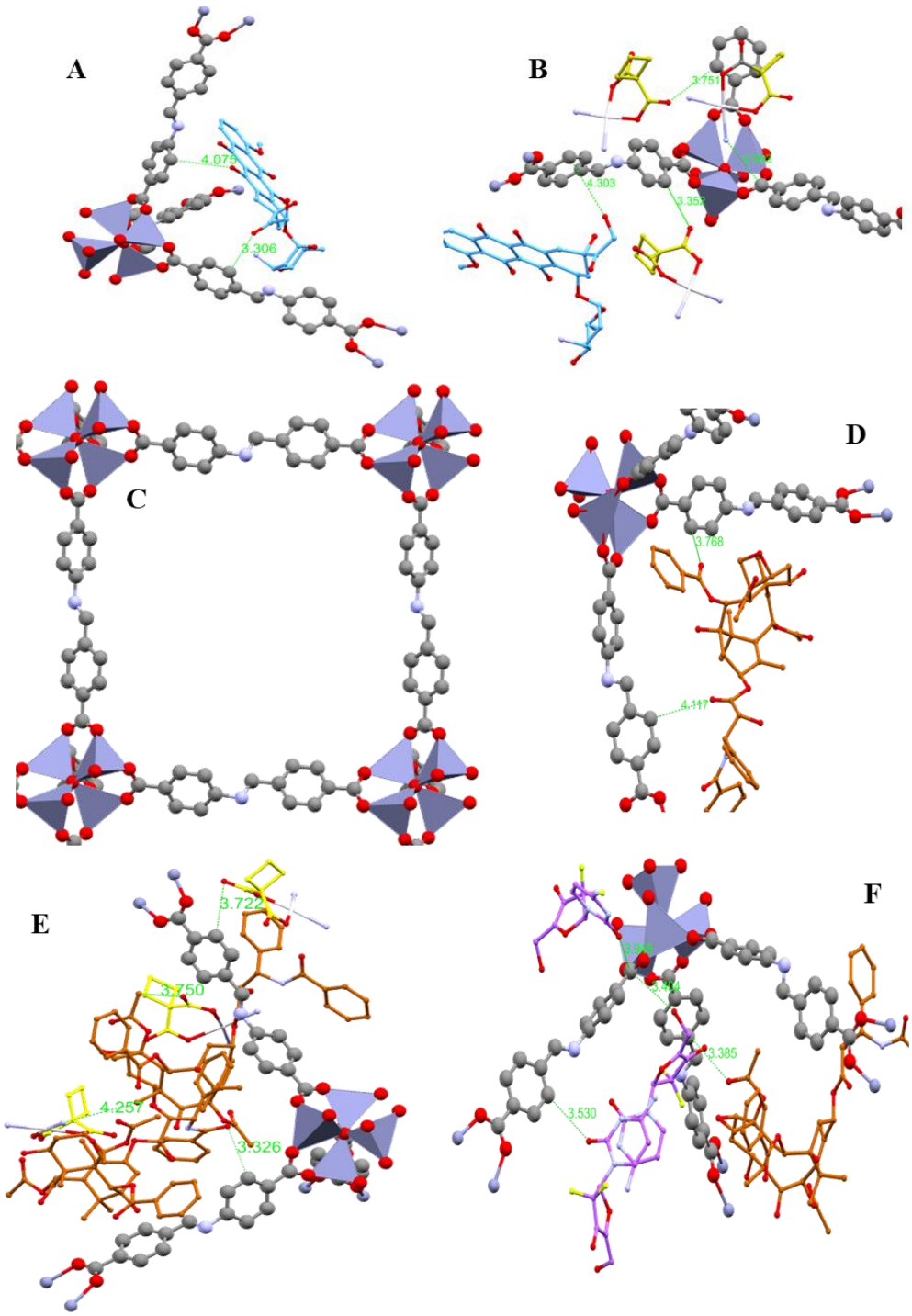


Figure 4.1: Images showing the site of adsorption in NUIG-4. A) DOX; B) DOX-CAR; C) NUIG-4 framework; D) PAL; E) PAL+CAR; F)PAL+GEM. The NUIG-4 atoms are in grey its metal cluster is represented as a blue-coloured polyhedron. DOX, PAL, CAR, and GEM are in the ball and stick representation

coloured in sky blue, brown, yellow, and violet respectively. Hydrogens are not shown for clarity.

3.2. Molecular dynamics simulation of MOFs

Drug diffusion is the other important process to be studied to understand the goodness of MOFs for drug delivery. The diffusion coefficient was calculated from a 200 ns trajectory at every 20 ns interval along with the error estimate using the MDAnalysis python package.[33,34] The diffusion coefficients with the small error are tabulated and presented in table 4.3, these coefficient values depict the diffusion behaviour of individual drugs and their combination. The individual drug diffusion rate of PAL is higher compared to DOX. DOX exhibits a slow diffusion rate in both cases, single component loading and co-loading with CAR highlighting DOX shows strong interactions in both cases and PAL diffusion rate is higher when co-loaded with CAR but the diffusion rate is reduced when co-loaded with GEM.

Table 4. 3: Drug diffusion coefficient in $Å^2/ps$ calculated during 200 ns molecular dynamics trajectory.

Drugs	Diffusion coeffecient
PAL	0.0044
PAL with CAR	0.1141
PAL with GEM	0.0023
DOX	0.0012
DOX with CAR	0.0097
CAR with DOX	0.0357
CAR with PAL	0.1833
GEM with PAL	0.0112

Among PAL-CAR and DOX-CAR drug combinations, CAR was diffusing faster in PAL-CAR compared to the DOX-CAR combination. Our binding energy analysis present in Table 4.2 also shows that DOX-CAR intermolecular energy is higher, hence the CAR diffusion is slow when loaded with DOX compared to PAL. Overall, the results of MD simulations suggest that intermolecular interactions with the co-loaded drugs might influence the drug release rate from the pores of NUIG-4. All these observations led to a molecular level of understanding of the adsorption and diffusion behaviors of individuals and combinations of drugs in NUIG-4. However, it is important to note that drug release under specific pH conditions is not simulated in this study to address the pH sensitivity of NUIG-4 and to mimic a drug release at acidic pH from pores of MOFs. These simulations would provide a potential opportunity to screen the pH-sensitive MOFs. But, currently, these calculations are computationally highly intensive as the multiple protonation states of NUIG-4 and drugs should be considered to simulate the drug release at constant pH.

4. Conclusion

This study was conducted to explore the drug delivery potential of MOFs, specifically NUIG-4. Through GCMC simulations, we observed that NUIG-4 shows selective loading of DOX and PAL while GEM and CAR remain unabsorbed as single components but co-adsorbed with DOX and PAL. Exploring further, binding energy analysis uncovered the role of intermolecular interactions in co-adsorption. Subsequently, MD simulations were carried out to investigate the drug diffusion. The analysis of MSD plots and hydrogen bond interactions reveals the diffusion dynamics highlighting controlled diffusion rates, particularly in the case of drug combinations. The findings in this study show that NUIG-4 could serve as an efficient carrier for delivering multiple drugs simultaneously. This is especially useful in ovarian cancer treatment as NUIG-4`s multidrug delivery capability can be used to target different cell types or metabolic pathways.

5. Bibliography

(1) Momenimovahed, Z.; Tiznobaik, A.; Taheri, S.; Salehiniya, H. Ovarian Cancer in the World: Epidemiology and Risk Factors. *International Journal of Women's Health*. 2019. https://doi.org/10.2147/IJWH.S197604.

(2) Momenimovahed, Z.; Tiznobaik, A.; Taheri, S.; Salehiniya, H. Ovarian Cancer in the World: Epidemiology and Risk Factors. *International Journal of Women's Health*. 2019. https://doi.org/10.2147/IJWH.S197604.

(3) Lheureux, S.; Braunstein, M.; Oza, A. M. Epithelial Ovarian Cancer: Evolution of Management in the Era of Precision Medicine. *CA Cancer J Clin* **2019**. https://doi.org/10.3322/caac.21559.

(4) Zhang H.; Zhang Y. Olaparib and Paclitaxel in Combination with Carboplatin in Treatment of Ovarian Cancer. *Am J Transl Res* **2022**, *14* (1), 468–475.

(5) Nguyen, J.; Solimando, D. A.; Waddell, J. A. Carboplatin and Liposomal Doxorubicin for Ovarian Cancer. *Hosp Pharm* **2016**, *51* (6), 442–449. https://doi.org/10.1310/hpj5106-442.

(6) Pfisterer, J.; Plante, M.; Vergote, I.; Du Bois, A.; Hirte, H.; Lacave, A. J.; Wagner, U.; Stähle, A.; Stuart, G.; Kimmig, R.; Olbricht, S.; Le, T.; Emerich, J.; Kuhn, W.; Bentley, J.; Jackisch, C.; Lück, H. J.; Rochon, J.; Zimmermann, A. H.; Eisenhauer, E. Gemcitabine plus Carboplatin Compared with Carboplatin in Patients with Platinum-Sensitive Recurrent Ovarian Cancer: An Intergroup Trial of the AGO-OVAR, the NCIC CTG, and the EORTC GCG. *Journal of Clinical Oncology* **2006**, *24* (29), 4699–4707. https://doi.org/10.1200/JCO.2006.06.0913.

(7) Garcia, A. A.; O'meara, A.; Bahador, A.; Facio, G.; Jeffers, S.; Kim, D.-Y.; Roman, L. Phase II Study of Gemcitabine and Weekly Paclitaxel in

Recurrent Platinum-Resistant Ovarian Cancer. https://doi.org/10.1016/j.ygyno.2004.02.007.

(8) Mitchell, M. J.; Billingsley, M. M.; Haley, R. M.; Wechsler, M. E.; Peppas, N. A.; Langer, R. Engineering Precision Nanoparticles for Drug Delivery. *Nature Reviews Drug Discovery*. 2021. https://doi.org/10.1038/s41573-020-0090-8.

(9) Megan Thompson. Molecular Simulations of MOF Nanoparticles for Drug Delivery, University of Bath, 2021. https://researchportal.bath.ac.uk/en/studentTheses/molecular-simulations-of-mof-nanoparticles-for-drug-delivery (accessed 2022-10-06).

(10) Wang, X.; Lan, P. C.; Ma, S. Metal-Organic Frameworks for Enzyme Immobilization: Beyond Host Matrix Materials. *ACS Cent Sci* **2020**, *6* (9), 1497–1506. https://doi.org/10.1021/acscentsci.0c00687.

(11) Majewski, M. B.; Howarth, A. J.; Li, P.; Wasielewski, M. R.; Hupp, J. T.; Farha, O. K. Enzyme Encapsulation in Metal-Organic Frameworks for Applications in Catalysis. *CrystEngComm*. Royal Society of Chemistry 2017, pp 4082–4091. https://doi.org/10.1039/c7ce00022g.

(12) Tajnšek, T. K.; Svensson Grape, E.; Willhammar, T.; Antonić Jelić, T.; Javornik, U.; Dražić, G.; Zabukovec Logar, N.; Mazaj, M. Design and Degradation of Permanently Porous Vitamin C and Zinc-Based Metal-Organic Framework. *Commun Chem* **2022**, *5* (1). https://doi.org/10.1038/s42004-022-00639-x.

(13) Maranescu, B.; Visa, A. Applications of Metal-Organic Frameworks as Drug Delivery Systems. *International Journal of Molecular Sciences*. MDPI April 1, 2022. https://doi.org/10.3390/ijms23084458.

(14) Horcajada, P.; Chalati, T.; Serre, C.; Gillet, B.; Sebrie, C.; Baati, T.; Eubank, J. F.; Heurtaux, D.; Clayette, P.; Kreuz, C.; Chang, J.-S.; Hwang, Y. K.;

Marsaud, V.; Bories, P.-N.; Cynober, L.; Gil, S.; Férey, G.; Couvreur, P.; Gref, R. Porous Metal--Organic-Framework Nanoscale Carriers as a Potential Platform for Drug Delivery and Imaging. **2009**. https://doi.org/10.1038/NMAT2608.

(15) Ahmed, A.; Efthymiou, C. G.; Sanii, R.; Patyk-Kazmierczak, E.; Alsharabasy, A. M.; Winterlich, M.; Kumar, N.; Sensharma, D.; Tong, W.; Guerin, S.; Farras, P.; Hudson, S.; Thompson, D.; Zaworotko, M. J.; Tasiopoulos, A. J.; Papatriantafyllopoulou, C. NUIG4: A Biocompatible Pcu Metal–Organic Framework with an Exceptional Doxorubicin Encapsulation Capacity. *J Mater Chem B* **2022**, *10* (9), 1378–1385. https://doi.org/10.1039/D1TB02176A.

(16) Dubbeldam, D.; Calero, S.; Ellis, D. E.; Snurr, R. Q. RASPA: Molecular Simulation Software for Adsorption and Diffusion in Flexible Nanoporous Materials. *Mol Simul* **2016**, *42* (2), 81–101. https://doi.org/10.1080/08927022.2015.1010082.

(17) Bader, R. Atoms in Molecules. *Acc Chem Res* **1985**, *18* (1), 9–15.

(18) Dal Corso, A. Pseudopotentials Periodic Table: From H to Pu. **2014**. https://doi.org/10.1016/j.commatsci.2014.07.043.

(19) Hamann, D. R. Optimized Norm-Conserving Vanderbilt Pseudopotentials. *Phys Rev B Condens Matter Mater Phys* **2013**, *88* (8). https://doi.org/10.1103/PHYSREVB.88.085117.

(20) Giannozzi, P.; Baroni, S.; Bonini, N.; Calandra, M.; Car, R.; Cavazzoni, C.; Ceresoli, D.; Chiarotti, G. L.; Cococcioni, m.; Dabo, I.; Corso, A. D.; Fabris, S.; Fratesi, G.; de Gironcoli, S.; Gebauer, R.; Gerstmann, U.; Gougoussis, C.; Kokalj, A.; Lazzeri, M.; Martin-Samos, L.; Marzari, N.; Mauri, F.; Mazzarello, R.; Paolini, S.; Pasquarello, A.; Paulatto, L.; Sbraccia, C.; Scandolo, S.; Sclauzero, G.; Seitsonen, A. P.; Smogunov, A.; Umari, P.; Wentzcovitch, R. M. Quantum ESPRESSO: A Modular and Open-Source Software Project for

Quantum Simulations of Materials. **2009**. https://doi.org/10.1088/0953-8984/21/39/395502.

(21) Otero-De-La-Roza, A.; Johnson, E. R.; Luaña, V. Critic2: A Program for Real-Space Analysis of Quantum Chemical Interactions in Solids. *Comput Phys Commun* **2014**, *185* (3), 1007–1018. https://doi.org/10.1016/j.cpc.2013.10.026.

(22) Henkelman, G.; Arnaldsson, A.; Jó Nsson, H. A Fast and Robust Algorithm for Bader Decomposition of Charge Density. https://doi.org/10.1016/j.commatsci.2005.04.010.

(23) Cundary, T. R.; Gordon, M. S. *UFF, a Full Periodic Table Force Field for Molecular Mechanics and Molecular Dynamics Simulations*; 1992; Vol. 114. https://pubs.acs.org/sharingguidelines.

(24) Abraham, M. J.; Murtola, T.; Schulz, R.; Páll, S.; Smith, J. C.; Hess, B.; Lindah, E. Gromacs: High Performance Molecular Simulations through Multi-Level Parallelism from Laptops to Supercomputers. *SoftwareX* **2015**, *1–2*, 19–25. https://doi.org/10.1016/j.softx.2015.06.001.

(25) Garberoglio, G. OBGMX: A Web-Based Generator of GROMACS Topologies for Molecular and Periodic Systems Using the Universal Force Field. *J Comput Chem* **2012**, *33* (27), 2204–2208. https://doi.org/10.1002/JCC.23049.

(26) Berendsen, H. J. C.; Postma, J. P. M.; Van Gunsteren, W. F.; Dinola, A.; Haak, J. R. Molecular Dynamics with Coupling to an External Bath. *J Chem Phys* **1984**, *81* (8), 3684–3690. https://doi.org/10.1063/1.448118.

(27) Li, X.; Porcino, M.; Qiu, J.; Constantin, D.; Martineau-Corcos, C.; Gref, R. Doxorubicin-Loaded Metal-Organic Frameworks Nanoparticles with Engineered Cyclodextrin Coatings: Insights on Drug Location by Solid State Nmr Spectroscopy. *Nanomaterials* **2021**, *11* (4). https://doi.org/10.3390/NANO11040945/S1.

(28) Safdar Ali, R.; Meng, H.; Li, Z. Zinc-Based Metal-Organic Frameworks in Drug Delivery, Cell Imaging, and Sensing. *Molecules* **2022**, *27* (1). https://doi.org/10.3390/MOLECULES27010100.

(29) Fytory, M.; Arafa, K. K.; El Rouby, W. M. A.; Farghali, A. A.; Abdel-Hafiez, M.; El-Sherbiny, I. M. Dual-Ligated Metal Organic Framework as Novel Multifunctional Nanovehicle for Targeted Drug Delivery for Hepatic Cancer Treatment. *Scientific Reports 2021 11:1* **2021**, *11* (1), 1–13. https://doi.org/10.1038/s41598-021-99407-5.

(30) Wells, B. A.; Liang, Z.; Marshall, M.; Chaffee, A. L. Energy Procedia Modeling Gas Adsorption in Metal Organic Frameworks. **2008**, 1273–1280. https://doi.org/10.1016/j.egypro.2009.01.167.

(31) Avci, G.; Velioglu, S.; Keskin, S. High-Throughput Screening of MOF Adsorbents and Membranes for H2 Purification and CO2 Capture. *ACS Appl Mater Interfaces* **2018**, *10* (39), 33693–33706. https://doi.org/10.1021/ACSAMI.8B12746/SUPPL_FILE/AM8B12746_SI_001.PDF.

(32) Lee, K.; Howe, J. D.; Lin, L. C.; Smit, B.; Neaton, J. B. Small-Molecule Adsorption in Open-Site Metal-Organic Frameworks: A Systematic Density Functional Theory Study for Rational Design. *Chemistry of Materials* **2015**, *27* (3), 668–678. https://doi.org/10.1021/CM502760Q.

(33) Michaud-Agrawal, N.; Denning, E. J.; Woolf, T. B.; Beckstein, O. MDAnalysis: A Toolkit for the Analysis of Molecular Dynamics Simulations. *J Comput Chem* **2011**, *32* (10), 2319–2327. https://doi.org/10.1002/JCC.21787.

(34) Gowers, R. J.; Linke, M.; Barnoud, J.; E Reddy, T. J.; Melo, M. N.; Seyler, S. L.; Domá nski, J.; Dotson, D. L.; Buchoux, S.; Kenney, I. M.; Beckstein, O. MDAnalysis: A Python Package for the Rapid Analysis of Molecular Dynamics Simulations. *PROC. OF THE 15th PYTHON IN SCIENCE CONF* **2016**.

Chapter 5: DFT Insights into the Mechanism of Enantioselective Synthesis of Homoallylic Alcohols from *Ortho*-Vinyl and *Ortho*-Alkynyl Benzaldehydes via Asymmetric Allylboration

Data generated from the study is planned to be submitted to the *Physical Chemistry Chemical Physics*

Abstract

Asymmetric allylboration of aldehydes is a valuable method for the synthesis of homoallylic alcohols, which are important building blocks in the synthesis of chiral drug compounds. Among all the available asymmetric allylation methods, chiral phosphoric acid (CPA)-catalyzed allylboration is regioselective and proceeds rapidly. Here, we studied the mechanism of the asymmetric allylboration reaction of *ortho*-vinyl and *ortho*-alkynyl benzaldehydes. We applied Density Functional Theory (DFT) calculations to understand the enantioselectivity of allylboration and account for the high enantiomeric excess *(ee)* observed for *ortho*-vinyl benzaldehydes. Our DFT results provide a detailed mechanistic understanding of the enantioselectivity in the asymmetric allylboration of aldehydes. Topology analysis using Atoms in Molecules (AIM) theory revealed that the most energetically favourable transition state conformation promotes hydrogen bonding interactions between the phosphoryl oxygens of the catalyst and the vinyl side chain of the benzaldehyde substrate and in turn promotes the dispersion interactions which are responsible for the high enantioselectivity observed for *o*-vinyl benzaldehydes compared to *o*-alkynyl benzaldehydes.

Reproduced with permission from:

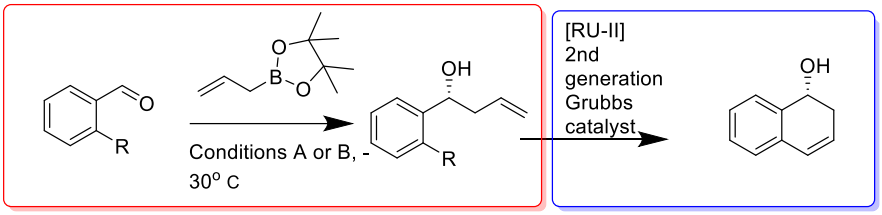
Vinay K R Cheemarla, Davide Tiana, Matthew N Grayson, Bruno N Falcone

1. Introduction

Homoallyl alcohols serve as essential building blocks for the synthesis of chiral drug compounds. Although there are several methods for synthesizing chiral drug compounds, asymmetric catalysis is the most widely used as it is highly enantioselective and has a wide substrate scope. To this aim, enzymes, chiral metal complexes, and organic compounds have been studied as chiral catalysts for asymmetric catalysis. Asymmetric allylation of aldehydes was found to be the most efficient method for the synthesis of homoallylic alcohols. Among the available asymmetric allylation methods, Lewis acid-catalyzed allylboration is of particular interest due to it being regioselective.[1] In 2002, Ishiyama *et al.*,[2] and Lachance *et al.*,[3] reported the first usage of Lewis acids to catalyze the allylboration of aldehydes. Rauniyar *et al.* [4] proposed that the Lewis acid $Sc(OTf)_3$ coordinate with a boronate oxygen, thus increasing the boron–carbonyl coordination strength and reducing the activation energy of the reaction. Further research on the Lewis-acid catalyzed allylboration found low yields when aromatic aldehydes were used due to steric hindrance of the allyl boronic acid pinacol ester.[5] To overcome this problem, a Brønsted acid catalyst, triflic acid, was employed and it showed excellent reactivity with aldehydes.[5] As a result, the focus on using chiral Brønsted acids as allylboration catalysts was increased and this led to the development of a BINOL-based catalyst that improved the enantioselectivity of the reaction on aromatic aldehydes.[6] Later, a chiral BINOL-phosphoric acid (TRIP-PA)- catalyzed allylboration reported by Antilla *et al.*[7] was found to have excellent enantioselectivity (*ee* greater than 90%) in the majority of the reactions over a wide range of aldehyde substrates used. The commercial availability of this catalyst led to the development of new synthetic methods such as dual-function catalysis,8, and many other tandem allylboration reactions, which evaluated different aldehyde substrates and chiral Brønsted acid catalysts.[9] These experimental results show that CPA is a highly efficient catalyst for asymmetric synthesis. This increased interest in CPA–catalyzed reactions drew the attention of computational chemists to carry out mechanistic studies[10,11] and provide key insights into the CPA activation modes.

Recently, Maji *et al.*[12] reviewed the numerous theoretical methods and provided a comprehensive review of computational tools to study the enantioselectivity of CPA-catalysed reactions.

This work studies the mechanism of the allylboration reaction reported by Santos Fustero *et al.*[9] using DFT methods. The authors developed a sequence of tandem allylboration and Ring-Closing Metathesis (RCM) reactions catalyzed by a CPA to synthesize benzo and heteroarene homoallyl alcohols as shown in Fig. 5.1 and achieved excellent enantioselectivity (>99% *ee*) in toluene. The enantioselectivity is higher (99% *ee*) for vinyl substituents compared to allyl substituents (82% *ee*) at the *ortho* position of benzaldehyde, which could associate the enantioselectivity to the steric demand at the ortho position.[9] This observation led Rodriguez *et al.*[13] to use *ortho*-ethynyl benzaldehyde as a substrate and reported 52% *ee* in toluene and 62% *ee* in DCM. Additional experiments performed to investigate the dependence of the enantioselectivity on the type of substituents at the alkynyl group found that the reaction achieves an *ee* of 99% when the phenyl ring is attached to an alkynyl group. That work also included DFT studies that explored the relationship between these interactions and the obtained stereoselectivity.[13] In the current work, we applied DFT methods to understand the role of steric and non-covalent interactions in the enantioselectivity of the allylboration of *o*-vinyl benzaldehydes and investigated the differences in the enantioselective levels achieved with alkene and alkyne-substituted benzaldehydes.



R	Conditions	Yield(%)	*ee* (%)
$H_2C{=}CH_2$	A	82	>99
$HC{\equiv}CH$	B	91	62

Conditions A: (R)-TRIP-PA/[Ru-II] (5 mol%), 4–5 h, toulene;
Conditions B: (R)-TRIP-PA (5 mol%), DCM

Figure 5.1: Allylboration of alkenes and alkynes catalyzed by BINOL phosphoric acid

2. Computational methods

Conformational searches were carried out with MacroModel version 12.3[14] using the OPLS3 force field[14] in the gas phase and a mixed torsional Monte Carlo Multiple Minimum (MCMM) and low-frequency mode (LMOD) sampling. A sufficient number of steps were chosen to obtain each conformation at least five times. Based on model calculations, the breaking B-C and the forming C-C bonds were fixed at 1.74 Å and 2.16 Å respectively. The obtained conformations were then subjected to PM6[15] and DFT (M06-2X[16]/6-31G(d)[17,18]) constrained optimizations in Gaussian 16,[19] keeping the braking and forming bonds fixed, and the obtained structures were clustered to remove redundant conformations.

The obtained TS structures were then subjected to full unconstrained DFT optimizations (M06-2X[16]/6-31G(d)[17,18]) and the location of the TSs were confirmed by the presence of a single imaginary frequency corresponding to the reaction coordinate. M06-2X /def2tzvpp[20,21] was used for the single point energy calculations with the SMD solvent model[22]. Atoms in molecules (AIM)[23]

analysis was carried out in Multiwfn[24] with electron density wavefunction files generated by Gaussian 09[25] using M06-2X/def2tzvpp, non-covalent interactions were also studied by analyzing the Reduced Density Gradient (RDG) and Non-Covalent Interactions (NCI) plots.[26]

3. Results and discussion:

Santos Fustero *et al.*[9] reported the synthesis of 1,2-dihydronapthol derivatives through tandem asymmetric catalysis (Fig. 5.2) and studied the enantioselectivity of the reaction with electron-withdrawing, electron-donating, and halogen substituents at 2,4,6 positions of *ortho*-vinyl benzaldehyde (**A**, Fig. 5.2). The proposed mechanism for this reaction occurs in two steps: first is the formation of the chiral homoallyl alcohol **2** catalyzed by CPA **C** and allyl-boronate pinacol ester **B**, followed by Ring-Closing Metathesis (RCM) catalyzed by a second-generation Grubbs catalyst **D**. As shown in Fig. 5.2, the first step is the Brønsted acid-base reaction between the carbonyl of the benzaldehyde and the boron atom of **B** catalyzed by **C**, this coordination results in increase in boron center electrophilicity which in turn enhances the electrophilicity of the carbonyl carbon in the chair-like transition state (Fig. 5.2).[9] The efficiency of this chiral synthesis relies on the interaction of the *ortho* vinyl side chain of benzaldehyde with the aryl side chains of the CPA catalyst at the transition state (TS) connecting **1** with **2**. These favourable interactions alongside the formyl hydrogen bond and vinyl hydrogen bond contribute to lowering the energy of the most favourable TS.

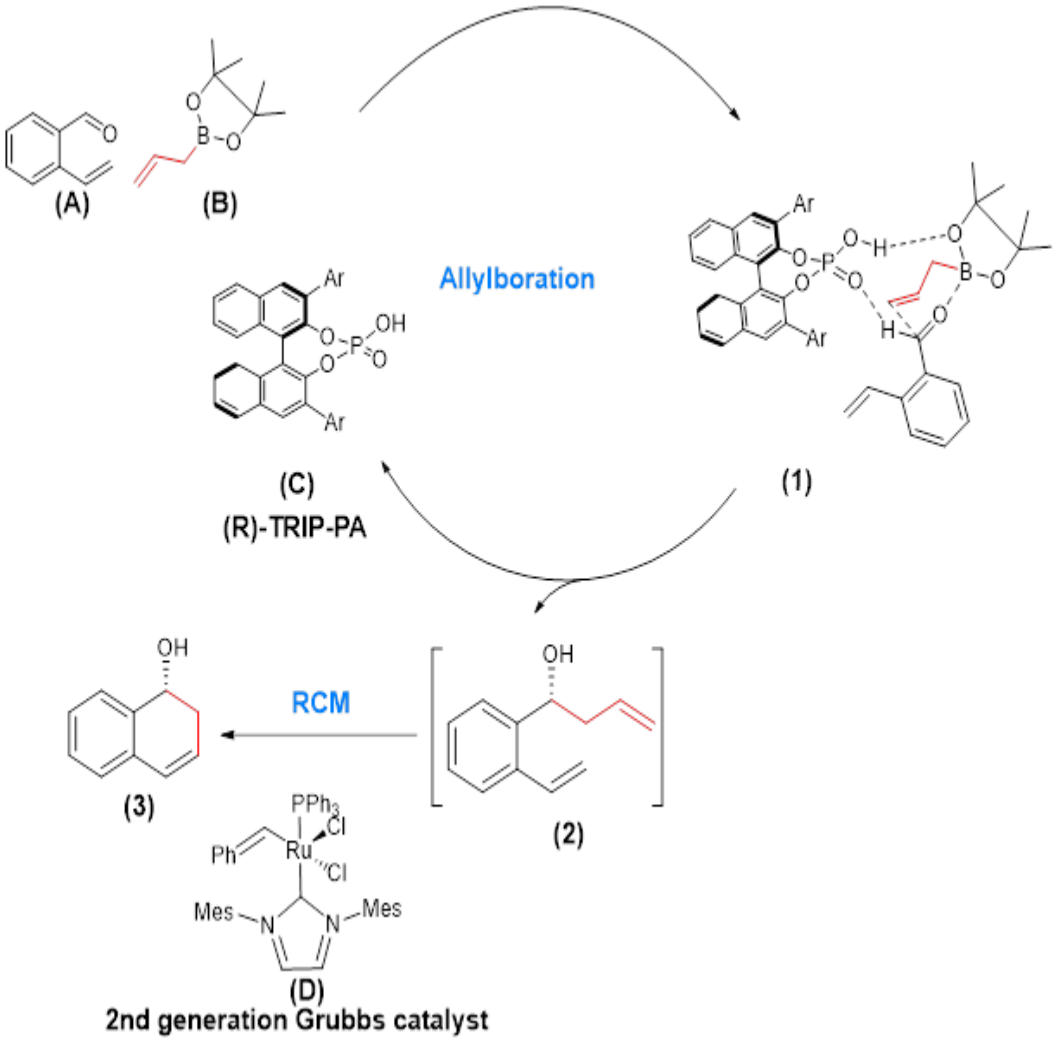


Figure 5.2: Mechanism of the asymmetric allylboration and Ring-Closing Metathesis (RCM)

The DFT optimizations and free energy calculations of 419 conformers of both major and minor pathways identified TS-1-ene-major and TS-1-ene-minor (see Fig. 5.6) as two low-energy transition structures, resulting in major and minor products, respectively. The energy difference between the two transition states was found to be +3.6 kcal/mol, indicating the major pathway is preferred, in agreement with the experimental studies. In addition to identifying these two structures, we performed cluster analysis of all the TS conformers of both major and minor pathways (details of cluster analysis are mentioned in SI) to analyze the most representative TS conformations. This resulted in 20 clusters from the major pathway and 9 clusters from the minor pathway. As shown in

Fig. 5.5 and Fig. 5.6, five structures from both pathways representing the spatial arrangement of formyl group, ortho vinyl, and allyl side chains were selected based on Goodman and Quadrant projection models.[27,28] These two models explain the steric interactions by defining the projections across and down the C_2 axis. The quadrant model projection along the C_2 symmetric axis of the CPA catalyst is shown in Fig. 5.3. The *re*-face attack of the substrate results in the positioning of the formyl and vinyl groups of the substrate into quadrant 3 (empty quadrant), resulting in hydrogen bonds between the oxygens (O1 and O2) of the phosphoryl group of CPA and the formyl hydrogen and the vinyl side chain of benzaldehyde (H5, H4). Besides, the presence of the vinyl group of the benzaldehyde near the aryl side chains promotes the vdW interactions with the catalyst in quadrants I and IV. Conversely, the presence of the ortho-vinyl side chain and allyl side chain in quadrant 4 results in steric hindrance which accounts for the high energy difference in TS-5-ene-major (5.88 kcal/mol), In TS-1-ene-minor and other activation modes of the minor pathway, as shown in Fig.5.6, the alkene chain and the carbonyl hydrogen of *ortho*-vinyl benzaldehyde are oriented away from the catalyst during the *si*-face attack, which impedes the formation of a formyl hydrogen bond and in turn results in less favourable interactions and a destabilization of the TS. Hydrogen bonding interactions and NCI interactions in the *re* and *si* face attacks are explained in greater detail in the following section.

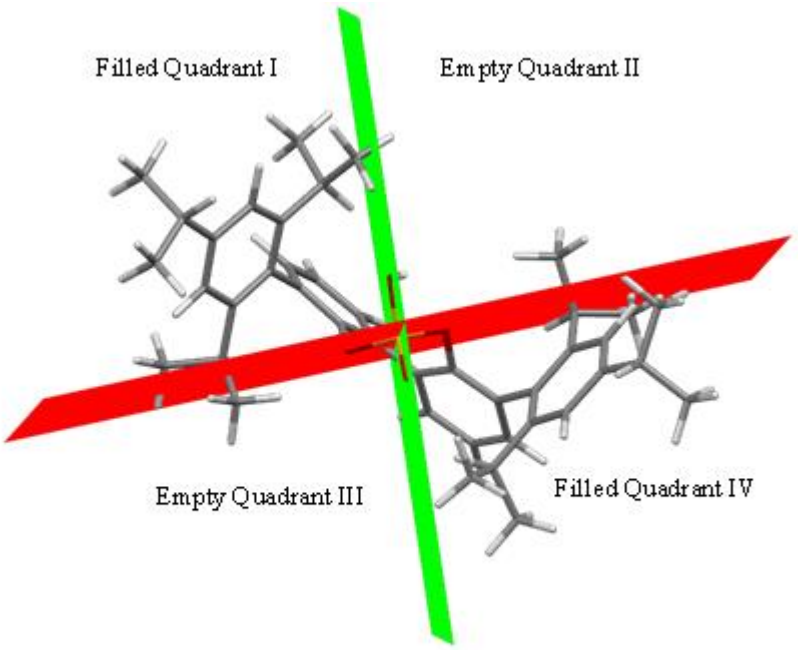


Figure 5.3: Quadrant projection of Chiral phosphoric acid ((R)-3,3'-Bis(2,4,6-triisopropylphenyl)-1,1'-binapthyl-2,2'-diyl hydrogen phosphate)catalyst down the C2 symmetry axis.

3.1. QTAIM Analysis:

The QTAIM method analyses the electron density and discloses inter and intra-molecular interactions between two atoms by mapping the critical points along the electron density topology as calculated from the wave function using DFT methods.[29] The critical points with the maximum electron density in all directions correspond to the atomic positions and a saddle point where the electron density is maximum in two directions and minimum in one direction represents a bond between two atoms, hence it is called a Bond Critical Point (BCP).[30]

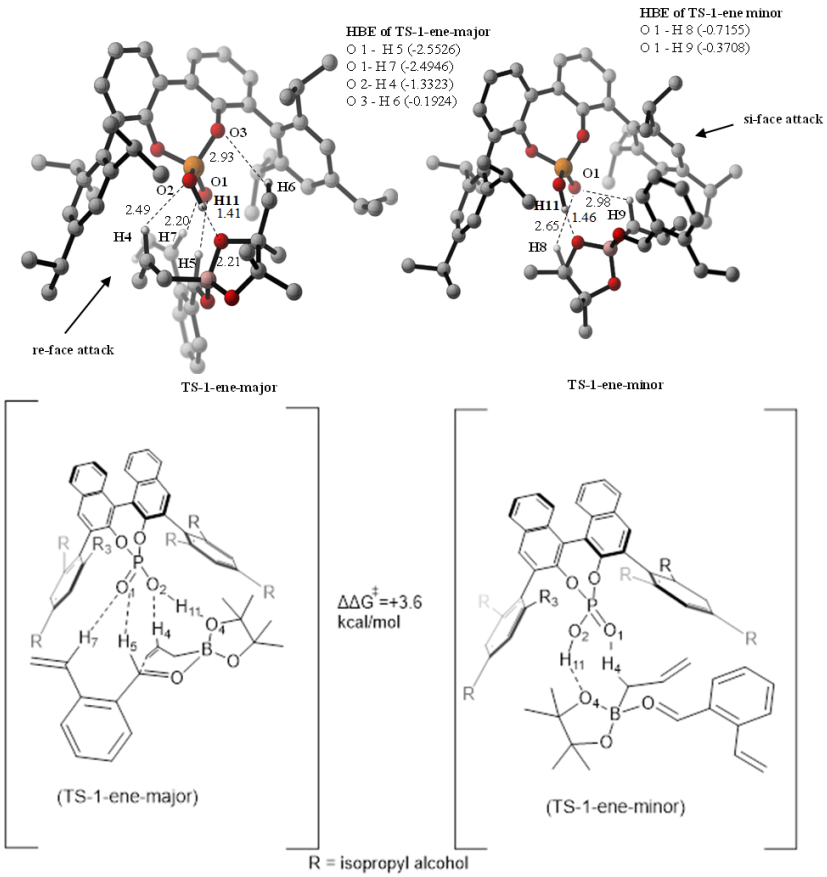


Figure 5.4: TS conformations of the major and minor pathways with hydrogen bond lengths located through QTAIM analysis. The estimated Hydrogen Binding Energies (HBE) of both conformers are in kJ/mol. and distances are in Angstroms.

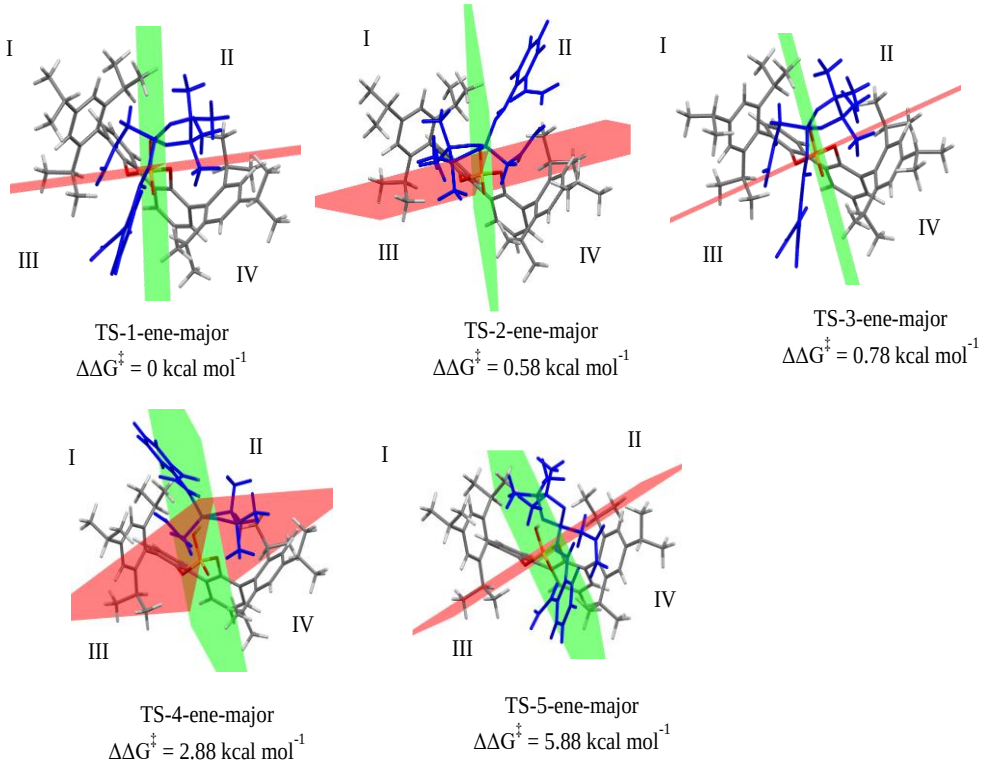


Figure 5.5: Quadrant projections of the TS conformers leading to the major product. The allyl boronic acid pinacol ester is coloured blue to distinguish it from the catalyst. II and III are empty quadrants and I and IV are filled quadrants

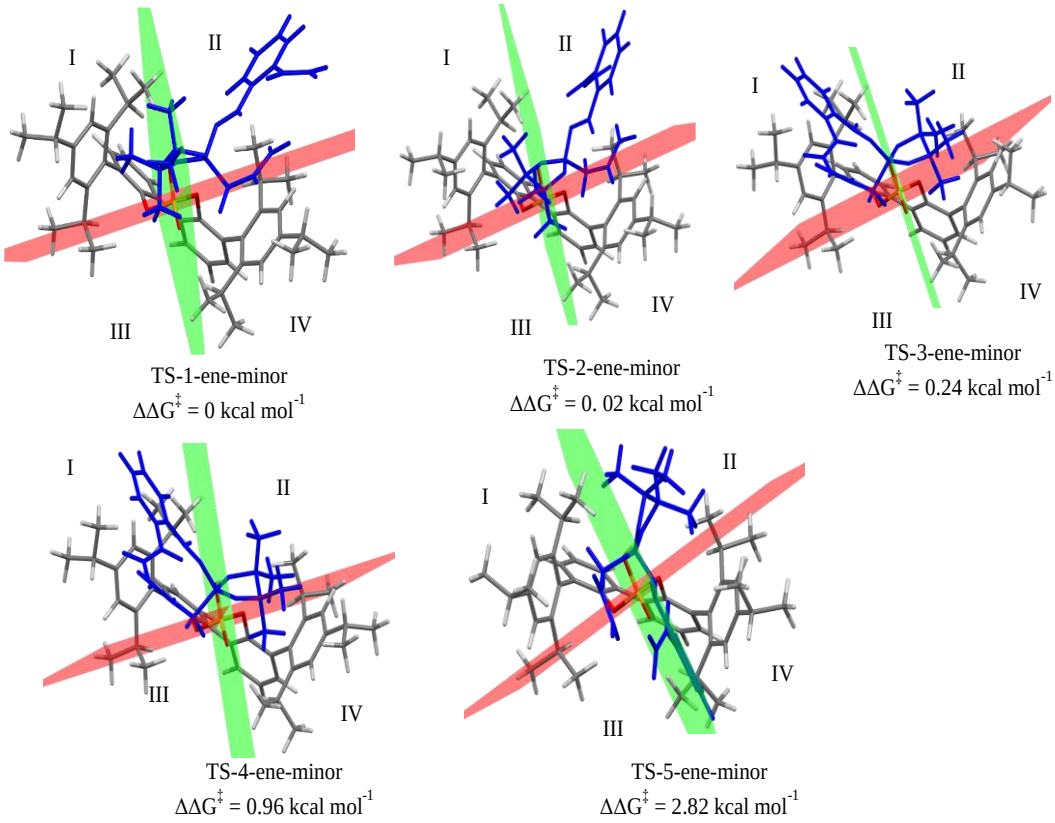


Figure 5.6: Quadrant projections of TS conformers leading to the minor product. Allyl boronic acid pinacol ester is coloured blue to distinguish it from the catalyst. II and III are empty quadrants and I and IV are filled quadrants

Earlier studies [7,13] reported that the hydrogen bond (CH---O) between the phosphoryl oxygen of CPA and the formyl hydrogen of benzaldehyde significantly contributes to the stereoselectivity. In our study, the BCP located between O1 and H7 corresponds to this hydrogen bond in TS-1-ene-major while no BCP was found between these two atoms in TS-1-ene-minor. Furthermore, two more BCPs were found in the *re*-face attack between O1, and O3 of CPA, and H5, H7, and H6 of the vinyl benzaldehyde and alkene side chain of boron pinacol respectively, confirming the presence of the hydrogen bond. The formation of these hydrogen bonds stabilizes the TS-CPA complex and induces the formation of vdW interactions between the alkene side chain of *o*-vinyl benzaldehyde and the aryl side chains. This highlights that the formation of hydrogen bonds and vdW interactions plays a crucial role in asymmetric

catalysis. The hydrogen bond distances between the atoms where BCPs were found are shown in Fig. 5.4. The estimated hydrogen bonding energies (HBE) shown in Fig. 5.4 and Fig. 5.8 were derived from the mathematical expression stated below,[31] where $\rho(bcp)$ is the electron density at a bond critical point.

$$H.B.E = -223.08 * \rho(bcp) + 0.7423$$

3.2. NCI and RDG Analysis:

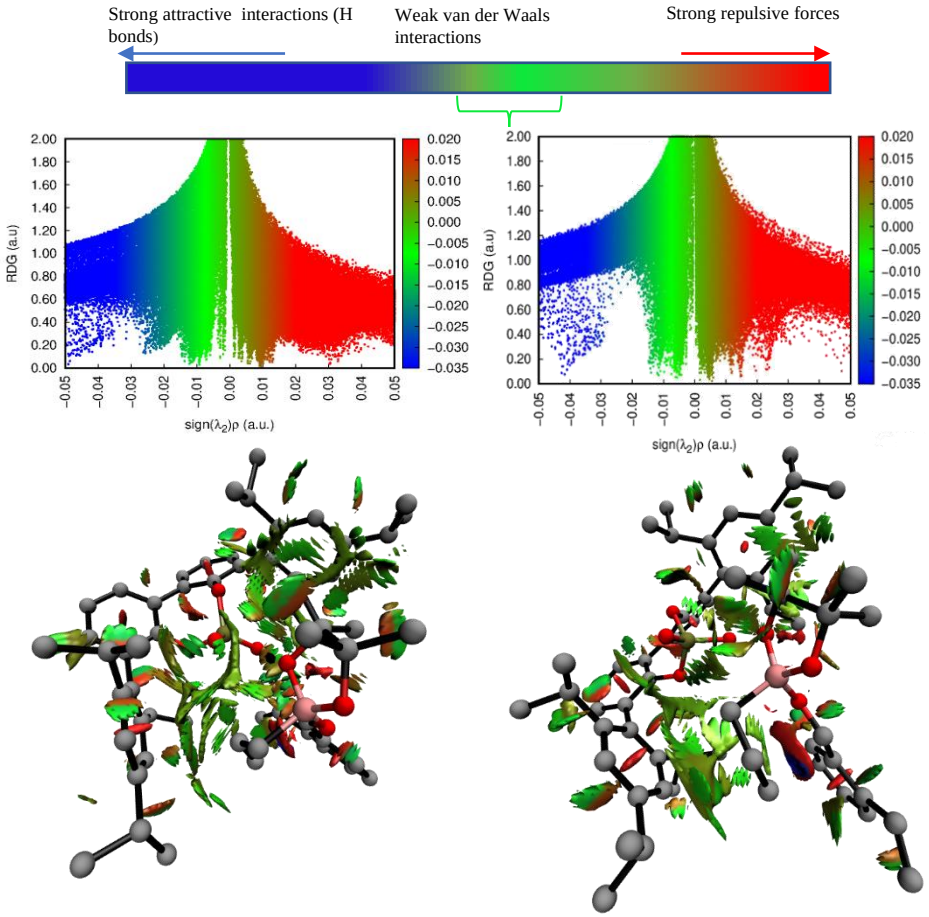


Figure 5.7: 2D and 3D NCI plots of TS-1-ene-major (right) and TS-1-ene-minor (left) conformers. Peaks towards negative s(ρ) represent strong hydrogen bond (blue) interactions, vdW interactions peaks are around 0 (green), and steric interactions peaks are towards positive.

Non-covalent interactions between the substrate and catalyst play an important role in the efficiency of chiral-catalyzed reactions. As there are some

reservations in identifying the long-range weak noncovalent interactions through BCPs,[32] we employed the Non-Covalent Interactions (NCI) index developed by Johnson and co-workers, which is a more appropriate descriptor for long-range dispersion interactions.[33] The reduced density gradient (RDG) plotted against the second eigenvalue of electron density ($sign\ (\lambda_2)\rho(r)$) in Fig. 7 is used to describe bonding and non-bonding interactions. Blue regions with negative eigenvalues represent strong attractive interactions such as hydrogen bonds, whereas red regions with positive values show strong repulsive interactions such as steric clashes, and green regions with values close to zero represent weak vdW interactions. The vinyl side chain in the vicinity of phosphoryl oxygens and aryl chains of CPA acts as a nucleophile and forms strong hydrogen bonds and long-range dispersion interactions and these interactions correspond to the troughs in the blue and green regions of the NCI plot in Fig. 5.7, respectively. On the other hand, the RDG values in Fig. 5.7 exhibit a narrow spread along the y-axis in the NCI plot of TS-1-ene-minor indicating a lower number of strong interactions. This is possibly due to the vinyl side chain not being in the vicinity of the aryl side chains and phosphoryl oxygens, thus hindering the formation of strong hydrogen bonds and reducing the likelihood of forming weak vdW interactions. Altogether, all these factors provide a rationale for the higher energy of TS-1-ene-minor (+3.6 kcal/mol) which results in the formation of the *syn* product (**2**, Fig. 5.2).

3.3. Comparative analysis of ortho-vinyl and alkynyl benzaldehydes

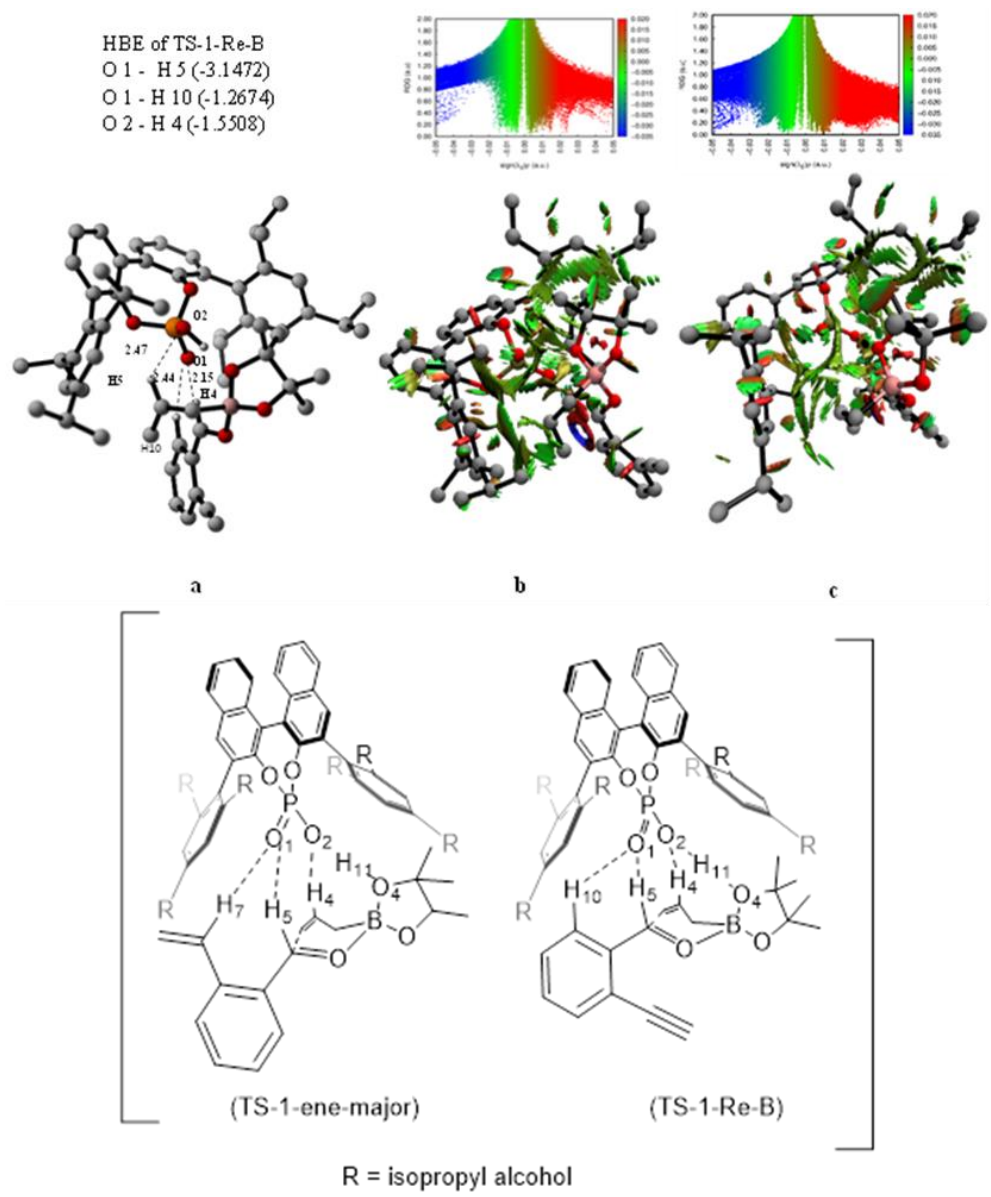


Figure 5.8: Hydrogen bond interactions in ortho-alkynyl benzaldehyde TS (a) and 3D and 2D NCI plots in Ortho alkynyl (b) and ortho-vinyl (c) benzaldehyde transition states achieving higher ee. Estimated hydrogen binding energies are in kJ/mol.

After having explained the mechanism of catalysis in *ortho*-vinyl benzaldehydes, to account for the low level of *ee* observed with *ortho*-alkynyl benzaldehydes, the lowest energy TSs (TS-1-Re-B and TS-1-Si-B) reported by

Elsa Rodriguez *et al.* were studied.[13] Similar to what was found in TS-1-ene-major, in both TS-1-Re-B and TS-1-Si-B the carbonyl group positioned in quadrant 3 as shown in Fig. 5.9 promotes the formation of a formyl hydrogen bond (CH—O). But in TS-1-ene-major, the allyl and vinyl side chains of TS of *ortho*-vinyl benzaldehyde in quadrant 3 are in gauche conformation, resulting in the formation of the hydrogen bond between the vinyl side chain and phosporyl oxygen of CPA (O1-H7) and it also promotes vdW interactions with aryl sides chains of CPA (blue and green troughs in the NCI plot of Fig. 5.8c). On the other hand, the alkynyl side chain of TS-1-Re-B and TS-1-Si-B is in filled quadrant I and IV respectively pointing to empty space (see Fig. 5.9), as a result no hydrogen boning and vdW interactions with CPA. The large energy difference between TS-1-ene-major and TS-1-ene-minor in contrast to small energy gap between TS-1-Re-B and TS-1-Si-B arises due to the spatial oreintation of benzaldehyde in TS-1-ene-minor pointing into the empty space as shown in Fig. 5.9, therby interactions with CPA catalyst were reduced and results in low enatioselectivity.

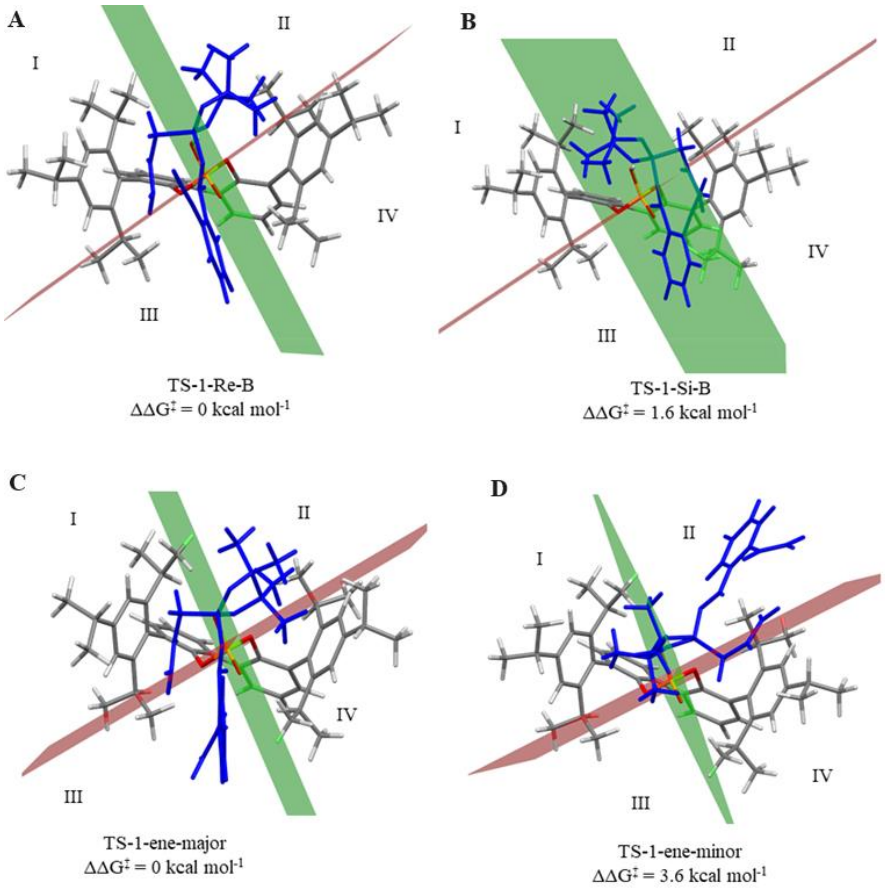


Figure 5.9: Low energy TS structures of ortho-alkynyl benzaldehyde (A and B) and Ortho-vinyl benzaldehyde (C and D). CPA catalyst atoms are coloured grey and allyl boron pinacol ester atoms are coloured blue. Red and blue planes are drawn to show quadrants (I, II, III, IV) of the TS catalyst. I and IV are filled quadrants and the presence of bulky substituents in these quadrants results in low enantioselectivity. II and III are empty quadrants

From the above comparative analysis, we can conclude that the formation of a hydrogen bond with alkenyl hydrogen not only stabilizes the TS complex but also promotes other weak vdW interactions. Our findings are in close agreement with the experimental results of phenyl-substituted *ortho*-alkynyl benzaldehyde.[13] The TS conformer of this structure as shown in Fig. 5.10 is similar to TS-1-ene-major, which supports our results of the quadrant model where hydrogen bonds are formed in empty quadrant III and π stacking

interactions of the phenyl ring of substrate and naphthyl ring of catalyst is observed in filled quadrant I and IV. These findings reveal that the benzaldehyde substituents showing vdW interactions with aryl side chains or aromatic rings in quadrants III and IV have high enatiocontrol leading to major product.

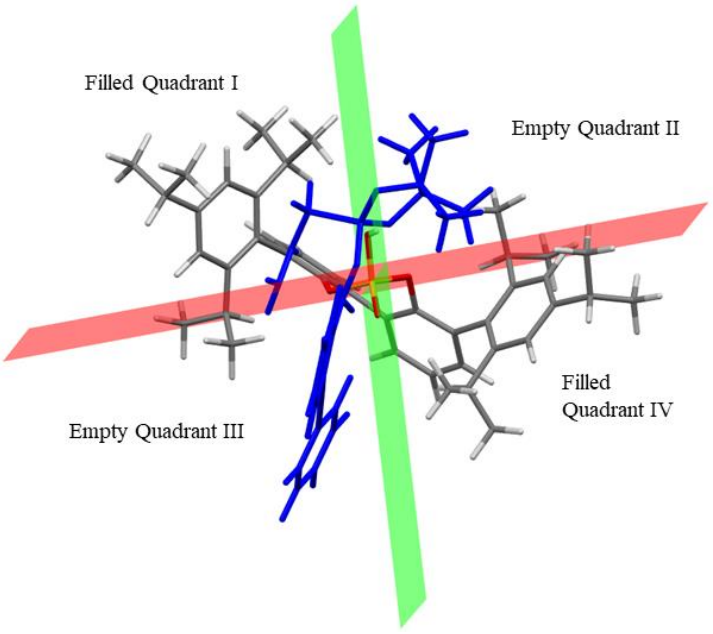


Figure 5.10: Quadrant projection of phenyl substituted ortho alkynyl benzaldehyde

4. Conclusion

In this study, we applied DFT methods to understand the enantioselectivity of the *ortho*-vinyl and *ortho*-alkynyl benzaldehydes and we performed QTAIM and NCI analysis to quantify and understand the key interactions and the conformational preference resulting in high *ee*. Our results show that the re-face attack results in a hydrogen bond between the vinyl side chain in *ortho*-vinyl benzaldehyde and phosphoryl oxygen that induces the formation of non-covalent interactions and promotes enantioselective synthesis. As shown in NCI plots, we anticipate that the presence of hydrogen bonding donors on the alkene side chain of vinyl benzaldehyde in the re-face attack of the catalyst promotes the formation of vdW interactions with aryl side chains of CPA. Overall, our research shows that DFT calculations, complemented by

QTAIM and NCI analysis, can provide valuable insights into the enantioselective synthesis catalyzed by CPA.

5. Bibliography

(1) Yamamoto, Y. From σ- to π-Electrophilic Lewis Acids. Application to Selective Organic Transformations. *Journal of Organic Chemistry*. October 12, 2007, pp 7817–7831. https://doi.org/10.1021/jo070579k.

(2) Ishiyama, T.; Ahiko, T.; Miyaura, N. Acceleration Effect of Lewis Acid in Allylboration of Aldehydes: Catalytic, Regiospecific, Diastereospecific, and Enantioselective Synthesis of Homoallyl Alcohols. *J Am Chem Soc* **2002**, *124* (42), 12414–12415. https://doi.org/10.1021/ja0210345.

(3) Lachance, H.; Lu, X.; Gravel, M.; Hall, D. G. Scandium-Catalyzed Allylboration of Aldehydes as a Practical Method for Highly Diastereo- and Enantioselective Construction of Homoallylic Alcohols. *J Am Chem Soc* **2003**, *125* (34), 10160–10161. https://doi.org/10.1021/ja036807j.

(4) Rauniyar, V.; Hall, D. G. Lewis Acids Catalyze the Addition of Allylboronates to Aldehydes by Electrophilic Activation of the Dioxaborolane in a Closed Transition Structure. *J. AM. CHEM. SOC* **2004**, *126*, 4518–4519. https://doi.org/10.1021/ja049446w.

(5) Yu, S. H.; Ferguson, M. J.; Mcdonald, R.; Hall, D. G. Brønsted Acid-Catalyzed Allylboration: Short and Stereodivergent Synthesis of All Four Eupomatilone Diastereomers with Crystallographic Assignments. **2005**. https://doi.org/10.1021/ja0541711.

(6) Rauniyar, V.; Hall, D. G. Preparation of a C2-Symmetric Binol-Derived Diol and Its Application in the Catalytic Enantioselective and Catalyst-Controlled Diastereoselective Allylboration of Aldehydes. *Synthesis (Stuttg)* **2007**, No. 21, 3421–3426. https://doi.org/10.1055/s-2007-983832.

(7) Jain, P.; Antilla, J. C. Chiral Brønsted Acid-Catalyzed Allylboration of Aldehydes. *J Am Chem Soc* **2010**, *132* (34), 11884–11886. https://doi.org/10.1021/ja104956s.

(8) Gao, S.; Duan, M.; Houk, K. N.; Chen, M. Chiral Phosphoric Acid Dual-Function Catalysis: Asymmetric Allylation with α-Vinyl Allylboron Reagents. *Angewandte Chemie - International Edition* **2020**, *59* (26), 10540–10548. https://doi.org/10.1002/anie.202000039.

(9) Fustero, S.; Rodríguez, E.; Lázaro, R.; Herrera, L.; Catalán, S.; Barrio, P. Relay Catalysis: Enantioselective Synthesis of Cyclic Benzo-Fused Homoallylic Alcohols by Chiral Brønsted Acid-Catalyzed Allylboration/Ring Closing Metathesis. *Adv Synth Catal* **2013**, *355* (6), 1058–1064. https://doi.org/10.1002/adsc.201201095.

(10) Farrar, E. H. E.; Grayson, M. N. Computational Studies of Chiral Hydroxyl Carboxylic Acids: The Allylboration of Aldehydes. *Journal of Organic Chemistry* **2020**, *85* (23), 15449–15456. https://doi.org/10.1021/acs.joc.0c02226.

(11) Grayson, M. N. Chiral Phosphoric Acid Catalysis: The Terada Model Revisited. *Journal of Organic Chemistry* **2021**, *86* (19), 13631–13635. https://doi.org/10.1021/acs.joc.1c01665.

(12) Maji, R.; Mallojjala, S. C.; Wheeler, S. E. Chiral Phosphoric Acid Catalysis: From Numbers to Insights. *Chemical Society Reviews*. Royal Society of Chemistry February 21, 2018, pp 1142–1158. https://doi.org/10.1039/c6cs00475j.

(13) Rodríguez, E.; Grayson, M. N.; Asensio, A.; Barrio, P.; Houk, K. N.; Fustero, S. Chiral Brønsted Acid-Catalyzed Asymmetric Allyl(Propargyl)Boration Reaction of Ortho-Alkynyl Benzaldehydes: Synthetic Applications and Factors Governing the Enantioselectivity. *ACS Catal* **2016**, *6* (4), 2506–2514. https://doi.org/10.1021/acscatal.6b00209.

(14) Mohamadi, F.; Richards, N. G. J.; Guida, W. C.; Liskamp, R.; Lipton, M.; Caufield, C.; Chang, G.; Hendrickson, T.; Still, W. C. Macromodel—an Integrated Software System for Modeling Organic and Bioorganic Molecules Using Molecular Mechanics. *J Comput Chem* **1990**, *11* (4), 440–467. https://doi.org/10.1002/JCC.540110405.

(15) Stewart, J. J. P. Optimization of Parameters for Semiempirical Methods V: Modification of NDDO Approximations and Application to 70 Elements. https://doi.org/10.1007/s00894-007-0233-4.

(16) Wang, Y.; Verma, P.; Jin, X.; Truhlar, D. G.; He, X. Revised M06 Density Functional for Main-Group and Transition-Metal Chemistry. *Proc Natl Acad Sci U S A* **2018**, *115* (41), 10257–10262. https://doi.org/10.1073/pnas.1810421115.

(17) Petersson, G. A.; Al-Laham, M. A. A Complete Basis Set Model Chemistry. II. Open-Shell Systems and the Total Energies of the First-Row Atoms. *J Chem Phys* **1991**, *94* (9), 6081–6090. https://doi.org/10.1063/1.460447.

(18) Petersson, G. A.; Bennett, A.; Tensfeldt, T. G.; Al-Laham, M. A.; Shirley, W. A.; Mantzaris, J. A Complete Basis Set Model Chemistry. I. The Total Energies of Closed-Shell Atoms and Hydrides of the First-Row Elements. *J Chem Phys* **1988**, *89* (4), 2193–2218. https://doi.org/10.1063/1.455064.

(19) Frisch, M. J.; Trucks, G. W.; Schlegel, H. B.; Scuseria, G. E.; Robb, M. A.; Cheeseman, J. R.; Scalmani, G.; Barone, V.; Petersson, G. A.; Nakatsuji, H.; others. Gaussian–16 Revision C. 01, 2019. *Gaussian Inc., Wallingford CT Search PubMed*.

(20) Weigend, F. Accurate Coulomb-Fitting Basis Sets for H to Rn. *Physical Chemistry Chemical Physics* **2006**, *8* (9), 1057–1065. https://doi.org/10.1039/b515623h.

(21) Weigend, F.; Ahlrichs, R. Balanced Basis Sets of Split Valence, Triple Zeta Valence and Quadruple Zeta Valence Quality for H to Rn: Design and Assessment of Accuracy. *Physical Chemistry Chemical Physics* **2005**, *7* (18), 3297–3305. https://doi.org/10.1039/b508541a.

(22) Marenich, A. v.; Cramer, C. J.; Truhlar, D. G. Universal Solvation Model Based on Solute Electron Density and on a Continuum Model of the Solvent Defined by the Bulk Dielectric Constant and Atomic Surface Tensions. *Journal of Physical Chemistry B* **2009**, *113* (18), 6378–6396. https://doi.org/10.1021/jp810292n.

(23) Bader, R. F. W. Atoms in Molecules. *Acc Chem Res* **1985**, *18* (1), 9–15. https://doi.org/10.1021/ar00109a003.

(24) Lu, T.; Chen, F. Multiwfn: A Multifunctional Wavefunction Analyzer. *J Comput Chem* **2012**, *33* (5), 580–592. https://doi.org/10.1002/jcc.22885.

(25) Frisch, M. J.; Trucks, G. W.; Schlegel, H. B.; Scuseria, G. E.; Robb, M. A.; Cheeseman, J. R.; Scalmani, G.; Barone, V.; Mennucci, B.; Petersson, G. A.; Nakatsuji, H.; Caricato, M.; Li, X.; Hratchian, H. P.; Izmaylov, A. F.; Bloino, J.; Zheng, G.; Sonnenberg, J. L.; Hada, M.; Ehara, M.; Toyota, K.; Fukuda, R.; Hasegawa, J.; Ishida, M.; Nakajima, T.; Honda, Y.; Kitao, O.; Nakai, H.; Vreven, T.; Montgomery Jr., J. A.; Peralta, J. E.; Ogliaro, F.; Bearpark, M.; Heyd, J. J.; Brothers, E.; Kudin, K. N.; Staroverov, V. N.; Kobayashi, R.; Normand, J.; Raghavachari, K.; Rendell, A.; Burant, J. C.; Iyengar, S. S.; Tomasi, J.; Cossi, M.; Rega, N.; Millam, J. M.; Klene, M.; Knox, J. E.; Cross, J. B.; Bakken, V.; Adamo, C.; Jaramillo, J.; Gomperts, R.; Stratmann, R. E.; Yazyev, O.; Austin, A. J.; Cammi, R.; Pomelli, C.; Ochterski, J. W.; Martin, R. L.; Morokuma, K.; Zakrzewski, V. G.; Voth, G. A.; Salvador, P.; Dannenberg, J. J.; Dapprich, S.; Daniels, A. D.; Farkas, Ö.; Foresman, J. B.; Ortiz, J. v; Cioslowski, J.; Fox, D. J. Gaussian~09 Revision E.01.

(26) Otero-de-la-Roza, A.; Johnson, E. R.; Contreras-García, J. Revealing Non-Covalent Interactions in Solids: NCI Plots Revisited. *Phys. Chem. Chem. Phys.* **2012**, *14* (35), 12165–12172. https://doi.org/10.1039/C2CP41395G.

(27) Simón, L.; Goodman, J. M. A Model for the Enantioselectivity of Imine Reactions Catalyzed by BINOL−Phosphoric Acid Catalysts. *J Org Chem* **2011**, *76* (6), 1775–1788. https://doi.org/10.1021/jo102410r.

(28) Reid, J. P.; Simón, L.; Goodman, J. M. A Practical Guide for Predicting the Stereochemistry of Bifunctional Phosphoric Acid Catalyzed Reactions of Imines. *Acc Chem Res* **2016**, *49* (5), 1029–1041. https://doi.org/10.1021/acs.accounts.6b00052.

(29) Bader, R. Atoms in Molecules. *Acc Chem Res* **1985**, *18* (1), 9–15.

(30) Bader, R. F. W. *A Bond Path: A Universal Indicator of Bonded Interactions*; 1998. https://pubs.acs.org/sharingguidelines.

(31) Emamian, S.; Lu, T.; Kruse, H.; Emamian, H. Exploring Nature and Predicting Strength of Hydrogen Bonds: A Correlation Analysis Between Atoms-in-Molecules Descriptors, Binding Energies, and Energy Components of Symmetry-Adapted Perturbation Theory. *J Comput Chem* **2019**, *40* (32), 2868–2881. https://doi.org/10.1002/jcc.26068.

(32) Lane, J. R.; Contreras-García, J.; Piquemal, J. P.; Miller, B. J.; Kjaergaard, H. G. Are Bond Critical Points Really Critical for Hydrogen Bonding? *J Chem Theory Comput* **2013**, *9* (8), 3263–3266. https://doi.org/10.1021/ct400420r.

(33) Johnson, E. R.; Keinan, S.; Mori-Sánchez, P.; Contreras-García, J.; Cohen, A. J.; Yang, W. Revealing Noncovalent Interactions. *J Am Chem Soc* **2010**, *132* (18), 6498–6506. https://doi.org/10.1021/ja100936w.

Chapter 6: Conclusions and future work:

The conclusion to each chapter is provided at the end of the respective chapter. This chapter provides the overall conclusion and further discusses the future aspects of work in each chapter. Three works formulated in this thesis cover the drug discovery, drug design, and drug delivery areas of pharmaceutical research and development. Through the predictive capability of computational chemistry tools, the experiments can be tailored to achieve the research aims and objectives. The work presented in this thesis serves as an example and shows the combination of computational prediction and experiments increases the accuracy and reduces the experimental workload.

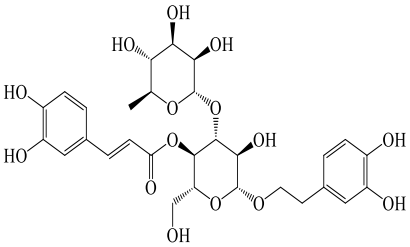
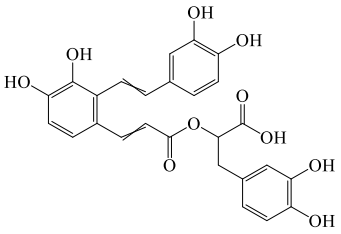
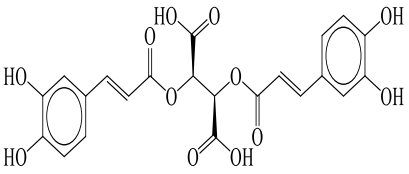
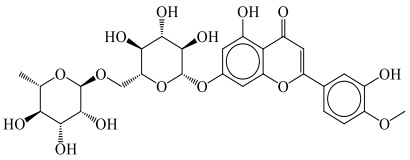
In Chapter 3, we performed in-silico screening of phytopharmaceuticals to identify the molecules that show binding affinity to sclerostin protein. The docking protocol used an empirical scoring function in ranking protein-ligand complexes. The emergence of machine learning opens new doors to integrate machine learning scoring functions in docking protocol to improve its accuracy in predicting the best-fit ligand. The 50 ns short duration of funnel metadynamics simulations show the verbascoside has affinity to multiple binding sites of sclerostin protein, increasing the length of simulations by adjusting the bias potential to provide an opportunity to converge the system through which binding kinetics and binding free energy can be calculated. Further, in-vitro testing of top-scored ligands needs to be performed and will be compared to the predicted results.

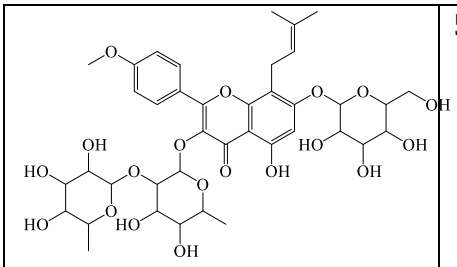
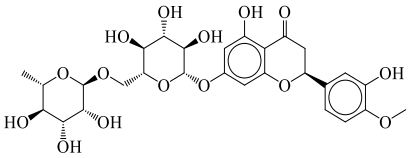
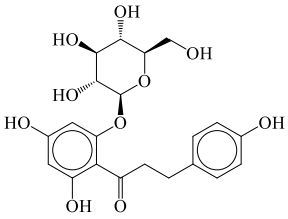
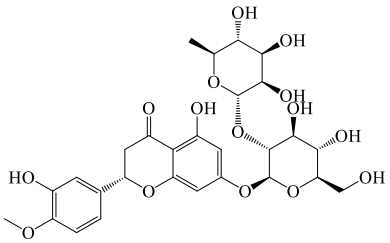
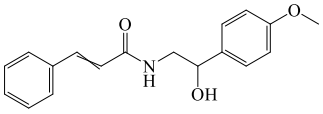
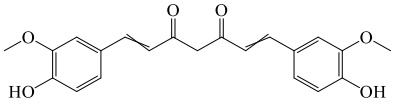
In Chapter 4, the computational study performed on NUIG-4 MOF demonstrated the application of NUIG-4 as a co-drug delivery agent. We conducted a simulation of drug release from pores through the molecular dynamics method. However, we were unsuccessful in modelling the drug release at acidic pH conditions which is an area of interest in anticancer drug therapy. Another interesting study that could be performed is drug kinetics modelling to understand the MOFs behaviour and drug release kinetics, this helps to improve the MOF-drug complexes to avoid disintegration before it reaches the target.

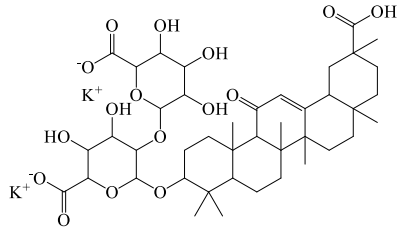
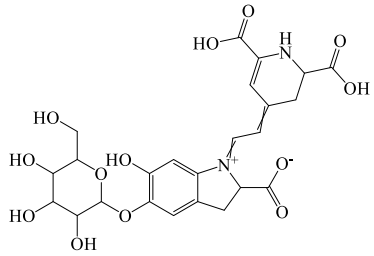
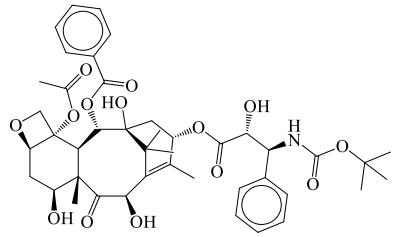
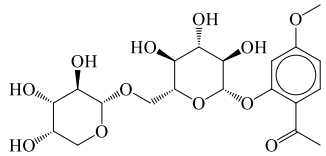
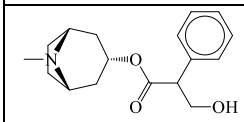
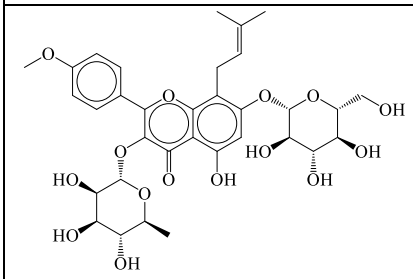
In Chapter 5, the comparative DFT study of two substrates shows the conformational preference of CPA catalysts. The current work investigated vinyl and allyl groups substituted in the ortho position of benzaldehyde, this could be extended to analyze how different substituents interact with catalysts at different temperatures and solvents. This process aids in designing the experiments efficiently.

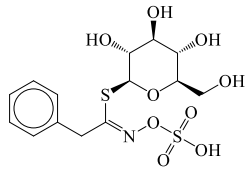
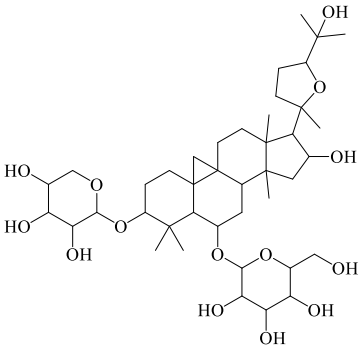
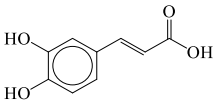
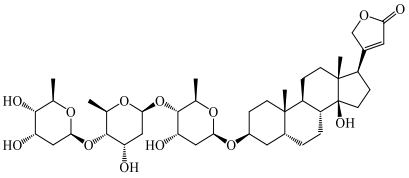
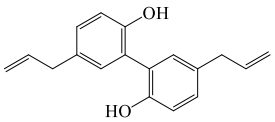
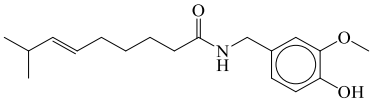
Supplementary data for Chapter 3

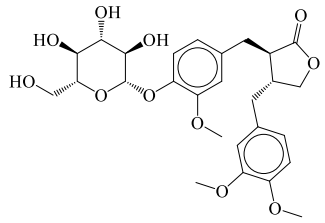
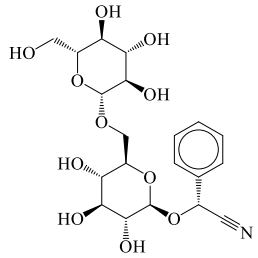
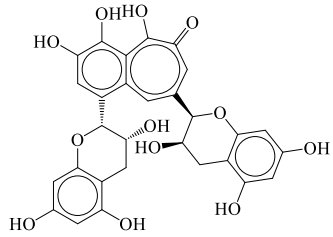
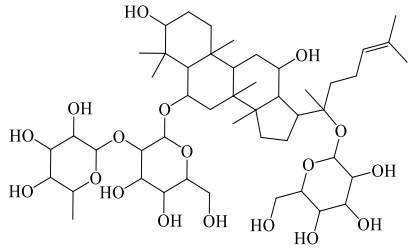
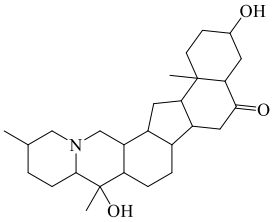
Table S 3.1: List of drugs and residue interactions of top 33 of GOLD docking

Compound name	PLP.Fitness	Hydrophobic interactions Residues	Hydrogen bond interactions Residues	Salt bridges
 Verbascoside	73.75	LEU91, ILE95,ARG97,LYS99	LEU91, ASN93, ILE95, TRP101, ARG102	ARG102
 Salvianolic acid	63.77	LEU91, ASN93,ILE95,LYS99	LEU91, ILE95, GLY96, ARG97, LYS99, TRP101, ARG102	ARG102
 Chicoric Acid	60.30	ARG89, LEU90, LEU91, ALA94, ILE95	ARG89, ASN93, ALA94, ILE95	ARG89, ARG102
 Diosmin	58.00	LEU91, PRO92, ILE95, ARG97	ARG89, ASN93, ILE95	ARG102

 Epimedin C	55.24	TRP100, ARG102	ARG89, ASN93, ILE95, GLY96, SER104	ARG89
 Hesperidin	54.91	LEU91, ALA94	ASN93, ILE95, GLY96	ARG89
 Phlorhizin Hydrate	54.33	ILE95, ARG97	ARG89, LEU91, ILE95, GLY96	
 Neo hesperidin	53.78	LEU91, ILE95	LEU91, ASN93, ALA94, GLY96	ARG102
 Aegeline	53.17	LEU91, LYS99, TRP100, TRP101, ARG102	ASN93, ILE95	ARG89
 Curcumin	52.70	TRP100, ARG102	ASN93, ILE95, GLY96	

 Dipotassium Glycyrrhizinate	51.96	ARG89, LEU91, ARG97	ASN93, ILE95, ARG102	ARG89, ARG102
 Betanin Red Beet Extract	51.63	LEU91, ALA94	ASN93, ILE95, GLY96, ARG102	ARG89, ARG102
 Docetaxel	51.24	ARG89, LEU91, ILE95, TRP100	ASN93, ILE95, ARG102, SER104	
 Paeonolide	50.85	ARG102	ASN93, ILE95, TRP101, ARG102	ARG102
 Atropine	50.46	ARG89, LEU90, LEU91	LEU91, PRO92	
 Icariin	49.98	ILE95, TRP100	ARG89, ASN93, GLY96, ARG102	

 Glucotro paeolin	49.94	TRP100, ARG102	ASN93, ILE95	ARG102
 Astragaloside IV	49.69	ALA94	ARG89, ASN93, ALA94, ILE95, GLY96, TRP101, TRP100	
 Caffeic Acid	48.46	ILE95, ARG97, LYS99	ASN93, ILE95	ARG102
 Digitoxin	48.16	LEU91, PRO92, ASN93, ILE95, TRP100	ASN93, ILE95, TRP101, ARG102	ARG102
 Magnolol	48.13	LEU90, LEU91, ALA94, ILE95, TRP100, ARG102	ASN93,ILE 95	ARG89
 Capsaicin	47.05	ARG97, TRP100	ALA94, GLY96	

 Arctiin	47.02	ILE95	ASN93, GLY96, ARG97, ARG102	
 Amygdalin	46.69	ARG102	ARG89, ASN93, ILE95, ARG102	ARG89, ARG102
 Theaflavine	46.39	LEU91, ILE95	ARG89, ASN93, ILE95, TRP101, ARG102	ARG102
 Gin Sennoside	46.05	TRP100	ALA94, ILE95, GLY96, TRP101	ARG102
 Peiminine	45.98	ALA94, TRP101	TRP101, ARG102	

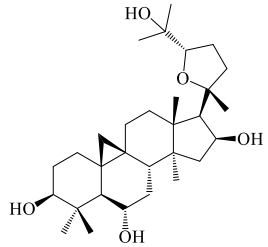
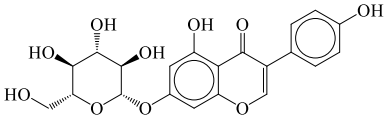
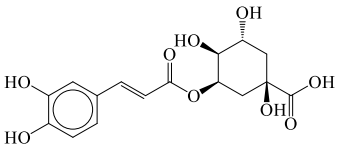
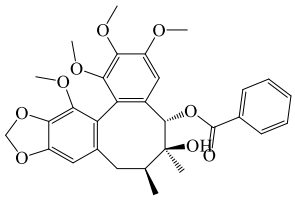
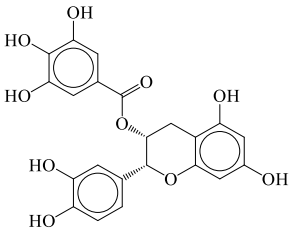
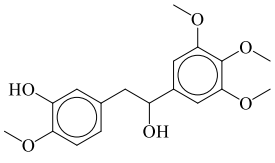
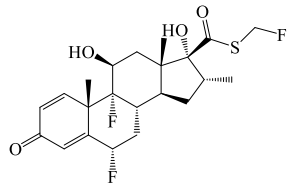
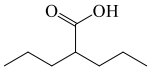
 Cyclo astragenol	45.46	ASN93, ILE95, ARG97	ASN93, ALA94, GLY96	
 Genistin	45.44	LEU91, ILE95, TRP100	ASN93, ILE95, SER104	
 Neo chlorogenic Acid	45.15	TRP100	ARG89, ILE95, GLY96, ARG102	
 Gomisin C	45.11	TRP100	GLY96, TRP101, ARG102, SER104	ARG89, ARG102
 Epicatechin Gallate	45.08	ARG89, LEU91, ALA94	ARG89, ASN93, ALA94, GLY96, ARG102	ARG89
 Combretastatin	44.43	LEU91	ARG102	

Table S 3.2: Docking score and list of ligand interaction residues reported experimentally

Compound name	PLP.Fitness	Hydrophobic interactions Residues	Hydrogen bond interactions Residues	Salt bridges
 Fluticasone	41.80	LEU91, ALA94	ILE95	-
 Valproic acid	30.12	LEU91, ARG89	LEU95	-

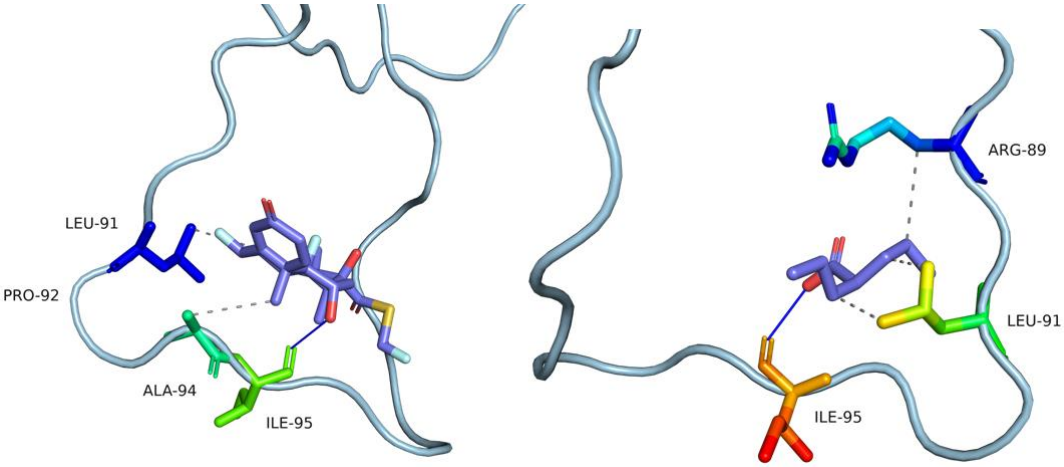


Figure S 3.1: Residue interactions of Fluticasone and Valproic acid

Supplementary data for Chapter 4

Table S 4.1: Cartesian coordinates of NUIG-4 and drugs to prepare input files and calculate the binding energy

104
NUIG-4_energy

Zn	1.746318	12.960757	5.099787
Zn	1.607303	10.777729	7.441760
O	3.774688	11.428734	22.280135
O	2.123657	12.749754	22.257142
C	2.995677	12.137749	21.684136
C	3.144668	12.238742	20.195152
C	4.158671	11.521743	19.569152
H	4.730681	10.991738	20.074152
C	2.288672	13.032744	19.441164
H	1.610653	13.512760	19.858153
Zn	3.852668	10.674727	5.103616
Zn	3.975678	12.955741	7.263764
O	5.873686	12.544744	6.799773
O	5.739687	10.788738	5.380785
O	19.114791	12.557744	4.935786
O	19.076806	10.958731	6.478780
O	4.030683	12.758753	9.141747
O	2.182664	11.649730	9.045751
O	3.237676	8.795711	5.107790
O	1.782657	8.894712	6.308768
O	2.866675	11.879744	6.220775
N	11.988740	11.345738	6.189778
N	3.652674	12.457747	15.937691
N	1.883668	2.418670	5.066780
C	6.235689	11.634739	6.088786
C	7.732714	11.529746	6.092768
C	8.401715	10.560734	5.352775
H	7.918713	9.953726	4.838795
C	9.789726	10.499737	5.382776
H	10.237731	9.850724	4.887789
C	10.508735	11.404745	6.151775
C	9.840730	12.373737	6.891767
H	10.323732	12.980745	7.405767
C	8.452719	12.436744	6.860771
H	8.004714	13.085758	7.355759
C	12.867748	11.981733	5.568775
H	12.536741	12.609743	4.966783
C	17.117781	11.801746	5.688779
C	16.476770	12.693754	4.836785
H	16.976774	13.254755	4.289798
C	15.086769	12.745753	4.803797
H	14.657757	13.342748	4.233798
C	14.339769	11.906740	5.621789
C	14.981756	11.014732	6.472768
H	14.481752	10.453730	7.021765
C	16.371777	10.962732	6.506770
H	16.800789	10.365737	7.076770
C	18.617793	11.766748	5.704785
C	4.315683	11.599742	18.162666
H	4.995693	11.119726	17.743666
C	3.459668	12.393744	17.409673
C	2.446661	13.110743	18.034678
H	1.872660	13.641762	17.529677
C	2.705661	11.894735	15.348698
H	2.004668	11.468729	15.788700
C	3.010668	12.124749	11.075729
C	3.992679	12.706753	11.871722
H	4.711688	13.143750	11.475736
C	3.898675	12.634747	13.255712
H	4.554676	13.022750	13.786713
C	2.822679	11.981733	13.845700
C	1.841663	11.399728	13.052713
H	1.121658	10.962732	13.446708
C	1.935667	11.471735	11.666732
H	1.278651	11.083732	11.135731
C	3.087671	12.187738	9.640736
C	2.412658	8.096709	5.653781
C	2.255665	6.610692	5.514785
C	1.255658	5.935699	6.204769
H	0.675645	6.404706	6.759778
C	1.125660	4.558678	6.065773
H	0.455644	4.106671	6.526778
C	1.992664	3.857684	5.235777
C	2.992671	4.533693	4.545793
H	3.572684	4.066677	3.989788
C	3.122669	5.912686	4.685785
H	3.792685	6.363696	4.222789
C	2.755669	1.996665	5.855785
H	3.293677	2.542676	6.380774
C	2.820668	0.547657	5.848778
H	4.301688	0.409656	7.218772
H	1.365668	0.224653	4.482785
O	3.895688	-4.253728	6.622773
O	2.287658	-4.213733	5.131779
C	3.740686	-0.089352	6.672762
C	3.819680	-1.478358	6.681779
H	4.436682	-1.904365	7.233763
C	2.979672	-2.228364	5.866775
C	2.059654	-1.589364	5.042791
H	1.497657	-2.090363	4.497795

C	1.980659	-0.202349	5.033792
C	3.086676	-3.723379	5.895780
Zn	1.746318	-6.184743	5.099787
Zn	1.746318	12.960757	24.245287
Zn	20.891818	12.960757	5.099787
Zn	20.752803	10.777729	7.441760
O	3.774688	11.428734	3.134635
O	2.123657	12.749754	3.111642
Zn	3.852668	10.674727	24.249116
Zn	3.975678	-6.189759	7.263764
O	-0.030709	12.557744	4.935786
O	-0.068694	10.958731	6.478780
O	3.895688	14.891772	6.622773
O	2.287658	14.931767	5.131779

376

dox__nuig-4

O	21.231498	7.058008	19.725494
C	20.220501	6.290005	19.186510
H	20.942497	7.945000	20.085506
H	19.475492	9.585999	20.258504
H	20.151500	5.348008	19.729495
O	20.101492	8.527004	17.979999
H	20.210507	9.381008	17.470001
H	20.436500	6.088997	18.108005
H	16.821007	19.238509	17.823005
H	17.214006	19.155494	15.889999
O	18.700003	11.879993	21.037497
O	17.961006	6.577992	19.921505
O	18.428003	14.396995	21.246508
C	18.601998	9.476008	19.613493
C	18.918990	7.028007	19.296501
C	18.313992	11.986998	19.716495
C	17.993994	13.245010	19.185495
C	18.080991	14.466991	20.060502
C	17.724004	15.781999	19.418496
C	17.781996	16.963009	20.171507
C	17.460007	18.194007	19.614507
H	18.911006	10.950996	21.342504
H	17.776003	9.191008	20.267503
H	18.080991	16.939000	21.212506
H	17.513002	19.088006	20.219505
O	16.655991	9.706998	15.890995
O	16.511998	9.219994	13.640996
O	13.004007	10.143994	13.376004
O	17.155000	12.202997	15.721997
O	16.894008	14.714006	15.975005
O	16.615997	17.242993	16.176990
N	13.847998	9.675006	15.979007
C	17.780005	9.654999	16.688998
C	18.864004	8.351995	18.565008
C	17.779009	8.336008	17.483996
C	17.850996	10.896010	17.582002
C	18.256000	10.816001	18.929998
C	16.549006	8.686007	14.967990
C	15.288007	7.840006	15.227010
C	14.006005	8.644997	14.957001
C	14.081994	9.303009	13.567995
C	15.397998	10.082001	13.385998
C	17.537010	12.147992	17.046004
C	17.596993	13.327010	17.802998
C	15.497000	10.609996	11.986002
C	17.241001	14.644010	17.160992
C	17.327999	15.868001	18.035004
C	17.008001	17.123008	17.495005
C	17.071008	18.280009	18.260001
C	16.330001	18.528996	15.768004
H	12.940003	10.902998	14.023007
H	17.137003	11.321998	15.250003
H	13.791997	9.240001	16.890007
H	14.641004	10.301007	15.953007
H	18.634009	9.672996	16.010003
H	16.801000	8.182002	17.945001
H	17.929990	7.495004	16.805996
H	17.444001	8.071992	15.079991
H	15.311997	6.960002	14.581998
H	15.291989	7.465998	16.252002
H	13.125006	8.004006	15.031994
H	14.011998	8.536998	12.794995
H	15.432996	10.950001	14.047991
H	14.650998	11.268007	11.786008
H	16.426992	11.169006	11.873005
H	15.486010	9.779004	11.282003
H	16.032997	18.519997	14.719999
H	15.515992	18.929998	16.373002
O	9.981009	15.175010	1.087005
O	12.265009	15.118991	0.773000
O	8.394000	18.004007	3.752997
O	4.426995	17.224996	1.295997
O	7.241996	15.273993	5.558992
O	7.259993	18.563994	5.940006
N	9.914995	12.453995	0.389994
C	9.241992	16.171993	1.691007
C	7.902994	16.714002	3.765996
C	8.930993	15.764003	3.143002
C	6.568993	16.653005	3.000004
C	7.988000	16.472003	0.868000
C	6.741992	16.718004	1.480005
C	11.191004	14.898990	1.691007
C	11.230999	13.446000	2.203992
C	11.221005	12.439999	1.040998
C	12.311992	12.806004	0.021003
C	7.678992	16.368005	5.207997
C	5.638005	17.000993	0.673003
C	8.026004	17.444997	6.194010

H	8.591007	18.371007	2.844007
H	4.447002	17.164994	2.293995
H	6.626009	18.476997	5.171008
H	9.200006	12.206998	1.059991
H	9.729992	13.379009	0.026000
H	9.875000	17.060995	1.688997
H	8.549002	14.741001	3.168006
H	9.849996	15.759006	3.731994
H	6.048006	15.725999	3.244990
H	5.920995	17.462993	3.339990
H	11.286004	15.595005	2.526000
H	12.131010	13.304993	2.803992
H	10.388004	13.261992	2.872993
H	11.364999	11.421995	1.411004
H	13.295995	12.616004	0.450991
H	9.081993	17.698004	6.099010
H	7.826010	17.090001	7.203992
O	12.216992	11.998006	-1.123496
O	9.309997	16.303006	-1.129508
O	8.238002	16.662999	-3.400490
O	3.393999	17.579992	-1.025490
O	7.209008	17.016999	-5.708499
C	12.222009	14.287999	-0.419497
C	8.078003	16.534992	-0.554492
C	6.973002	16.822002	-1.367506
C	5.721996	17.060000	-0.753509
C	13.367005	14.645006	-1.320503
C	7.141999	16.870000	-2.864492
C	4.490003	17.373010	-1.561507
C	5.911001	17.184005	-3.674500
C	4.659996	17.419993	-3.057498
C	6.004010	17.241997	-5.073500
C	3.558000	17.704993	-3.874494
C	4.899008	17.526001	-5.863501
C	3.674998	17.758006	-5.257507
C	7.167003	17.103001	-7.084505
H	11.355005	12.069993	-1.624496
H	10.047999	16.105999	-0.483500
H	11.308998	14.480010	-0.987506
H	13.339991	14.015004	-2.209506
H	13.286001	15.691996	-1.613506
H	14.306992	14.487993	-0.792509
H	2.582996	17.892006	-3.440504
H	4.991998	17.566992	-6.940493
H	2.806998	17.979999	-5.862505
H	8.160004	16.911010	-7.491500
H	6.466010	16.365995	-7.474499
H	6.843004	18.101994	-7.376493
O	6.590992	7.500996	14.193995
O	5.898997	6.286999	16.028000
O	9.572999	10.409006	14.724996
O	3.057996	4.789993	14.318996
O	8.009003	5.713994	13.050990
O	10.141008	9.834009	10.064004
O	7.177993	12.686995	13.667992
O	10.289002	12.831008	14.793996
O	8.816005	4.059995	11.304001
O	10.932004	8.143998	8.341005
O	9.604991	2.356007	9.577000
N	4.058999	7.054006	13.061998
C	7.716000	8.294003	14.089001
C	8.481993	10.698008	13.929998
C	7.319995	9.767996	14.291005
C	8.860997	10.547007	12.444996
C	8.420995	8.035998	12.755000
C	8.975008	9.088005	11.995996
C	5.937000	7.574994	15.406997
C	4.503998	8.112006	15.227010
C	3.623994	7.115999	14.452995
C	3.726997	5.720005	15.090004
C	5.194997	5.293003	15.276003
C	8.548006	6.727001	12.284997
C	8.120009	12.124003	14.222005
C	9.619006	8.786004	10.794003
C	9.197000	6.419008	11.080994
C	9.744006	7.474001	10.315997
C	5.266008	3.985002	16.005006
C	8.981996	12.816993	15.234993
C	9.293992	4.982999	10.632989
C	10.453003	7.220993	9.011997
C	10.004002	4.728000	9.327994
C	10.549994	5.786000	8.565007
C	10.126993	3.411996	8.857991
C	11.196001	5.474005	7.361004
C	10.769995	3.126001	7.661991
C	11.304997	4.162998	6.914991
C	9.792004	1.113004	9.007000
H	9.927995	9.478994	14.633001
H	3.409009	4.680998	13.389999
H	7.564004	6.013008	13.895000
H	10.011010	10.738998	10.469008
H	10.440003	12.393993	13.907004
H	3.984006	7.970999	12.642999
H	5.020008	6.743007	13.022003
H	8.383010	7.979998	14.895008
H	6.451000	10.007008	13.673008
H	7.008995	9.930005	15.324996
H	8.109996	11.037993	11.823993
H	9.798992	11.072991	12.258002
H	6.517990	8.255004	16.031006
H	4.068993	8.300991	16.209997
H	4.526992	9.076001	14.715002
H	2.586002	7.455009	14.433007
H	3.231990	5.721996	16.062002
H	5.681006	5.135991	14.309998
H	4.731006	3.222992	15.436998

H	6.308997	3.687998	16.119994
H	4.808009	4.092006	16.989008
H	8.925000	12.284997	16.184993
H	8.632993	13.839995	15.370007
H	11.627005	6.256003	6.747008
H	10.855001	2.102999	7.317008
H	11.808006	3.951995	5.981992
H	9.348997	0.349999	9.646001
H	9.317004	1.087005	8.027000
H	10.859998	0.919999	8.898005
H	19.838510	20.735495	10.457004
H	19.366497	20.219505	12.093006
O	20.659507	18.454003	9.666008
C	19.639492	18.030007	10.493993
H	20.403493	18.571001	8.706990
H	19.902494	15.895992	10.141008
H	20.070496	17.949998	11.493005
O	15.825000	19.611501	8.160004
O	15.854006	21.184496	6.169006
O	15.919005	22.796509	4.192003
C	14.470992	19.222503	6.209001
C	19.015004	20.373492	11.072991
C	15.024010	20.477510	5.583000
C	14.516003	20.827490	4.208009
C	13.567995	20.016505	3.541994
C	14.992994	21.983495	3.571000
C	13.139997	20.403493	2.263994
C	14.556994	22.347508	2.305003
C	13.627001	21.552491	1.653999
C	16.308003	23.900496	3.462004
H	16.082009	19.272492	9.064992
H	18.152997	19.289493	9.507004
H	18.208998	21.108507	11.074006
H	12.414995	19.809504	1.721008
H	14.936994	23.243499	1.831995
H	13.280008	21.826502	0.668006
H	17.034996	24.476507	4.033000
H	16.757003	23.576496	2.522994
H	15.436998	24.522495	3.251002
O	16.291997	17.568007	9.615004
O	17.428991	18.606995	11.331992
O	12.326007	16.360998	10.277994
O	12.125994	16.455002	5.552999
O	13.479006	13.142007	9.688006
O	10.613002	14.532009	10.591003
O	12.185000	18.056006	3.580993
N	18.774001	16.700007	8.626005
C	14.934007	17.340003	9.525997
C	13.186004	15.514996	9.607001
C	14.636007	15.885998	9.935998
C	12.929990	15.603008	8.091003
C	14.431993	17.686000	8.122000
C	13.479006	16.884991	7.460006
C	16.831996	17.391006	10.872002
C	17.881993	16.262992	10.866009
C	19.120994	16.653005	10.043002
C	18.507993	19.075006	10.517006
C	14.901996	18.838004	7.487001
C	12.877991	14.132002	10.098007
C	13.049994	17.263000	6.184992
C	13.523003	18.415003	5.542010
C	11.786008	14.037002	11.122999
C	13.014000	18.761996	4.166999
H	12.421007	17.329990	10.046008
H	11.838007	15.652001	6.075001
H	10.679992	14.858995	9.649007
H	18.441003	15.793008	8.329996
H	18.051009	17.388996	8.478010
H	14.465995	18.023995	10.236008
H	15.315998	15.207003	9.417997
H	14.830009	15.753990	11.002000
H	13.394996	14.750000	7.591995
H	11.860005	15.518002	7.901999
H	16.002996	17.129000	11.531009
H	18.177006	16.045997	11.894008
H	17.440995	15.342993	10.475996
H	12.060995	14.620002	12.002008
H	11.645001	12.995008	11.407004
Zn	1.746318	12.960757	5.099787
Zn	1.607303	10.777729	7.441760
O	3.774688	11.428734	22.280135
O	2.123657	12.749754	22.257142
C	2.995677	12.137749	21.684136
C	3.144668	12.238742	20.195152
C	4.158671	11.521743	19.569152
H	4.730681	10.991738	20.074152
C	2.288672	13.032744	19.441164
H	1.610653	13.512760	19.858153
Zn	3.852668	10.674727	5.103616
Zn	3.975678	12.955741	7.263764
O	5.873686	12.544744	6.799773
O	5.739687	10.788738	5.380785
O	19.114791	12.557744	4.935786
O	19.076806	10.958731	6.478780
O	4.030683	12.758753	9.141747
O	2.182664	11.649730	9.045751
O	3.237676	8.795711	5.107790
O	1.782657	8.894712	6.308768
O	2.866675	11.879744	6.220775
N	11.988740	11.345738	6.189778
N	3.652674	12.457747	15.937691
N	1.883668	2.418670	5.066780
C	6.235689	11.634739	6.088786
C	7.732714	11.529746	6.092768
C	8.401715	10.560734	5.352775
H	7.918713	9.953726	4.838795

C	9.789726	10.499737	5.382776
H	10.237731	9.850724	4.887789
C	10.508735	11.404745	6.151775
C	9.840730	12.373737	6.891767
H	10.323732	12.980745	7.405767
C	8.452719	12.436744	6.860771
H	8.004714	13.085758	7.355759
C	12.867748	11.981733	5.568775
H	12.536741	12.609743	4.966783
C	17.117781	11.801746	5.688779
C	16.476770	12.693754	4.836785
H	16.976774	13.254755	4.289798
C	15.086769	12.745753	4.803797
H	14.657757	13.342748	4.233798
C	14.339769	11.906740	5.621789
C	14.981756	11.014732	6.472768
H	14.481752	10.453730	7.021765
C	16.371777	10.962732	6.506770
H	16.800789	10.365737	7.076770
C	18.617793	11.766748	5.704785
C	4.315683	11.599742	18.162666
H	4.995693	11.119726	17.743666
C	3.459668	12.393744	17.409673
C	2.446661	13.110743	18.034678
H	1.872660	13.641762	17.529677
C	2.705661	11.894735	15.348698
H	2.004668	11.468729	15.788700
C	3.010668	12.124749	11.075729
C	3.992679	12.706753	11.871722
H	4.711688	13.143750	11.475736
C	3.898675	12.634747	13.255712
H	4.554676	13.022750	13.786713
C	2.822679	11.981733	13.845700
C	1.841663	11.399728	13.052713
H	1.121658	10.962732	13.446708
C	1.935667	11.471735	11.666732
H	1.278651	11.083732	11.135731
C	3.087671	12.187738	9.640736
C	2.412658	8.096709	5.653781
C	2.255665	6.610692	5.514785
C	1.255658	5.935699	6.204769
H	0.675645	6.404706	6.759778
C	1.125660	4.558678	6.065773
H	0.455644	4.106671	6.526778
C	1.992664	3.857684	5.235777
C	2.992671	4.533693	4.545793
H	3.572684	4.066677	3.989788
C	3.122669	5.912686	4.685785
H	3.792685	6.363696	4.222789
C	2.755669	1.996665	5.855785
H	3.293677	2.542676	6.380774
C	2.820668	0.547657	5.848778
H	4.301688	0.409656	7.218772
H	1.365668	0.224653	4.482785
O	3.895688	-4.253728	6.622773
O	2.287658	-4.213733	5.131779
C	3.740686	-0.089352	6.672762
C	3.819680	-1.478358	6.681779
H	4.436682	-1.904365	7.233763
C	2.979672	-2.228364	5.866775
C	2.059654	-1.589364	5.042791
H	1.497657	-2.090363	4.497795
C	1.980659	-0.202349	5.033792
C	3.086676	-3.723379	5.895780
Zn	1.746318	-6.184743	5.099787
Zn	1.746318	12.960757	24.245287
Zn	20.891818	12.960757	5.099787
Zn	20.752803	10.777729	7.441760
O	3.774688	11.428734	3.134635
O	2.123657	12.749754	3.111642
Zn	3.852668	10.674727	24.249116
Zn	3.975678	-6.189759	7.263764
O	-0.030709	12.557744	4.935786
O	-0.068694	10.958731	6.478780
O	3.895688	14.891772	6.622773
O	2.287658	14.931767	5.131779

458

dox_car_nuig_4

H	19.414494	16.117007	-0.155500
O	13.883991	19.424507	6.263010
O	11.744003	20.271504	6.420003
O	12.703997	23.645497	5.460009
N	14.830009	22.070492	6.301990
C	12.909007	19.855492	7.140008
C	13.425992	21.015498	8.012009
C	13.678005	22.280499	7.173991
C	12.436993	22.601492	6.322993
C	11.965995	21.368503	5.528991
C	10.688990	21.676497	4.804008
H	13.436006	23.473493	4.801998
H	15.644994	21.866497	6.862992
H	14.646001	21.295501	5.680010
H	12.691992	21.230502	8.790005
H	14.339003	20.715508	8.530009
H	13.933004	23.124509	7.816993
H	11.625990	22.939506	6.969000
H	12.697008	21.092502	4.765009
H	10.851995	22.512504	4.123003
H	10.371998	20.801490	4.236995
H	9.917005	21.941509	5.525008
C	15.073999	19.362495	-2.513498
H	14.176994	19.965502	-2.656496
H	15.948010	19.933510	-2.824497
O	14.625994	15.565004	7.738994

O	13.912001	18.885006	3.769998
O	18.367006	15.816997	4.854992
O	16.821007	17.107002	9.939003
O	15.691996	14.033996	9.443001
O	14.572999	18.938997	1.321001
O	18.992011	15.894996	2.393992
C	14.280992	18.113998	6.432007
C	15.535003	16.571005	7.995008
C	14.849001	17.933992	7.852010
C	16.728993	16.455998	7.028007
C	15.268996	17.716001	5.332003
C	16.402007	16.922995	5.608004
C	15.033008	18.121005	4.015998
C	15.998995	16.365995	9.405993
C	17.258003	16.583009	4.558007
C	15.888008	17.777994	2.957999
C	17.028008	16.990004	3.235992
C	15.392006	15.195994	10.122992
C	15.573007	18.251003	1.563000
C	17.992003	16.584004	2.153007
C	16.536007	17.845004	0.476991
C	17.677002	17.057990	0.757989
H	14.228993	15.577009	6.821006
H	13.352991	19.086991	4.573994
H	18.463001	15.566000	5.817992
H	16.242008	14.158002	8.615992
H	13.380005	17.508005	6.318991
H	15.565004	18.730004	8.069005
H	14.050002	18.035999	8.587006
H	17.560999	17.055998	7.403010
H	17.081002	15.423998	7.013992
H	12.655003	18.998003	7.766008
H	14.309998	15.319999	10.171009
H	15.795995	15.139993	11.132993
O	15.194003	19.024003	-1.181507
C	16.297990	18.256000	-0.871503
C	18.528996	16.718004	-0.329494
C	17.155995	17.907992	-1.905494
C	18.273001	17.137003	-1.628497
H	16.952996	18.234997	-2.917506
H	18.947995	16.860006	-2.426501
H	15.000997	18.454003	-3.113499
O	9.064992	20.131493	20.040495
H	9.064992	19.473501	20.794502
O	10.802006	20.414502	14.222005
O	8.628992	22.349499	18.856001
O	10.367001	22.639496	13.050990
C	9.611003	19.667502	18.833007
C	10.220002	20.008503	16.514008
C	9.659996	20.508506	17.711004
C	10.311000	20.852494	15.268996
C	9.120993	21.911508	17.807995
C	9.771997	22.257505	15.363996
C	9.210996	22.754503	16.563002
C	9.827002	23.092498	14.237991
C	8.729008	24.069493	16.577993
C	9.343004	24.392497	14.274004
C	8.794007	24.878505	15.449997
C	10.362004	23.556508	12.020004
H	8.291993	24.487497	17.477008
H	9.395003	25.020507	13.394996
H	8.414007	25.889502	15.489992
H	10.807003	23.108504	11.132993
H	9.335997	23.852498	11.803009
H	10.938992	24.434502	12.311992
O	12.202997	16.597004	20.255499
O	9.408003	14.814999	21.278500
O	12.022991	16.218000	22.746501
C	10.885002	16.239998	20.051503
C	9.991003	17.492994	20.098506
C	10.526004	15.314007	21.173506
C	11.622008	15.034999	22.160495
H	12.582001	17.223005	19.572502
H	11.537997	17.033005	22.429508
H	8.947994	17.193004	20.220501
H	10.242000	18.080991	20.981496
H	12.466994	14.578992	21.644505
H	11.255008	14.356004	22.928498
O	10.856992	15.859998	16.318992
O	12.206998	14.638994	14.901996
O	9.653008	14.256007	12.340002
O	11.256999	18.181007	15.338992
N	8.648999	14.966995	14.828994
C	11.209001	16.434995	17.522000
C	10.747997	15.525009	18.674999
C	10.646008	17.854998	17.612998
C	10.095001	18.356993	18.811009
C	11.403998	14.614009	16.085992
C	10.302998	13.545996	15.949006
C	9.463008	13.764006	14.679008
C	10.387008	13.915007	13.458999
C	11.485003	14.965999	13.709997
C	10.701990	18.691005	16.494997
C	12.438008	15.004998	12.553992
H	9.162002	15.124007	12.405997
H	11.577992	17.237000	15.405005
H	8.038008	14.862996	15.626997
H	9.251010	15.767008	14.966995
H	12.298993	16.498003	17.519990
H	9.707994	15.228005	18.519997
H	11.329005	14.601009	18.674004
H	12.041007	14.391002	16.943002
H	10.765993	12.559008	15.916994
H	9.662006	13.553004	16.832992
H	8.762991	12.939008	14.533004
H	10.856992	12.957004	13.234001

H	11.054995	15.967002	13.791997
H	11.894008	15.254005	11.642991
H	13.203005	15.760001	12.738994
H	12.910998	14.031009	12.439004
O	19.263494	5.043997	16.062998
O	19.920491	6.563001	11.631006
O	21.561490	7.550009	16.753997
O	21.633496	4.254992	16.439992
C	19.666506	6.356000	15.914008
C	19.920491	6.658996	14.426000
C	20.944507	6.489999	16.688003
C	21.417496	5.244010	17.376992
H	20.683496	6.463004	12.271002
H	21.445506	4.520004	15.493994
H	20.498493	7.581005	14.334006
H	20.540499	5.869991	13.998998
H	20.661498	4.912008	18.087998
H	22.347508	5.452007	17.905006
H	16.469993	9.466990	19.187505
O	16.382000	8.096996	16.127997
O	14.699991	7.989992	17.702006
O	13.487009	11.356996	17.048991
O	15.043002	7.393992	14.073991
O	13.942002	7.495999	11.788995
O	18.778002	6.670005	9.365998
O	12.786992	7.606009	9.516998
N	16.058997	10.888008	16.113006
C	17.252010	7.090995	15.760997
C	18.596005	7.292004	16.484007
C	17.388001	7.041007	14.237991
C	18.632994	6.818000	13.613006
C	16.101997	8.161995	17.478004
C	16.566008	9.505990	18.071993
C	15.738003	10.678996	17.521004
C	14.236996	10.377991	17.670990
C	13.881004	8.994996	17.095993
C	16.251007	7.189997	13.438992
C	18.687999	6.769006	12.219003
C	16.301991	7.137998	12.038997
C	17.551005	6.922994	11.412996
C	12.439999	8.679000	17.362001
C	15.034999	7.309005	11.239998
C	17.685005	6.856004	9.914995
C	15.167008	7.242992	9.741001
C	16.417994	7.029002	9.117011
C	14.024002	7.396002	8.942002
C	16.465992	6.978994	7.717991
C	14.093003	7.344003	7.556997
C	15.319999	7.133996	6.947998
C	11.744003	7.742000	8.623995
H	18.412993	4.806995	15.592995
H	13.640001	11.445008	16.066004
H	15.087994	7.418996	15.072008
H	17.043994	11.092003	16.017010
H	15.834994	10.053991	15.588994
H	16.792997	6.157997	16.094990
H	18.921995	8.329996	16.380009
H	18.471004	7.120001	17.553992
H	16.641996	7.337992	17.945996
H	17.626994	9.659996	17.866006
H	15.997999	11.607993	18.034008
H	13.959999	10.406996	18.726003
H	14.006005	8.978991	16.010999
H	11.809997	9.440991	16.901992
H	12.197005	7.703000	16.939996
H	12.262999	8.663990	18.437002
H	17.405002	6.817004	7.202001
H	13.199003	7.464007	6.959006
H	15.385994	7.090995	5.869991
H	10.815006	7.901999	9.171001
H	11.933007	8.592998	7.970999
H	11.658997	6.835001	8.023994
O	17.954995	2.262998	13.718995
O	17.796010	2.814006	10.819007
C	16.563997	3.216999	11.150990
O	15.970008	4.020000	10.441994
C	16.701998	2.734992	13.687999
O	16.203009	3.212002	14.699991
C	15.912993	2.569001	12.380993
C	15.550990	1.053003	12.111003
C	14.400001	2.877990	12.522995
C	14.049006	1.391993	12.257007
Pt	18.838004	1.593997	12.037006
H	14.145997	3.247996	13.523003
H	14.050002	3.584995	11.762995
H	13.463001	1.211010	11.347002
H	13.558001	0.876002	13.092995
H	15.859998	0.698007	11.118998
H	15.954998	0.365009	12.865010
N	19.691491	1.062996	10.193007
H	19.491497	0.103003	9.899008
H	19.191507	1.709004	9.561990
H	20.698506	1.230998	10.105990
N	19.872493	0.441993	13.455993
H	19.455504	0.800990	14.330005
H	20.884505	0.587001	13.490991
H	19.684503	-0.563490	13.398002
H	5.821993	19.812510	10.069997
O	9.801003	17.672005	8.972998
O	6.969996	16.834006	9.132001
C	7.308010	16.138010	8.040000
O	6.668990	15.138998	7.729000
C	9.784001	16.870000	7.901003
O	10.825000	16.368005	7.495999
C	8.445999	16.688998	7.170009
C	8.009999	18.014001	6.422990

C	8.575997	15.988005	5.793007
C	8.148995	17.287008	5.064999
Pt	8.083000	18.402004	9.732002
N	6.218994	18.977000	10.508008
H	9.602004	15.655007	5.595004
H	7.884002	15.143995	5.691995
H	7.209008	17.215002	4.503002
H	8.912996	17.720998	4.405992
H	6.995995	18.347994	6.678008
H	8.700002	18.853991	6.580998
H	5.644993	18.162991	10.238994
H	6.178004	19.088006	11.524997
N	9.404002	19.920491	10.331008
H	10.298996	19.541506	9.981009
H	9.236995	20.824503	9.879997
H	9.482000	20.066494	11.341009
C	5.180006	20.354500	16.303006
C	5.786995	20.331506	14.879997
H	5.116003	20.723491	14.105007
H	6.749995	20.853508	14.801003
H	4.150993	20.732509	16.369996
H	5.785004	20.862507	17.064997
O	5.905008	18.505006	18.727994
O	3.191995	18.291994	17.572008
C	3.889006	18.130004	16.439992
O	3.383010	17.547004	15.488997
C	6.261000	18.316998	17.451008
O	7.366001	17.858999	17.185001
C	5.279008	18.775992	16.364003
C	5.886992	18.784990	14.938008
H	6.904997	18.380005	14.919992
H	5.259001	18.247997	14.218004
Pt	4.048010	19.135008	19.217506
N	2.042997	19.652492	19.570492
H	1.855007	20.657497	19.520503
H	1.636002	19.283501	20.434509
H	1.587009	19.194493	18.736992
N	5.095996	19.892500	20.872501
H	6.045996	19.544492	20.669501
H	5.126993	20.914506	20.917493
H	4.801998	19.532507	21.784497
O	6.650994	9.585003	2.210003
C	6.294007	7.060994	0.495007
O	5.708001	6.062001	0.097010
C	6.425000	8.368000	2.721992
O	5.925992	8.255999	3.834997
C	6.892993	7.155994	1.904996
C	8.471003	7.055997	1.869003
C	6.852998	5.820002	2.692010
C	8.399992	5.725002	2.654007
Pt	7.349000	9.791009	0.332002
N	8.105994	11.555994	1.183000
H	6.416002	5.941002	3.688993
H	6.321997	5.034003	2.143990
H	8.796993	4.863991	2.102004
H	8.889007	5.763006	3.635998
H	8.883991	6.983991	0.854004
H	8.975008	7.883006	2.387004
H	7.724003	11.482992	2.138993
H	9.127004	11.587010	1.243998
H	7.773992	12.427995	0.760995
O	6.502003	8.090008	-0.364492
N	7.937992	9.871994	-1.710497
H	8.946998	9.782010	-1.855505
H	7.478003	9.023006	-2.074492
H	7.599998	10.682002	-2.238492
O	6.981005	5.528991	9.072995
O	5.525008	7.487997	10.742004
C	4.900004	6.381999	11.166000
O	4.360005	6.368999	12.266005
C	6.174003	4.668994	9.706998
O	6.498002	3.493001	9.817008
C	4.817008	5.195993	10.194998
C	3.847997	5.509998	8.985002
C	3.842004	4.080997	10.652997
C	2.893995	4.391001	9.465995
Pt	6.527007	7.490007	8.994001
N	6.014999	9.524006	9.110003
N	7.655003	7.320990	7.231006
H	4.309997	3.090007	10.631994
H	3.427006	4.278005	11.648007
H	1.896994	4.749999	9.752009
H	2.772996	3.571000	8.744994
H	3.432003	6.524997	9.007000
H	4.307010	5.345998	8.001000
H	5.358002	9.831999	8.386993
H	5.531001	9.543993	10.021004
H	7.927003	6.325999	7.275998
H	7.115999	7.470995	6.373001
H	6.801994	10.177997	9.140004
H	8.502995	7.893000	7.192007
O	15.640993	6.606002	1.840993
C	16.845991	6.022006	1.852002
O	17.815998	6.630010	2.287007
C	16.930002	4.559999	1.391993
C	16.239002	3.588001	2.430004
C	18.290002	3.885005	1.704007
C	17.609993	2.934010	2.721992
Pt	14.058005	5.672008	1.014999
N	13.065004	6.865998	2.427994
H	18.721006	3.397005	0.823008
H	19.012994	4.589004	2.132005
H	17.945001	3.051008	3.760004
H	17.656995	1.868007	2.461001
H	15.774992	4.109007	3.277997
H	15.487006	2.926007	1.978994

H	12.604995	6.337007	3.174994
H	13.863008	7.379001	2.835008
H	12.397994	7.543997	2.046003
O	15.164002	4.644009	-0.346495
C	16.428007	4.307010	-0.065497
O	17.116996	3.751006	-0.913508
H	12.026992	3.971006	0.568009
N	12.526001	4.659996	-0.031494
H	13.074998	4.154995	-0.744492
H	11.839998	5.254999	-0.503508
Zn	1.746318	12.960757	5.099787
Zn	1.607303	10.777729	7.441760
O	3.774688	11.428734	22.280135
O	2.123657	12.749754	22.257142
C	2.995677	12.137749	21.684136
C	3.144668	12.238742	20.195152
C	4.158671	11.521743	19.569152
H	4.730681	10.991738	20.074152
C	2.288672	13.032744	19.441164
H	1.610653	13.512760	19.858153
Zn	3.852668	10.674727	5.103616
Zn	3.975678	12.955741	7.263764
O	5.873686	12.544744	6.799773
O	5.739687	10.788738	5.380785
O	19.114791	12.557744	4.935786
O	19.076806	10.958731	6.478780
O	4.030683	12.758753	9.141747
O	2.182664	11.649730	9.045751
O	3.237676	8.795711	5.107790
O	1.782657	8.894712	6.308768
O	2.866675	11.879744	6.220775
N	11.988740	11.345738	6.189778
N	3.652674	12.457747	15.937691
N	1.883668	2.418670	5.066780
C	6.235689	11.634739	6.088786
C	7.732714	11.529746	6.092768
C	8.401715	10.560734	5.352775
H	7.918713	9.953726	4.838795
C	9.789726	10.499737	5.382776
H	10.237731	9.850724	4.887789
C	10.508735	11.404745	6.151775
C	9.840730	12.373737	6.891767
H	10.323732	12.980745	7.405767
C	8.452719	12.436744	6.860771
H	8.004714	13.085758	7.355759
C	12.867748	11.981733	5.568775
H	12.536741	12.609743	4.966783
C	17.117781	11.801746	5.688779
C	16.476770	12.693754	4.836785
H	16.976774	13.254755	4.289798
C	15.086769	12.745753	4.803797
H	14.657757	13.342748	4.233798
C	14.339769	11.906740	5.621789
C	14.981756	11.014732	6.472768
H	14.481752	10.453730	7.021765
C	16.371777	10.962732	6.506770
H	16.800789	10.365737	7.076770
C	18.617793	11.766748	5.704785
C	4.315683	11.599742	18.162666
H	4.995693	11.119726	17.743666
C	3.459668	12.393744	17.409673
C	2.446661	13.110743	18.034678
H	1.872660	13.641762	17.529677
C	2.705661	11.894735	15.348698
H	2.004668	11.468729	15.788700
C	3.010668	12.124749	11.075729
C	3.992679	12.706753	11.871722
H	4.711688	13.143750	11.475736
C	3.898675	12.634747	13.255712
H	4.554676	13.022750	13.786713
C	2.822679	11.981733	13.845700
C	1.841663	11.399728	13.052713
H	1.121658	10.962732	13.446708
C	1.935667	11.471735	11.666732
H	1.278651	11.083732	11.135731
C	3.087671	12.187738	9.640736
C	2.412658	8.096709	5.653781
C	2.255665	6.610692	5.514785
C	1.255658	5.935699	6.204769
H	0.675645	6.404706	6.759778
C	1.125660	4.558678	6.065773
H	0.455644	4.106671	6.526778
C	1.992664	3.857684	5.235777
C	2.992671	4.533693	4.545793
H	3.572684	4.066677	3.989788
C	3.122669	5.912686	4.685785
H	3.792685	6.363696	4.222789
C	2.755669	1.996665	5.855785
H	3.293677	2.542676	6.380774
C	2.820668	0.547657	5.848778
H	4.301688	0.409656	7.218772
H	1.365668	0.224653	4.482785
O	3.895688	-4.253728	6.622773
O	2.287658	-4.213733	5.131779
C	3.740686	-0.089352	6.672762
C	3.819680	-1.478358	6.681779
H	4.436682	-1.904365	7.233763
C	2.979672	-2.228364	5.866775
C	2.059654	-1.589364	5.042791
H	1.497657	-2.090363	4.497795
C	1.980659	-0.202349	5.033792
C	3.086676	-3.723379	5.895780
Zn	1.746318	-6.184743	5.099787
Zn	1.746318	12.960757	24.245287
Zn	20.891818	12.960757	5.099787
Zn	20.752803	10.777729	7.441760

O 3.774688 11.428734 3.134635
O 2.123657 12.749754 3.111642
Zn 3.852668 10.674727 24.249116
Zn 3.975678 -6.189759 7.263764
O -0.030709 12.557744 4.935786
O -0.068694 10.958731 6.478780
O 3.895688 14.891772 6.622773
O 2.287658 14.931767 5.131779

330
pal_nuig_4
C 9.944000 5.583996 9.309002
C 8.885005 5.690004 8.159008
O 7.626993 5.721001 8.726002
C 7.055997 6.917997 8.438992
O 7.612997 7.788006 7.779008
C 5.685007 6.973002 9.046000
C 4.899008 8.108004 8.886996
C 3.630006 8.157993 9.448993
C 3.147003 7.073994 10.173000
C 3.933003 5.940006 10.332003
C 5.202005 5.889003 9.769011
C 8.847002 4.558007 7.080006
O 7.759001 4.844999 6.279992
C 8.609999 3.122995 7.665992
C 9.775999 2.102004 7.464007
O 9.722008 1.119993 8.432999
C 8.531005 0.476991 8.329001
O 7.682993 0.767007 7.491998
C 11.110995 2.832002 7.513001
C 12.215001 2.288998 8.371006
C 11.253993 4.042994 6.940990
C 12.435998 4.948997 7.236999
O 13.173004 5.126993 6.084000
C 14.433007 4.672995 6.303005
C 15.250999 4.857998 5.059007
O 14.798993 4.196004 7.370998
C 11.978995 6.322993 7.759001
O 12.206998 7.332995 7.089004
C 11.243999 6.450004 9.119002
C 10.820998 7.888003 9.171001
C 12.250995 6.225006 10.273992
O 13.427007 6.912004 10.056997
C 11.646993 6.692003 11.605007
C 10.277994 6.049997 11.914991
O 9.348001 7.118010 12.396998
C 8.663990 7.111998 11.063993
C 9.331000 5.768999 10.730000
O 8.485994 4.706002 10.973990
C 8.152001 4.714005 12.289994
C 7.232998 3.565007 12.577004
O 8.563993 5.554990 13.082005
C 10.077004 4.602004 6.148003
C 9.849000 3.750010 4.935002
C 10.319003 5.987008 5.626996
H 10.283010 4.550005 9.342008
H 8.971007 6.662002 7.671008
H 5.275006 8.951995 8.323008
H 3.018001 9.041998 9.325007
H 2.159000 7.112994 10.610991
H 3.557004 5.095000 10.896010
H 5.813991 5.004997 9.892997
H 7.249999 5.666991 6.538992
H 8.397006 3.198007 8.734005
H 7.699995 2.695993 7.239009
H 9.685996 1.596007 6.502003
H 11.930997 1.305991 8.748996
H 13.126002 2.199990 7.779008
H 12.390010 2.962996 9.208009
H 13.097992 4.496991 7.975001
H 14.633997 5.310004 4.283002
H 16.097996 5.506992 5.275006
H 15.613998 3.889006 4.715996
H 10.288007 8.075993 10.103004
H 11.701002 8.527999 9.119997
H 10.164997 8.104003 8.328005
H 12.522995 5.168998 10.341997
H 14.248005 6.343000 10.008999
H 12.337992 6.498002 12.426004
H 11.541003 7.777993 11.566007
H 10.366006 5.253008 12.655999
H 7.581005 7.099994 11.199007
H 8.995992 7.979998 10.488996
H 7.056993 3.001995 11.659992
H 7.689005 2.911992 13.321994
H 6.285008 3.943992 12.958000
H 9.008992 4.146992 4.365002
H 10.743995 3.756002 4.313003
H 9.628004 2.728004 5.245005
H 9.442005 6.324008 5.073002
H 10.501996 6.662998 6.462008
H 11.184993 5.980997 4.965998
C 8.451992 -0.595502 9.373005
O 9.720994 -1.067496 9.646001
C 7.598007 -1.721506 8.871010
N 8.185008 -2.271499 7.651997
C 7.685999 -3.283492 6.940990
O 6.653004 -3.869497 7.249003
C 8.536998 -3.596501 5.746005
C 7.998990 -4.305497 4.676997
C 8.787000 -4.595494 3.570004
C 10.112002 -4.178505 3.531005
C 10.648995 -3.470505 4.598998
C 9.862000 -3.179493 5.707006
C 7.518993 -2.794496 9.915991

C	8.455993	-3.820504	9.931001
C	8.384006	-4.815495	10.899993
C	7.374004	-4.783503	11.853994
C	6.436009	-3.756500	11.839003
C	6.509011	-2.762504	10.869992
H	8.014996	-0.185501	10.284005
H	10.362004	-0.380498	9.987997
H	6.597003	-1.349490	8.656006
H	9.029994	-1.762496	7.435997
H	6.967009	-4.630492	4.707993
H	8.368996	-5.147497	2.737998
H	10.725998	-4.405494	2.668998
H	11.681991	-3.144495	4.568997
H	10.280004	-2.627509	6.538992
H	9.243007	-3.845508	9.188002
H	9.113009	-5.613499	10.911001
H	7.317008	-5.557498	12.607005
H	5.649990	-3.731496	12.582001
H	5.778993	-1.964501	10.859002
C	19.611501	9.090992	19.697503
C	19.986504	9.170005	21.034491
H	21.008510	9.408999	21.295501
H	19.340497	8.999993	23.073506
C	19.694497	7.119005	17.235009
O	19.396498	6.282998	18.083001
C	20.816500	6.990003	16.248001
C	21.342504	5.737007	15.954998
C	22.382506	5.617998	15.040992
C	22.895510	6.749995	14.420008
C	22.369506	8.001996	14.713010
C	21.329504	8.122995	15.626997
H	19.246493	8.984007	16.405990
H	20.942497	4.856007	16.438996
H	22.792507	4.641999	14.811993
H	23.705499	6.656010	13.708006
H	22.769494	8.885005	14.228993
H	20.919503	9.097999	15.855997
H	20.341500	9.270002	18.890999
H	19.986504	14.650003	9.334006
C	18.298005	8.783994	19.360504
C	19.047992	8.940010	22.033503
C	17.734994	8.632993	21.696504
C	17.359991	8.553999	20.360493
H	17.003999	8.453006	22.474500
H	16.338004	8.315006	20.098506
C	13.856000	13.542991	13.496008
C	13.497999	12.175006	12.820995
O	12.531993	11.551993	13.584996
C	11.403002	11.438000	12.841002
O	11.314990	11.839998	11.685992
C	10.338991	10.761992	13.653001
C	9.084004	10.532993	13.100998
C	8.097991	9.905997	13.853990
C	8.367005	9.509991	15.160000
C	9.620997	9.740005	15.711008
C	10.607009	10.366006	14.957996
C	14.639989	11.125010	12.624007
O	14.020996	9.994008	12.129000
C	15.357008	10.701990	13.952992
C	16.874001	11.066003	14.055994
O	17.250995	11.161999	15.380001
C	17.029003	9.965003	15.980002
O	16.566008	8.994996	15.389995
C	17.432992	10.048994	17.421007
O	18.462006	10.958999	17.557993
C	17.893001	8.700998	17.889996
N	19.034992	8.269994	17.089005
C	17.137003	12.375996	13.325000
C	17.933992	13.449005	14.004991
C	16.521992	12.647996	12.159001
C	16.486994	14.045005	11.563001
O	17.168995	14.045005	10.363000
C	18.195998	14.927000	10.450992
C	18.951001	14.942010	9.154995
O	18.428999	15.587998	11.456993
C	15.043002	14.520005	11.321998
O	14.656991	14.724996	10.168003
C	14.075006	14.752010	12.511010
C	12.753009	15.025005	11.857000
C	14.486998	16.036003	13.270991
O	14.768992	17.068003	12.398990
C	13.359998	16.482993	14.210996
C	12.897998	15.375004	15.182994
O	11.402007	15.357008	15.208994
C	11.411005	14.127005	14.353994
C	12.901004	13.920999	14.667999
O	13.084992	13.005998	15.683994
C	12.461997	13.467002	16.797994
C	12.650006	12.484991	17.915000
O	11.848997	14.528007	16.834006
C	15.648996	11.560991	11.540008
C	16.514008	10.405005	11.131998
C	14.951008	12.002008	10.289002
H	14.805005	13.410006	14.012994
H	12.996004	12.357003	11.869999
H	8.874992	10.839991	12.085999
H	7.120996	9.727005	13.424997
H	7.599002	9.023006	15.746006
H	9.831004	9.431992	16.727002
H	11.584004	10.544997	15.387009
H	13.031997	10.073998	12.005990
H	14.836997	11.145993	14.802994
H	15.250003	9.625994	14.102997
H	17.491003	10.284005	13.611991
H	16.580999	10.371002	18.019993
H	18.243000	11.891002	17.267997

H	17.081002	7.982008	17.781996
H	18.359003	13.056006	14.928991
H	18.739003	13.777006	13.346998
H	17.284998	14.293992	14.234009
H	16.986002	14.758998	12.216992
H	18.490992	14.240997	8.458999
H	18.924006	15.945004	8.730999
H	11.999002	15.200991	12.624007
H	12.837996	15.906005	11.221005
H	12.462993	14.166004	11.252997
H	15.401004	15.864000	13.844992
H	15.696993	17.432992	12.461002
H	13.661999	17.365007	14.776995
H	12.516007	16.806992	13.599010
H	13.299000	15.527996	16.187003
H	10.720006	13.385998	14.757007
H	11.161999	14.404998	13.327010
H	13.242004	11.641000	17.561995
H	13.168007	12.971000	18.742009
H	11.676994	12.129000	18.255005
H	15.894001	9.625994	10.688990
H	17.250000	10.743000	10.401003
H	17.026993	10.007008	12.007005
H	14.347006	11.180991	9.901000
H	14.306992	12.852010	10.513005
H	15.690005	12.292005	9.542998
Zn	1.746318	12.960757	5.099787
Zn	1.607303	10.777729	7.441760
O	3.774688	11.428734	22.280135
O	2.123657	12.749754	22.257142
C	2.995677	12.137749	21.684136
C	3.144668	12.238742	20.195152
C	4.158671	11.521743	19.569152
H	4.730681	10.991738	20.074152
C	2.288672	13.032744	19.441164
H	1.610653	13.512760	19.858153
Zn	3.852668	10.674727	5.103616
Zn	3.975678	12.955741	7.263764
O	5.873686	12.544744	6.799773
O	5.739687	10.788738	5.380785
O	19.114791	12.557744	4.935786
O	19.076806	10.958731	6.478780
O	4.030683	12.758753	9.141747
O	2.182664	11.649730	9.045751
O	3.237676	8.795711	5.107790
O	1.782657	8.894712	6.308768
O	2.866675	11.879744	6.220775
N	11.988740	11.345738	6.189778
N	3.652674	12.457747	15.937691
N	1.883668	2.418670	5.066780
C	6.235689	11.634739	6.088786
C	7.732714	11.529746	6.092768
C	8.401715	10.560734	5.352775
H	7.918713	9.953726	4.838795
C	9.789726	10.499737	5.382776
H	10.237731	9.850724	4.887789
C	10.508735	11.404745	6.151775
C	9.840730	12.373737	6.891767
H	10.323732	12.980745	7.405767
C	8.452719	12.436744	6.860771
H	8.004714	13.085758	7.355759
C	12.867748	11.981733	5.568775
H	12.536741	12.609743	4.966783
C	17.117781	11.801746	5.688779
C	16.476770	12.693754	4.836785
H	16.976774	13.254755	4.289798
C	15.086769	12.745753	4.803797
H	14.657757	13.342748	4.233798
C	14.339769	11.906740	5.621789
C	14.981756	11.014732	6.472768
H	14.481752	10.453730	7.021765
C	16.371777	10.962732	6.506770
H	16.800789	10.365737	7.076770
C	18.617793	11.766748	5.704785
C	4.315683	11.599742	18.162666
H	4.995693	11.119726	17.743666
C	3.459668	12.393744	17.409673
C	2.446661	13.110743	18.034678
H	1.872660	13.641762	17.529677
C	2.705661	11.894735	15.348698
H	2.004668	11.468729	15.788700
C	3.010668	12.124749	11.075729
C	3.992679	12.706753	11.871722
H	4.711688	13.143750	11.475736
C	3.898675	12.634747	13.255712
H	4.554676	13.022750	13.786713
C	2.822679	11.981733	13.845700
C	1.841663	11.399728	13.052713
H	1.121658	10.962732	13.446708
C	1.935667	11.471735	11.666732
H	1.278651	11.083732	11.135731
C	3.087671	12.187738	9.640736
C	2.412658	8.096709	5.653781
C	2.255665	6.610692	5.514785
C	1.255658	5.935699	6.204769
H	0.675645	6.404706	6.759778
C	1.125660	4.558678	6.065773
H	0.455644	4.106671	6.526778
C	1.992664	3.857684	5.235777
C	2.992671	4.533693	4.545793
H	3.572684	4.066677	3.989788
C	3.122669	5.912686	4.685785
H	3.792685	6.363696	4.222789
C	2.755669	1.996665	5.855785
H	3.293677	2.542676	6.380774
C	2.820668	0.547657	5.848778

H 4.301688 0.409656 7.218772
H 1.365668 0.224653 4.482785
O 3.895688 -4.253728 6.622773
O 2.287658 -4.213733 5.131779
C 3.740686 -0.089352 6.672762
C 3.819680 -1.478358 6.681779
H 4.436682 -1.904365 7.233763
C 2.979672 -2.228364 5.866775
C 2.059654 -1.589364 5.042791
H 1.497657 -2.090363 4.497795
C 1.980659 -0.202349 5.033792
C 3.086676 -3.723379 5.895780
Zn 1.746318 -6.184743 5.099787
Zn 1.746318 12.960757 24.245287
Zn 20.891818 12.960757 5.099787
Zn 20.752803 10.777729 7.441760
O 3.774688 11.428734 3.134635
O 2.123657 12.749754 3.111642
Zn 3.852668 10.674727 24.249116
Zn 3.975678 -6.189759 7.263764
O -0.030709 12.557744 4.935786
O -0.068694 10.958731 6.478780
O 3.895688 14.891772 6.622773
O 2.287658 14.931767 5.131779

430
pal_car_nuig_4
C 5.945999 0.600996 0.301006
C 7.020999 0.613001 1.434994
O 7.833994 1.719993 1.308001
C 7.063005 2.833993 1.399000
O 5.849008 2.798000 1.567002
C 7.928994 4.050001 1.264005
O 9.192003 3.773004 1.749994
C 7.330008 5.181002 2.045007
N 7.236999 4.804008 3.453006
C 6.752005 5.571991 4.430001
O 6.321002 6.705999 4.235004
C 6.800999 4.879996 5.759005
C 5.989000 5.315997 6.800003
C 6.035006 4.675006 8.031997
C 6.892993 3.597995 8.224007
C 7.703996 3.161994 7.184004
C 7.659004 3.803005 5.950996
C 8.195997 6.398005 1.909993
C 9.223996 6.623998 2.816992
C 10.027992 7.750998 2.690996
C 9.802994 8.653000 1.658000
C 8.774000 8.427007 0.750006
C 7.970999 7.300007 0.876002
H 5.137006 1.275990 0.584991
H 6.547991 0.682997 2.415990
H 8.000005 4.330999 0.212994
H 9.668994 3.027995 1.285008
H 6.334001 5.398993 1.661006
H 7.599998 3.868004 3.567994
H 5.320994 6.153996 6.649998
H 5.402994 5.013996 8.842005
H 6.928010 3.099006 9.184001
H 8.372997 2.323996 7.332995
H 8.290997 3.463995 5.139992
H 9.400000 5.922009 3.621008
H 10.828006 7.926007 3.397005
H 10.427999 9.530994 1.559994
H 7.171004 7.124002 0.169993
H 9.637998 0.440002 1.658996
C 1.681990 0.389994 -5.653494
C 2.059003 1.727996 -5.674496
C 3.088992 2.172000 -4.854495
C 3.742007 1.278996 -4.013509
O 7.285992 0.718990 -3.141509
C 7.789998 1.385005 -4.211493
C 7.603999 2.858998 -4.012495
O 8.307003 0.821993 -5.169496
H 0.880004 0.043001 -6.291498
H 1.550001 2.422001 -6.329502
H 3.383010 3.213993 -4.870500
H 4.543993 1.626008 -3.374509
H 6.378993 1.057999 -0.619510
H 8.599010 9.128996 -0.082498
H 7.108992 3.036993 -3.056502
H 8.575997 3.351994 -4.015501
H 6.990003 3.260996 -4.818501
C 7.842992 -0.668503 1.376006
C 9.339003 -0.583497 1.426991
C 7.257006 -1.849494 1.102991
C 8.052999 -3.082502 0.708996
O 7.892005 -4.054500 1.674006
C 9.111994 -4.359507 2.185995
C 8.959003 -5.417506 3.238997
O 10.150006 -3.825501 1.810992
C 5.738002 -1.880490 0.971998
C 5.120004 -1.567500 2.301997
C 5.203000 -3.227491 0.587001
H 9.715001 -1.255504 2.199990
H 9.753005 -0.873494 0.462000
H 9.117011 -2.855494 0.652996
H 7.906000 -5.682499 3.336008
H 9.530994 -6.298506 2.953002
H 9.326998 -5.036492 4.191007
H 4.033995 -1.589498 2.213009
H 5.439007 -2.311494 3.034007
H 5.437992 -0.577505 2.628007
H 4.116991 -3.178498 0.510993
H 5.480993 -3.959500 1.345010
C 7.167003 -1.368501 -2.000494

C	5.666991	-1.264503	-1.559497
O	5.030001	-0.362501	-2.387501
C	4.071003	-1.022504	-3.084493
O	3.851002	-2.221491	-2.956506
C	3.364994	-0.058509	-3.992507
C	2.335004	-0.503508	-4.812509
C	5.354996	-0.805489	-0.097508
O	3.981000	-0.689506	-0.030499
C	7.594005	-3.640498	-0.678497
O	7.076004	-4.758499	-0.731492
C	7.782990	-2.816495	-1.979492
C	7.059999	-3.613503	-3.024491
C	9.282006	-2.801504	-2.368509
O	9.843008	-4.057506	-2.257503
C	9.451999	-2.313504	-3.812501
C	8.785008	-0.947492	-4.080500
O	8.036994	-1.025490	-5.373491
C	6.748999	-1.119495	-4.612496
C	7.466994	-0.634501	-3.342498
H	7.754004	-0.788507	-1.290502
H	5.158008	-2.206500	-1.766498
H	2.041006	-1.544506	-4.795507
H	3.497998	-0.908492	-0.878510
H	7.137002	-3.106491	-3.985500
H	7.505993	-4.605507	-3.098508
H	6.010998	-3.707507	-2.746499
H	9.845995	-2.155496	-1.691505
H	10.609000	-4.124496	-1.619499
H	10.509003	-2.264491	-4.076498
H	9.023006	-3.066496	-4.477501
H	9.520004	-0.139494	-4.109505
H	6.010002	-0.443506	-5.043499
H	6.407999	-2.157506	-4.615501
H	5.621999	-3.523500	-0.403491
C	12.184005	6.740001	11.420004
C	11.644006	6.745994	9.948997
O	12.710008	6.557008	9.093002
C	12.529007	5.384997	8.432999
O	11.558004	4.657009	8.609004
C	13.678005	5.160995	7.494008
C	13.716009	4.017990	6.704007
C	14.780996	3.811008	5.834993
C	15.807003	4.745002	5.756994
C	15.768004	5.886992	6.547991
C	14.703993	6.095008	7.417005
C	10.897006	8.021007	9.438004
O	10.648000	7.793999	8.100002
C	11.746990	9.336992	9.521995
C	11.200003	10.443009	10.482008
O	12.228997	11.264006	10.897006
C	12.784006	11.844995	9.801998
O	12.392001	11.635008	8.658993
C	13.904994	12.742996	10.230991
O	13.639005	13.242004	11.490995
C	14.033996	13.880009	9.261999
N	12.786992	14.638994	9.231998
C	12.552996	15.713995	8.479006
O	13.388008	16.187003	7.712994
C	11.168010	16.251007	8.690008
C	10.591999	17.078992	7.733001
C	9.309002	17.577005	7.927998
C	8.602992	17.246994	9.079007
C	9.179999	16.420004	10.034999
C	10.462997	15.921991	9.840998
C	15.155999	14.779005	9.690993
C	14.904006	15.843993	10.547007
C	15.943989	16.676994	10.945999
C	17.233994	16.443993	10.487005
C	17.487002	15.379006	9.631010
C	16.446999	14.546004	9.231998
C	10.517006	9.792004	11.678008
C	10.850004	10.263998	13.061003
C	9.758002	8.691004	11.520001
C	9.333010	7.819999	12.690001
O	7.958995	7.859994	12.811001
C	7.647995	8.347993	14.037998
C	6.156006	8.398997	14.188998
O	8.492006	8.680991	14.862001
C	9.780000	6.360001	12.500997
O	8.929002	5.475996	12.378006
C	11.286004	5.989000	12.472011
C	11.295998	4.537005	12.094997
C	11.873005	6.097995	13.900992
O	11.036998	5.519992	14.834010
C	13.238998	5.402994	13.968997
C	14.237991	5.911001	12.906996
O	14.914995	4.729992	12.284997
C	14.062006	4.896002	11.065008
C	13.678005	6.309993	11.525993
O	14.447003	7.274007	10.907000
C	15.750007	7.050005	11.216008
C	16.603992	8.087997	10.552004
O	16.121009	6.126005	11.930997
C	9.512997	8.187994	10.100993
C	8.691004	9.197000	9.355008
C	8.726002	6.913000	10.052000
H	12.223004	7.776002	11.753997
H	11.023002	5.863999	9.784001
H	12.918005	3.290997	6.763990
H	14.810997	2.922005	5.219006
H	16.636004	4.582992	5.082001
H	16.567003	6.615000	6.488008
H	14.672996	6.983991	8.031997
H	10.976996	6.913995	7.753009
H	12.767004	9.090992	9.823996
H	11.856004	9.769011	8.526008

H	10.479002	11.079999	9.967990
H	14.836001	12.176997	10.255000
H	13.536003	12.549990	12.206003
H	14.244003	13.487009	8.267008
H	12.129995	14.217008	9.873009
H	11.140996	17.335006	6.836992
H	8.859006	18.221002	7.184004
H	7.603999	17.634997	9.231003
H	8.630006	16.163990	10.932004
H	10.912992	15.277994	10.584992
H	13.899001	16.024994	10.903994
H	15.747001	17.504999	11.611995
H	18.044002	17.093007	10.797009
H	18.492007	15.197009	9.274004
H	16.644006	13.717004	8.566003
H	11.467006	11.161999	13.000005
H	9.930005	10.492998	13.599010
H	11.395995	9.483991	13.591008
H	9.749003	8.195997	13.624991
H	5.686003	8.031997	13.276007
H	5.855000	7.775007	15.029007
H	5.843992	9.428010	14.370000
H	12.324992	4.182009	12.047995
H	10.747001	3.963999	12.841997
H	10.824004	4.412004	11.122004
H	11.977004	7.146000	14.192004
H	10.711007	6.135999	15.549994
H	13.673008	5.512009	14.964008
H	13.080991	4.330004	13.838004
H	14.974002	6.592006	13.339991
H	14.676002	4.824991	10.165992
H	13.268999	4.144005	11.079999
H	15.971004	8.769998	9.983000
H	17.150998	8.648003	11.309994
H	17.310002	7.602008	9.878006
H	8.513008	8.842005	8.339990
H	7.736007	9.335001	9.863991
H	9.224991	10.147000	9.318996
H	8.588001	6.611994	9.012993
H	9.265005	6.131997	10.587002
H	7.753009	7.068002	10.517006
O	13.324004	0.050008	19.594500
C	13.285005	2.871997	19.226505
H	12.466994	3.599009	19.294490
H	13.397006	2.345994	20.181501
H	15.501996	3.229003	19.207493
O	11.790010	1.581993	15.950997
C	13.231991	0.414998	18.399993
C	11.887996	2.219002	17.124999
O	11.067994	3.078003	17.425009
C	13.100002	1.894007	18.010000
C	14.442006	2.446010	17.380993
C	14.599995	3.411001	18.579999
Pt	13.050990	0.078994	15.493994
N	12.599998	0.757989	13.558996
H	14.578992	4.472006	18.299996
H	15.225995	1.684000	17.281992
H	14.304005	2.927002	16.403998
H	11.924009	1.507995	13.774996
H	13.394996	1.173006	13.064009
H	12.150002	0.074993	12.944005
O	13.325996	-0.481509	17.409999
N	14.328990	-1.562503	15.202006
H	15.249008	-1.315506	14.826007
H	14.448994	-1.882500	16.175995
H	13.942002	-2.331501	14.647992
O	17.245003	15.795995	3.762991
O	14.720994	15.888008	2.224994
C	15.509999	15.404010	1.257993
O	15.022000	14.766005	0.332998
C	17.716997	15.323005	2.603003
O	18.726003	14.629996	2.590999
C	17.003004	15.758010	1.315009
C	17.244007	17.290990	1.007991
C	17.779009	15.404010	0.021003
Pt	15.515992	16.828990	3.819010
N	13.635999	17.762008	3.761995
N	16.473994	17.659005	5.493993
H	18.683002	14.821010	0.228999
H	16.317001	17.858003	0.851994
H	17.837001	17.804990	1.777009
H	13.669006	18.760005	3.535006
H	13.201990	17.262004	2.970003
H	17.349001	17.111003	5.501000
H	16.713007	18.649000	5.393000
H	13.050990	17.631991	4.593005
H	15.994993	17.525006	6.389007
C	18.013005	16.905993	-0.305505
H	17.151994	14.874005	-0.733502
H	17.544994	17.272994	-1.228490
H	19.064993	17.219999	-0.303494
H	13.088993	12.021996	19.288498
O	13.762992	9.560995	17.123008
O	14.196005	11.333006	14.797002
C	15.168999	10.449997	14.539993
O	15.583001	10.310005	13.394996
C	14.789994	8.899996	16.575006
O	14.945992	7.707997	16.809998
C	15.787992	9.709009	15.734002
C	16.648008	10.683993	16.635008
C	17.082994	8.932008	15.384003
C	17.923002	9.890010	16.266993
Pt	13.415003	11.486994	16.646993
N	13.075994	13.441003	15.958004
N	12.586998	11.447994	18.576994
H	17.046004	7.892005	15.725003

H	17.307991	8.964995	14.310993
H	18.673008	10.480993	15.724008
H	18.412993	9.414991	17.127009
H	16.628001	11.727997	16.295003
H	16.369000	10.661995	17.695994
H	13.613006	14.158997	16.451996
H	13.438992	13.366010	14.995004
H	12.724999	10.454994	18.821003
H	12.094997	13.732991	15.918009
H	11.588005	11.666004	18.634009
C	2.496994	4.646000	19.876494
C	1.364998	5.651005	20.208496
H	2.401994	3.661003	20.348507
H	3.515994	5.026996	20.007507
H	1.705998	6.631006	20.565503
H	0.603007	5.276002	20.904493
O	0.892008	3.226993	16.707991
O	2.721992	5.480993	16.147008
C	3.104002	5.241004	17.406993
O	4.218998	5.581009	17.782991
C	1.502998	3.271009	17.897998
O	1.533995	2.271996	18.607990
C	2.068997	4.621992	18.358007
C	0.914006	5.647004	18.700003
Pt	0.941997	4.818003	15.472991
N	1.192994	6.486993	14.223000
H	1.010002	6.606997	18.176010
H	0.513004	7.236003	14.382999
H	2.120996	6.816009	14.533004
H	1.233008	6.286999	13.220006
H	-0.093507	5.251994	18.515000
N	-0.867502	3.950999	14.853002
H	-0.889500	3.110991	15.453003
H	-1.695506	4.516998	15.057993
H	-0.904491	3.657001	13.873997
Zn	1.746318	12.960757	5.099787
Zn	1.607303	10.777729	7.441760
O	3.774688	11.428734	22.280135
O	2.123657	12.749754	22.257142
C	2.995677	12.137749	21.684136
C	3.144668	12.238742	20.195152
C	4.158671	11.521743	19.569152
H	4.730681	10.991738	20.074152
C	2.288672	13.032744	19.441164
H	1.610653	13.512760	19.858153
Zn	3.852668	10.674727	5.103616
Zn	3.975678	12.955741	7.263764
O	5.873686	12.544744	6.799773
O	5.739687	10.788738	5.380785
O	19.114791	12.557744	4.935786
O	19.076806	10.958731	6.478780
O	4.030683	12.758753	9.141747
O	2.182664	11.649730	9.045751
O	3.237676	8.795711	5.107790
O	1.782657	8.894712	6.308768
O	2.866675	11.879744	6.220775
N	11.988740	11.345738	6.189778
N	3.652674	12.457747	15.937691
N	1.883668	2.418670	5.066780
C	6.235689	11.634739	6.088786
C	7.732714	11.529746	6.092768
C	8.401715	10.560734	5.352775
H	7.918713	9.953726	4.838795
C	9.789726	10.499737	5.382776
H	10.237731	9.850724	4.887789
C	10.508735	11.404745	6.151775
C	9.840730	12.373737	6.891767
H	10.323732	12.980745	7.405767
C	8.452719	12.436744	6.860771
H	8.004714	13.085758	7.355759
C	12.867748	11.981733	5.568775
H	12.536741	12.609743	4.966783
C	17.117781	11.801746	5.688779
C	16.476770	12.693754	4.836785
H	16.976774	13.254755	4.289798
C	15.086769	12.745753	4.803797
H	14.657757	13.342748	4.233798
C	14.339769	11.906740	5.621789
C	14.981756	11.014732	6.472768
H	14.481752	10.453730	7.021765
C	16.371777	10.962732	6.506770
H	16.800789	10.365737	7.076770
C	18.617793	11.766748	5.704785
C	4.315683	11.599742	18.162666
H	4.995693	11.119726	17.743666
C	3.459668	12.393744	17.409673
C	2.446661	13.110743	18.034678
H	1.872660	13.641762	17.529677
C	2.705661	11.894735	15.348698
H	2.004668	11.468729	15.788700
C	3.010668	12.124749	11.075729
C	3.992679	12.706753	11.871722
H	4.711688	13.143750	11.475736
C	3.898675	12.634747	13.255712
H	4.554676	13.022750	13.786713
C	2.822679	11.981733	13.845700
C	1.841663	11.399728	13.052713
H	1.121658	10.962732	13.446708
C	1.935667	11.471735	11.666732
H	1.278651	11.083732	11.135731
C	3.087671	12.187738	9.640736
C	2.412658	8.096709	5.653781
C	2.255665	6.610692	5.514785
C	1.255658	5.935699	6.204769
H	0.675645	6.404706	6.759778
C	1.125660	4.558678	6.065773

H	0.455644	4.106671	6.526778
C	1.992664	3.857684	5.235777
C	2.992671	4.533693	4.545793
H	3.572684	4.066677	3.989788
C	3.122669	5.912686	4.685785
H	3.792685	6.363696	4.222789
C	2.755669	1.996665	5.855785
H	3.293677	2.542676	6.380774
C	2.820668	0.547657	5.848778
H	4.301688	0.409656	7.218772
H	1.365668	0.224653	4.482785
O	3.895688	-4.253728	6.622773
O	2.287658	-4.213733	5.131779
C	3.740686	-0.089352	6.672762
C	3.819680	-1.478358	6.681779
H	4.436682	-1.904365	7.233763
C	2.979672	-2.228364	5.866775
C	2.059654	-1.589364	5.042791
H	1.497657	-2.090363	4.497795
C	1.980659	-0.202349	5.033792
C	3.086676	-3.723379	5.895780
Zn	1.746318	-6.184743	5.099787
Zn	1.746318	12.960757	24.245287
Zn	20.891818	12.960757	5.099787
Zn	20.752803	10.777729	7.441760
O	3.774688	11.428734	3.134635
O	2.123657	12.749754	3.111642
Zn	3.852668	10.674727	24.249116
Zn	3.975678	-6.189759	7.263764
O	-0.030709	12.557744	4.935786
O	-0.068694	10.958731	6.478780
O	3.895688	14.891772	6.622773
O	2.287658	14.931767	5.131779

438

pal_gem_nuig-4

Zn	1.746318	12.960757	5.099787
Zn	1.607303	10.777729	7.441760
O	3.774688	11.428734	22.280135
O	2.123657	12.749754	22.257142
C	2.995677	12.137749	21.684136
C	3.144668	12.238742	20.195152
C	4.158671	11.521743	19.569152
H	4.730681	10.991738	20.074152
C	2.288672	13.032744	19.441164
H	1.610653	13.512760	19.858153
Zn	3.852668	10.674727	5.103616
Zn	3.975678	12.955741	7.263764
O	5.873686	12.544744	6.799773
O	5.739687	10.788738	5.380785
O	19.114791	12.557744	4.935786
O	19.076806	10.958731	6.478780
O	4.030683	12.758753	9.141747
O	2.182664	11.649730	9.045751
O	3.237676	8.795711	5.107790
O	1.782657	8.894712	6.308768
O	2.866675	11.879744	6.220775
N	11.988740	11.345738	6.189778
N	3.652674	12.457747	15.937691
N	1.883668	2.418670	5.066780
C	6.235689	11.634739	6.088786
C	7.732714	11.529746	6.092768
C	8.401715	10.560734	5.352775
H	7.918713	9.953726	4.838795
C	9.789726	10.499737	5.382776
H	10.237731	9.850724	4.887789
C	10.508735	11.404745	6.151775
C	9.840730	12.373737	6.891767
H	10.323732	12.980745	7.405767
C	8.452719	12.436744	6.860771
H	8.004714	13.085758	7.355759
C	12.867748	11.981733	5.568775
H	12.536741	12.609743	4.966783
C	17.117781	11.801746	5.688779
C	16.476770	12.693754	4.836785
H	16.976774	13.254755	4.289798
C	15.086769	12.745753	4.803797
H	14.657757	13.342748	4.233798
C	14.339769	11.906740	5.621789
C	14.981756	11.014732	6.472768
H	14.481752	10.453730	7.021765
C	16.371777	10.962732	6.506770
H	16.800789	10.365737	7.076770
C	18.617793	11.766748	5.704785
C	4.315683	11.599742	18.162666
H	4.995693	11.119726	17.743666
C	3.459668	12.393744	17.409673
C	2.446661	13.110743	18.034678
H	1.872660	13.641762	17.529677
C	2.705661	11.894735	15.348698
H	2.004668	11.468729	15.788700
C	3.010668	12.124749	11.075729
C	3.992679	12.706753	11.871722
H	4.711688	13.143750	11.475736
C	3.898675	12.634747	13.255712
H	4.554676	13.022750	13.786713
C	2.822679	11.981733	13.845700
C	1.841663	11.399728	13.052713
H	1.121658	10.962732	13.446708
C	1.935667	11.471735	11.666732
H	1.278651	11.083732	11.135731
C	3.087671	12.187738	9.640736
C	2.412658	8.096709	5.653781
C	2.255665	6.610692	5.514785
C	1.255658	5.935699	6.204769
H	0.675645	6.404706	6.759778

C	1.125660	4.558678	6.065773
H	0.455644	4.106671	6.526778
C	1.992664	3.857684	5.235777
C	2.992671	4.533693	4.545793
H	3.572684	4.066677	3.989788
C	3.122669	5.912686	4.685785
H	3.792685	6.363696	4.222789
C	2.755669	1.996665	5.855785
H	3.293677	2.542676	6.380774
C	2.820668	0.547657	5.848778
H	4.301688	0.409656	7.218772
H	1.365668	0.224653	4.482785
O	3.895688	-4.253728	6.622773
O	2.287658	-4.213733	5.131779
C	3.740686	-0.089352	6.672762
C	3.819680	-1.478358	6.681779
H	4.436682	-1.904365	7.233763
C	2.979672	-2.228364	5.866775
C	2.059654	-1.589364	5.042791
H	1.497657	-2.090363	4.497795
C	1.980659	-0.202349	5.033792
C	3.086676	-3.723379	5.895780
Zn	1.746318	-6.184743	5.099787
Zn	1.746318	12.960757	24.245287
Zn	20.891818	12.960757	5.099787
Zn	20.752803	10.777729	7.441760
O	3.774688	11.428734	3.134635
O	2.123657	12.749754	3.111642
Zn	3.852668	10.674727	24.249116
Zn	3.975678	-6.189759	7.263764
O	-0.030709	12.557744	4.935786
O	-0.068694	10.958731	6.478780
O	3.895688	14.891772	6.622773
O	2.287658	14.931767	5.131779
C	19.457495	8.394000	-0.163503
H	20.431503	8.627996	-0.571493
H	19.541506	6.327990	-0.739495
H	19.579490	-2.839507	-1.782503
C	13.137010	5.453998	0.622995
C	14.085995	5.880004	1.795005
O	15.331008	6.157997	1.269002
C	15.603008	7.470995	1.477994
O	14.831004	8.234996	2.047994
C	16.954010	7.793999	0.912991
C	17.455010	9.088005	1.006996
C	18.706991	9.387000	0.483003
C	17.703997	6.801994	0.294994
C	14.323993	4.865006	2.961005
O	15.277994	5.449001	3.770993
C	14.908007	3.484998	2.500000
C	13.993006	2.241000	2.743990
O	14.315990	1.231994	1.860004
C	15.614993	0.888007	2.054006
O	16.333007	1.420998	2.892004
C	12.531993	2.642002	2.594005
C	11.623003	1.800998	1.747008
C	12.090996	3.824007	3.062993
C	10.751002	4.413995	2.656993
O	9.936993	4.498005	3.768007
C	8.825003	3.755007	3.545000
C	7.924993	3.834001	4.743010
O	8.630006	3.131993	2.505993
C	10.912992	5.815005	2.042002
O	10.428994	6.791005	2.621995
C	11.667000	6.010998	0.700993
C	11.757003	7.500996	0.548002
C	13.070997	4.692007	3.846005
C	13.424997	4.002003	5.129998
C	12.497991	6.018005	4.247008
H	13.041991	4.369999	0.660998
H	13.759009	6.838007	2.201005
H	16.870995	9.861005	1.488007
H	19.097004	10.393996	0.556004
H	17.314999	5.794998	0.221992
H	15.600998	6.345010	3.463995
H	15.151002	3.531005	1.437004
H	15.868001	3.308993	2.988995
H	14.146993	1.838006	3.747004
H	16.364003	0.224998	0.174990
H	12.140008	0.885001	1.458006
H	10.726994	1.549005	2.314997
H	11.342005	2.357003	0.853009
H	10.246997	3.770993	1.935993
H	8.384006	4.469000	5.500004
H	6.964999	4.256006	4.447997
H	7.772996	2.833993	5.150005
H	10.752993	7.923997	0.519992
H	12.304009	7.919000	1.391993
H	14.124995	4.620001	5.694006
H	12.521004	3.847997	5.720005
H	13.885006	3.039004	4.910993
H	13.247001	6.584999	4.801002
H	12.207994	6.573990	3.355000
H	11.623003	5.860993	4.878005
C	18.955998	7.102004	-0.257507
C	10.795994	5.480993	-0.492499
O	9.485006	5.894995	-0.370504
C	11.343996	5.979006	-1.836494
C	12.837000	5.647004	-2.049507
O	13.523998	6.862992	-2.585504
C	14.124995	7.107001	-1.234502
C	13.761996	5.673003	-0.815503
O	14.836001	4.817008	-0.946496
C	15.224999	4.810001	-2.247509
C	16.391994	3.883990	-2.411491
O	14.673992	5.475996	-3.116504

H	12.279005	7.738994	-0.406497
H	10.772005	4.387995	-0.485492
H	8.812999	5.158008	-0.303494
H	10.755999	5.574997	-2.661493
H	11.200003	7.060994	-1.880490
H	12.966998	4.800007	-2.727506
H	15.187991	7.332995	-1.332508
H	13.578008	7.914003	-0.741505
H	16.645002	3.441997	-1.447496
H	16.132994	3.092994	-3.116504
H	17.249004	4.442005	-2.790495
C	15.984999	-0.209509	1.101000
O	14.870004	-0.976497	0.825994
C	17.045009	-1.072493	1.718998
N	16.537002	-1.655492	2.957999
C	17.215002	-2.473503	3.764005
O	18.368001	-2.827503	3.536997
C	16.398006	-2.887505	4.952003
C	17.028008	-3.377496	6.089992
C	16.270995	-3.762493	7.190992
C	14.887005	-3.657499	7.153008
C	14.257003	-3.167508	6.014999
C	15.013001	-2.782492	4.913999
C	17.414996	-2.169491	0.765992
C	16.736001	-3.381497	0.803001
H	14.109008	-0.480495	0.409005
H	17.923998	-0.467495	1.935993
H	15.588994	-1.338500	3.105994
H	18.107010	-3.459496	6.118998
H	16.761005	-4.143507	8.078003
H	14.297993	-3.956494	8.010994
H	13.178001	-3.085508	5.985994
H	14.523010	-2.401497	4.027007
H	15.938993	-3.533493	1.519004
C	17.078992	-4.398506	-0.109493
C	18.101994	-4.203490	-1.029492
C	18.782004	-2.991504	-1.066500
C	18.438993	-1.974495	-0.182495
H	16.550002	-5.340503	-0.080507
H	18.369992	-4.995501	-1.716509
H	18.968002	-1.031502	-0.211500
C	4.788002	0.419995	19.790493
H	5.250998	1.073010	20.528494
H	3.791996	0.134995	20.129502
C	6.225006	1.994004	13.264002
C	6.602996	0.526003	12.867997
O	6.834005	0.487004	11.507001
C	8.133008	0.154006	11.300995
C	8.406004	0.105989	9.827002
C	8.909990	0.017997	7.094997
C	7.639993	0.340005	7.556997
C	7.388000	0.384001	8.922990
O	1.948993	0.483998	12.842993
C	0.447009	0.523993	11.059992
C	3.424996	0.513999	14.722009
C	2.629003	1.679003	15.229001
C	4.620996	0.240008	15.276003
C	5.267999	1.145992	16.308998
O	5.376995	0.466001	17.504999
C	4.680998	1.144001	18.451993
O	4.075005	2.184999	18.222993
C	6.666004	1.606001	15.862008
O	7.655998	1.252996	16.507001
C	6.842008	2.513996	14.616000
C	8.327010	2.581005	14.420008
C	6.356995	3.946002	14.948002
O	6.822997	4.364006	16.178005
C	6.842008	4.934006	13.877999
C	6.451000	4.523010	12.443005
O	7.642003	4.698995	11.554003
C	7.850000	3.215008	11.554998
C	6.429997	3.017005	12.107002
O	5.531996	2.716000	11.104007
C	5.518001	3.742007	10.215005
C	4.546999	3.433994	9.115996
O	6.213002	4.744006	10.336005
H	5.146004	2.024005	13.402999
H	7.569997	0.267999	13.299996
H	6.847005	0.557000	6.852998
H	6.399000	0.634999	9.282006
H	4.214997	0.470998	11.830004
H	0.872001	1.200997	10.319003
H	0.259000	1.931992	12.492994
H	1.695009	1.752005	14.671005
H	2.409002	1.536005	16.287996
H	3.203004	2.595996	15.099003
H	4.651993	2.025000	16.494001
H	8.550993	3.203999	13.554995
H	8.791997	3.009003	15.307995
H	8.716008	1.576996	14.254993
H	5.266008	3.976003	15.009000
H	6.114001	4.597007	16.842009
H	6.468996	5.937000	14.088006
H	7.928994	5.008003	13.954006
H	5.604998	5.107005	12.072999
H	8.034007	2.862999	10.539004
H	8.675994	2.971994	12.228997
H	4.088005	2.461996	9.296997
H	3.773004	4.201001	9.088005
H	5.072007	3.414006	8.160004
H	5.397997	-0.474502	19.661490
O	8.922990	-0.067507	12.211995
C	9.676002	-0.216497	9.365998
C	9.927995	-0.261508	7.998990
C	5.570996	-0.611507	13.165001
O	6.109004	-1.754494	12.608997

C	4.171000	-0.397499	12.491003
C	2.963991	-0.214506	13.466007
C	1.550001	-0.219503	11.752006
O	2.047994	-1.290502	11.425001
C	5.441994	-0.898498	14.676002
C	4.728000	-2.197501	14.905997
C	6.787003	-1.060508	15.318008
H	10.469008	-0.434507	10.069001
H	10.918009	-0.512506	7.639993
H	9.106997	-0.016503	6.032000
H	6.993009	-1.628497	12.159001
H	3.951995	-1.233506	11.823993
H	2.547002	-1.181507	13.752002
H	0.103998	-1.028496	9.646001
H	5.311996	-3.013502	14.480010
H	4.606005	-2.360506	15.976996
H	3.748000	-2.163499	14.429006
H	7.318999	-1.886502	14.844004
H	7.361004	-0.141504	15.195994
H	6.661007	-1.271510	16.380009
O	-0.272498	1.251005	11.987993
C	-1.567500	0.288006	9.685996
C	-2.750500	0.562993	10.361009
C	-3.774497	1.251005	9.719998
C	-3.614498	1.665008	8.402998
C	-2.430502	1.390002	7.727009
C	-1.407501	0.700993	8.368000
H	-2.875501	0.241004	11.386001
H	-4.694496	1.464995	10.246002
H	-4.410491	2.199990	7.902994
H	-2.305501	1.711991	6.701997
H	-0.487502	0.488000	7.841997
C	-0.463493	-0.455491	10.379005
N	-1.034508	-1.361494	11.370991
C	-1.886502	-2.354494	11.113005
O	-2.285494	-2.613495	9.981009
C	-2.276496	-3.092496	12.359990
C	-2.800508	-4.376508	12.271002
C	-3.162492	-5.059505	13.425992
C	-3.000502	-4.458508	14.667999
C	-2.476490	-3.174496	14.757007
C	-2.114506	-2.491500	13.601997
H	-0.680508	-1.114498	12.284002
H	-2.926505	-4.844501	11.303005
H	-3.569506	-6.060508	13.358007
H	-3.282496	-4.991500	15.568010
H	-2.349497	-2.706504	15.725003
H	-1.706496	-1.490496	13.670002
F	6.382995	10.630998	12.301998
F	6.994004	8.700002	13.153992
O	7.918004	8.670997	9.910994
O	4.597007	8.391990	11.273004
O	6.095008	8.544005	7.508004
O	10.275007	11.145993	11.257994
N	9.365002	9.076996	11.751010
N	11.637994	9.624003	12.301998
N	12.998990	8.057996	13.264998
C	5.905008	8.682006	10.997998
C	6.834005	9.360005	11.938004
C	6.579006	8.339990	9.883998
C	8.147999	9.470992	11.110995
C	6.097995	7.673995	8.644997
C	9.529998	7.822009	12.266005
C	10.466998	10.039000	11.753001
C	10.707006	7.448002	12.828997
C	11.774004	8.406004	12.802998
H	4.158996	9.184001	11.640005
H	7.008995	8.834002	7.332995
H	13.743004	8.746009	13.240990
H	13.155007	7.182990	13.748996
H	8.291993	10.519993	10.811004
H	6.711991	6.774999	8.458003
H	5.057992	7.362000	8.799004
H	8.677009	7.150002	12.193003
H	10.830992	6.456992	13.261992
H	9.680999	19.178507	17.683990
O	12.307991	15.707006	19.322500
H	13.221002	15.908992	19.604494
H	9.885990	16.935994	19.459505
F	14.282007	16.560992	17.141004
F	13.246006	14.715002	16.554003
O	11.000009	17.218008	16.300000
O	9.755992	18.773005	18.567995
O	13.238003	18.038009	13.503991
N	12.175006	16.232991	14.483992
N	12.478999	16.383991	12.106006
N	11.636999	14.762004	
	10.730995		
C	12.093006	16.222997	18.045993
C	13.009003	16.045001	16.891003
C	11.001004	16.897991	17.642004
C	12.310001	16.860006	15.763007
C	9.817008	17.350992	18.418009
C	11.521992	15.040992	14.335997
C	12.678993	16.960003	13.320003
C	11.360997	14.481005	13.109996
C	11.852003	15.224004	11.986998
H	11.990999	15.297006	9.947006
H	11.252997	13.841009	10.562994
H	12.880997	17.784006	15.586007
H	8.902007	16.960003	17.939008
H	11.140996	14.577996	15.243992
H	10.863999	13.519997	12.995008
H	19.613493	5.428994	9.784997

F	17.845999	7.167003	8.627001
F	16.692004	5.315997	8.364994
O	15.937001	6.511997	11.425996
O	18.990000	4.935997	10.352010
O	17.756992	6.610999	13.833007
O	14.295007	9.020000	9.303009
N	14.578992	6.731998	9.489008
N	12.521999	7.691992	8.704004
N	10.742004	6.347997	8.195997
C	17.824997	5.643002	10.471995
C	17.080007	6.238006	9.334006
C	17.133002	5.847993	11.607993
C	15.882992	6.947998	10.034003
C	17.465004	5.478006	13.008008
C	14.051993	5.475996	9.365998
C	13.783994	7.913007	9.153004
C	12.794995	5.289997	8.890998
C	12.034995	6.468001	8.584000
H	16.965995	7.180003	13.874993
H	10.219006	7.189001	7.980993
H	10.331008	5.446990	7.988996
H	16.046992	8.035998	10.000001
H	16.636004	4.880992	13.428998
H	18.371007	4.860009	12.998990
H	14.689998	4.649006	9.672996
H	12.383999	4.289990	8.769003
F	5.042006	14.080998	2.972990
F	5.677005	14.693999	0.961008
O	8.484998	14.127005	2.740008
O	6.200998	16.895004	3.023993
O	9.546999	15.785005	5.029006
O	7.213010	10.699003	2.383002
N	7.534003	12.633005	1.156005
N	7.816993	10.454994	0.182993
C	6.813998	15.685008	2.846993
C	6.164009	14.490999	2.249998
C	8.104003	15.401004	3.107008
C	7.282010	13.408991	2.331003
C	9.159992	16.242008	3.727993
C	7.504998	11.177009	1.290005
H	5.331007	16.759990	3.445999
H	9.918001	14.886009	4.947006
H	7.020004	12.686000	3.117998
H	10.027992	16.291002	3.048002
H	8.762991	17.254997	3.861992
N	8.501004	10.244010	-2.017495
C	7.875999	13.220006	-0.058509
C	8.159008	12.469005	-1.153497
C	8.137010	11.044005	-0.986491
H	8.479006	9.239006	-1.886502
H	8.665004	10.613997	-2.945497
H	7.914003	14.306992	-0.071508
H	8.407000	12.936002	-2.104493

Supplementary data for Chapter 5

Cluster Analysis:

Hierarchical agglomerative clustering is carried using cpptraj module of AMBER tools. We identified ten and twenty clusters from both major and minor pathway transition structures respectively. Low energy conformer from each cluster were chosen for further analysis. After visual analysis of all the low energy activation modes from each cluster they were categorized based on re-face and si-face attack and presence of ortho vinyl benzaldehyde in the quadrants of quadrant projection model. Here is the list of transition structures of each cluster in major and minor pathway.

Table S 5.1: List of structures with details of major conformers identified in cluster analysis. Structures are selected based on the presence of benzaldehydehyde substituents in quadrants.

	Transition state name	**Free energy difference**	**Total energy in toluene**
quadrant 3	TS-1-ene-major	0	-3224.76116
quadrant 2	TS-2-ene-major	0.58201	-3224.75868
quadrant 3	TS-3-ene-major	0.78955	-3224.75934
quadrant 1	TS-4-ene-major	2.86686	-3224.75187
quadrant 4	TS-5-ene-major	5.88026	-3224.74758

Table S 5.2: List of structures with details of minor conformers identified in cluster analysis. Structures are selected based on the presence of benzaldehydehyde substituents in quadrants

	Transition state name	**Free energy difference**	**Total energy in toluene**
quadrant 2	TS-1-ene-minor	0	-3224.75159
quadrant 2	TS-2-ene-minor	0.02634	-3224.75312
quadrant 1	TS-3-ene-minor	0.24937	-3224.75402
quadrant 3	TS-4-ene-minor	0.96223	-3224.75290
quadrant 4	TS-5-ene-minor	2.82544	-3224.74892

Table S 5.3: Cartesian co-ordinates of major and minor conformers included in the study

147
TS-1-ene-major Energy: -2024552.3786

C	-3.57999	-1.96448	-0.25092
C	-3.76783	-1.54974	-1.58334
C	-4.67012	-0.51420	-1.84255
C	-5.36484	0.13746	-0.82694
C	-5.11009	-0.24829	0.48901
C	-4.23344	-1.28863	0.79764
O	-1.04499	-1.74847	0.97193
P	0.09794	-0.94805	0.16205
C	-1.44066	-3.01531	0.57783
O	-0.48835	-0.59103	-1.23267
O	1.13174	-2.12928	-0.20864
C	-0.59460	-4.10386	0.82585
C	-2.72072	-3.15542	0.04051
C	1.60673	-2.90889	0.83407
C	0.77960	-3.91223	1.35004
C	-3.17891	-4.45214	-0.20400
C	-1.08743	-5.38327	0.55053
C	-2.37258	-5.55816	0.05185
C	2.92365	-2.71013	1.24804
C	1.31840	-4.75106	2.33098
C	3.42687	-3.57992	2.21736
C	2.63057	-4.58770	2.75858
C	3.76501	-1.64084	0.62321
C	4.01702	-0.43927	1.31623
C	4.87014	0.50045	0.73783
C	5.45088	0.30391	-0.51523
C	5.14397	-0.86760	-1.19991
C	4.30906	-1.84723	-0.65681
O	0.62561	0.14832	0.99777
H	-4.84127	-0.20486	-2.87153
H	-5.62055	0.26621	1.30171
H	-4.18533	-4.58419	-0.58978
H	-0.44171	-6.24045	0.71758
H	-2.74385	-6.55776	-0.14923
H	0.69253	-5.52743	2.76137
H	4.45977	-3.46875	2.53313
H	3.03748	-5.24926	3.51644
H	5.08309	1.41760	1.28146
H	5.57216	-1.02414	-2.18889
H	-0.23224	0.41258	-1.49058
C	-2.30431	2.46699	-1.75618
C	-2.51124	1.84247	-0.46343
C	-2.63335	2.55800	0.69730
O	-0.26098	3.59040	-2.97697
B	-0.66116	2.87995	-1.81919
O	-0.48086	3.71537	-0.57208
O	0.21649	1.69501	-1.74509
C	-0.53724	3.15720	0.58656
C	1.16782	1.74261	-2.83492
C	-0.52005	4.05728	1.76195
C	-0.46281	3.55320	3.07817
C	-0.54666	5.43851	1.53366
C	-0.49911	6.33101	2.59391
C	-0.39416	4.47544	4.13031
C	-0.41728	5.84406	3.89818
C	1.10274	3.25284	-3.23355
C	2.01768	4.12111	-2.36376
C	1.39540	3.52026	-4.70360
C	2.50504	1.24668	-2.30251
C	0.65754	0.82909	-3.94787
H	-2.48419	1.79491	-2.59944
H	-2.84736	3.40743	-1.88428
H	-2.36986	0.76150	-0.38855
H	-2.93350	3.60242	0.66380
H	-2.71979	2.05475	1.65684
H	-0.14355	2.14357	0.68656
H	-0.51029	7.39977	2.40631
H	-0.29798	4.10273	5.14518
H	-0.35878	6.53313	4.73515
H	1.89619	3.90166	-1.30002
H	1.75496	5.17003	-2.52708
H	3.06978	3.97853	-2.63205
H	1.35990	4.59768	-4.88800
H	0.65348	3.04121	-5.34520
H	2.39252	3.15751	-4.97678
H	2.43458	0.18452	-2.03882
H	2.79968	1.78626	-1.39924
H	3.29422	1.35124	-3.05705
H	-0.30921	1.18152	-4.32237
H	0.53466	-0.18852	-3.56392
H	1.36589	0.79463	-4.78104
C	4.01881	-3.09394	-1.47918
C	3.24907	-2.73982	-2.75790
C	5.30622	-3.86035	-1.80515
H	3.38428	-3.76068	-0.88741
H	3.03769	-3.64355	-3.33949
H	2.29799	-2.25616	-2.51584
H	3.83105	-2.06078	-3.39177
H	5.84941	-4.12236	-0.89199
H	5.97487	-3.26384	-2.43505
H	5.07432	-4.78369	-2.34602
C	3.39870	-0.14944	2.67647
C	2.94596	1.30838	2.81637
C	4.37488	-0.50384	3.80638
H	2.50564	-0.77521	2.77665
H	2.33820	1.60892	1.95881

H	2.34331	1.42348	3.72339
H	3.79901	1.99068	2.90377
H	4.65309	-1.56129	3.78720
H	5.29343	0.08710	3.71340
H	3.92824	-0.28628	4.78248
C	6.42297	1.31183	-1.09991
C	7.76311	1.24984	-0.35563
C	5.87214	2.74078	-1.09488
H	6.60226	1.02317	-2.14402
H	8.18145	0.23943	-0.38184
H	7.62827	1.53058	0.69500
H	8.48867	1.93892	-0.80069
H	6.57995	3.42415	-1.57537
H	4.91870	2.80075	-1.62726
H	5.70931	3.09957	-0.07302
C	-3.03076	-2.20220	-2.74398
C	-2.48326	-1.16802	-3.73310
C	-3.93282	-3.20332	-3.47755
H	-2.17207	-2.74396	-2.33372
H	-1.91301	-0.39771	-3.20904
H	-1.81753	-1.65395	-4.45425
H	-3.28518	-0.68492	-4.30239
H	-4.27587	-4.00177	-2.81385
H	-4.81759	-2.69542	-3.87816
H	-3.39641	-3.66222	-4.31479
C	-4.02016	-1.65963	2.25632
C	-3.36634	-0.50293	3.01933
C	-5.33086	-2.09443	2.92214
H	-3.33332	-2.51018	2.29975
H	-2.41553	-0.22199	2.55556
H	-3.16977	-0.79023	4.05826
H	-4.01765	0.37939	3.03620
H	-5.14921	-2.40543	3.95611
H	-5.78530	-2.93241	2.38478
H	-6.05688	-1.27445	2.94277
C	-6.39028	1.21025	-1.14495
C	-6.02637	2.56516	-0.52964
C	-7.78922	0.77044	-0.69576
H	-6.40842	1.33044	-2.23582
H	-5.06911	2.92801	-0.91337
H	-5.94402	2.49168	0.56082
H	-6.79706	3.30843	-0.75955
H	-7.82901	0.66016	0.39363
H	-8.53943	1.51340	-0.98561
H	-8.06239	-0.19090	-1.14043
C	-0.48782	2.10368	3.36149
C	-0.99752	1.57864	4.47886
H	-0.59142	5.79282	0.50947
H	-0.97429	0.50686	4.64502
H	-1.46411	2.18673	5.24955
H	-0.07172	1.42942	2.61467

TS-2-ene-major

C	4.09543	-0.70705	0.82443
C	3.76636	0.47562	1.51916
C	4.33916	1.67529	1.09813
C	5.20398	1.74657	0.00482
C	5.49508	0.56827	-0.67529
C	4.95103	-0.65990	-0.28817
O	1.83413	-1.97564	-0.33060
P	0.38547	-1.25583	-0.26813
C	2.40393	-2.58645	0.77403
O	0.53954	0.08026	0.52889
O	-0.36931	-2.15625	0.83843
C	1.87210	-3.79328	1.25339
C	3.56519	-2.02144	1.30614
C	-0.50114	-3.50254	0.53334
C	0.59523	-4.34330	0.74065
C	4.24134	-2.73129	2.30157
C	2.57156	-4.46202	2.26281
C	3.75570	-3.94677	2.77381
C	-1.74957	-3.95566	0.10799
C	0.41236	-5.71095	0.51122
C	-1.89439	-5.32932	-0.09384
C	-0.82245	-6.19871	0.10075
C	-2.87083	-2.98845	-0.09994
C	-3.30817	-2.68577	-1.40361
C	-4.38058	-1.80347	-1.56630
C	-5.01774	-1.20683	-0.48255
C	-4.54898	-1.50528	0.79546
C	-3.47848	-2.36971	1.01171
O	-0.22698	-1.18882	-1.60449
H	4.09823	2.59566	1.62694
H	6.14764	0.59816	-1.54479
H	5.16439	-2.31646	2.69659
H	2.16141	-5.38764	2.65589
H	4.29148	-4.48279	3.55038
H	1.25263	-6.38558	0.64687
H	-2.86179	-5.71335	-0.40283
H	-0.95201	-7.26223	-0.07177
H	-4.71247	-1.56932	-2.57378
H	-5.02685	-1.02615	1.64976
H	0.43292	0.87665	-0.13751
C	-2.29232	1.58882	-1.76517
C	-2.65598	1.06165	-0.45679
C	-3.37969	1.76098	0.45754
O	-0.56841	3.28639	-2.77969
B	-0.95577	2.58957	-1.60832
O	-1.42379	3.59778	-0.53183
O	0.24027	1.90513	-1.11478
C	-1.52929	3.18949	0.66426
C	1.37757	2.33833	-1.89318
C	-2.12276	4.01343	1.72578
C	-3.01049	5.08837	1.49612
C	-1.76477	3.65980	3.03227

C	-2.25133	4.36623	4.12278
C	-3.48105	5.79014	2.61096
C	-3.11270	5.43883	3.90573
C	0.68109	2.76003	-3.22298
C	0.41292	1.55594	-4.13053
C	1.42245	3.84426	-3.99209
C	2.34381	1.16934	-2.00742
C	2.01884	3.51398	-1.15973
H	-3.07367	2.21745	-2.20378
H	-1.99464	0.79973	-2.46003
H	-2.19901	0.12030	-0.14306
H	-3.95067	2.63980	0.16174
H	-3.56854	1.36062	1.44994
H	-0.87692	2.37525	0.99305
H	-1.95839	4.08741	5.12932
H	-4.13473	6.64116	2.44684
H	-3.49470	6.00995	4.74618
H	-0.01422	0.72093	-3.56526
H	-0.29899	1.85949	-4.90329
H	1.32965	1.20672	-4.61672
H	1.47911	4.76775	-3.41191
H	2.43780	3.51791	-4.24474
H	0.88972	4.05840	-4.92302
H	2.73577	0.91035	-1.01814
H	1.84669	0.28982	-2.42475
H	3.19721	1.42954	-2.64411
H	1.31485	4.34834	-1.07873
H	2.92087	3.86136	-1.67486
H	2.30650	3.19134	-0.15347
C	-3.00684	-2.59304	2.44063
C	-2.55057	-1.27497	3.08034
C	-4.09573	-3.26593	3.28485
H	-2.14485	-3.26562	2.42441
H	-1.78530	-0.78836	2.46668
H	-2.12985	-1.45946	4.07469
H	-3.39479	-0.58581	3.20130
H	-4.39732	-4.22177	2.84574
H	-4.98681	-2.63264	3.35600
H	-3.73380	-3.45198	4.30154
C	-2.66382	-3.29641	-2.64031
C	-2.36788	-2.25628	-3.72636
C	-3.54812	-4.41568	-3.20681
H	-1.70294	-3.72785	-2.34326
H	-1.74610	-1.45429	-3.32417
H	-3.28658	-1.82911	-4.14310
H	-1.82709	-2.73182	-4.55142
H	-3.07415	-4.87610	-4.08011
H	-3.73905	-5.19929	-2.46741
H	-4.51786	-4.01246	-3.52089
C	-6.19707	-0.26609	-0.64244
C	-6.15888	0.54521	-1.93760
C	-7.51305	-1.04799	-0.53195
H	-6.15196	0.44231	0.19657
H	-6.32931	-0.09199	-2.81221
H	-5.19319	1.04445	-2.06289
H	-6.94661	1.30509	-1.93041
H	-8.37468	-0.37522	-0.60021
H	-7.57175	-1.59206	0.41562
H	-7.58477	-1.77978	-1.34432
C	2.82986	0.46232	2.71889
C	3.62271	0.29832	4.02318
C	1.94984	1.71402	2.80553
H	2.16047	-0.39764	2.61003
H	4.18871	-0.63675	4.03537
H	2.94814	0.29896	4.88618
H	4.33108	1.12612	4.14234
H	1.47663	1.93326	1.84396
H	2.52296	2.59340	3.11994
H	1.16359	1.55425	3.55140
C	5.26988	-1.89760	-1.11101
C	6.77873	-2.15151	-1.19687
C	4.64457	-1.78462	-2.50694
H	4.81880	-2.76366	-0.61665
H	7.22185	-2.23697	-0.19981
H	6.97751	-3.07911	-1.74327
H	7.29092	-1.33980	-1.72464
H	5.05783	-0.92727	-3.05110
H	4.84838	-2.68660	-3.09367
H	3.56083	-1.65481	-2.43468
C	5.81287	3.08179	-0.38234
C	7.13357	3.29545	0.36993
C	6.02400	3.24284	-1.88895
H	5.10934	3.86021	-0.05665
H	6.98531	3.23297	1.45209
H	7.85807	2.52447	0.08471
H	7.56412	4.27448	0.13430
H	6.81121	2.57502	-2.25493
H	6.33296	4.26697	-2.12000
H	5.10849	3.02461	-2.44878
C	-3.47760	5.47180	0.14568
C	-4.74009	5.82601	-0.10313
H	-1.09525	2.81606	3.18263
H	-5.05375	6.11611	-1.10024
H	-5.50202	5.81868	0.67217
H	-2.75630	5.44009	-0.66302

147
TS-3-ene-major

C	-3.50866	-1.99580	-0.23832
C	-3.65236	-1.59625	-1.58163
C	-4.55647	-0.57424	-1.88296
C	-5.29654	0.07816	-0.89989
C	-5.08663	-0.29258	0.42782
C	-4.20666	-1.31694	0.77858
O	-1.00577	-1.74503	1.05462
P	0.11495	-0.94428	0.21624

C	-1.38508	-3.01953	0.66445	H	-2.87868	3.37633	-1.86366
O	-0.49579	-0.64619	-1.18338	H	-2.36133	0.76863	-0.31334
O	1.16488	-2.11823	-0.12978	H	-2.95852	3.62635	0.67474
C	-0.53101	-4.09657	0.93445	H	-2.72531	2.10481	1.70401
C	-2.64961	-3.17573	0.09662	H	-0.14712	2.19196	0.68507
C	1.65142	-2.87399	0.92537	H	-0.47939	7.46258	2.36451
C	0.83983	-3.88104	1.45785	H	-0.30409	4.18306	5.12757
C	-3.09117	-4.47972	-0.14112	H	-0.33881	6.61098	4.69919
C	-1.00699	-5.38363	0.66642	H	2.14225	4.44802	-3.51315
C	-2.28178	-5.57548	0.14731	H	2.60454	3.19204	-4.68856
C	2.96638	-2.64822	1.33354	H	1.27886	4.31457	-5.05202
C	1.39526	-4.69926	2.44695	H	-0.48559	2.61665	-5.37420
C	3.48717	-3.49823	2.31036	H	-0.61597	1.22727	-4.28324
C	2.70713	-4.51159	2.86584	H	0.81319	1.40279	-5.32641
C	3.76306	-1.56129	0.68221	H	2.52291	2.05681	-0.70473
C	3.95096	-0.32856	1.33286	H	1.96413	3.63528	-1.32044
C	4.69954	0.66343	0.69198	H	3.29744	2.78050	-2.13206
C	5.22964	0.48328	-0.58256	H	2.30025	0.02903	-2.02972
C	4.99815	-0.73665	-1.21808	H	1.18167	-0.06495	-3.40925
C	4.27869	-1.76521	-0.61307	H	2.77054	0.71567	-3.59057
O	0.63268	0.18687	1.01083	C	4.07849	-3.06558	-1.37797
H	-4.69302	-0.27569	-2.92032	C	5.42474	-3.73188	-1.68768
H	-5.63267	0.22273	1.21641	C	3.26728	-2.84255	-2.66013
H	-4.08694	-4.62543	-0.54904	H	3.51148	-3.75601	-0.74603
H	-0.35566	-6.23276	0.85186	H	5.99658	-3.90782	-0.77138
H	-2.64088	-6.58061	-0.04822	H	5.26999	-4.69316	-2.18859
H	0.78322	-5.47962	2.88992	H	6.03339	-3.10461	-2.34818
H	4.51929	-3.36926	2.62152	H	2.28255	-2.42579	-2.43030
H	3.12687	-5.15836	3.62945	H	3.78347	-2.15254	-3.33793
H	4.84526	1.61121	1.19979	H	3.12749	-3.79025	-3.19117
H	5.38617	-0.88448	-2.22558	C	3.37442	-0.05174	2.71395
H	-0.25856	0.33687	-1.47716	C	2.89242	1.39373	2.87933
C	-2.32639	2.44363	-1.71931	C	4.40143	-0.38219	3.80597
C	-2.52020	1.84552	-0.41138	H	2.50260	-0.70150	2.84581
C	-2.65434	2.58396	0.73133	H	2.30695	1.48559	3.80004
O	-0.25846	3.55066	-2.97369	H	3.73169	2.09407	2.95697
B	-0.68517	2.86243	-1.80680	H	2.25920	1.69202	2.03936
O	-0.50141	3.74367	-0.58831	H	5.29955	0.23308	3.67842
O	0.15694	1.66484	-1.70019	H	3.98657	-0.17677	4.79862
C	-0.53623	3.20658	0.57866	H	4.70653	-1.43162	3.77460
C	1.34189	1.90489	-2.48824	C	6.05296	1.54515	-1.29429
C	-0.51763	4.11613	1.74393	C	7.51105	1.08212	-1.42823
C	-0.46853	3.62040	3.06415	C	6.00372	2.91965	-0.62871
C	-0.53201	5.49566	1.50525	H	5.63889	1.64389	-2.30872
C	-0.47802	6.39509	2.55944	H	7.58253	0.12096	-1.94534
C	-0.39318	4.54920	4.10964	H	8.10245	1.81703	-1.98433
C	-0.40242	5.91647	3.86711	H	7.95804	0.96243	-0.43527
C	0.75200	2.78856	-3.63208	H	6.53206	3.65377	-1.24440
C	1.76212	3.74269	-4.25478	H	4.97649	3.26851	-0.48485
C	0.08208	1.94835	-4.72105	H	6.49470	2.89673	0.35074
C	2.34413	2.65062	-1.60840	C	-2.86858	-2.25336	-2.70925
C	1.92431	0.56455	-2.91056	C	-2.30807	-1.22925	-3.70294
H	-2.51126	1.75247	-2.54650	C	-3.73199	-3.28163	-3.45217

H	-2.01365	-2.77321	-2.26446
H	-1.61596	-1.72036	-4.39507
H	-3.09950	-0.76861	-4.30454
H	-1.76415	-0.43993	-3.17839
H	-3.16349	-3.74549	-4.26516
H	-4.08104	-4.07448	-2.78494
H	-4.61284	-2.79569	-3.88713
C	-4.03143	-1.66152	2.24875
C	-5.35492	-2.09827	2.88712
C	-3.41051	-0.48344	3.00745
H	-3.33717	-2.50366	2.32603
H	-5.78596	-2.95072	2.35326
H	-5.19798	-2.38860	3.93110
H	-6.08980	-1.28610	2.87357
H	-3.23678	-0.74978	4.05601
H	-2.45194	-0.19877	2.56186
H	-4.07262	0.39070	2.99095
C	-6.32684	1.12995	-1.26805
C	-7.73923	0.63410	-0.93248
C	-6.05539	2.48027	-0.59801
H	-6.26926	1.27616	-2.35440
H	-7.85034	0.49050	0.14815
H	-8.49180	1.36118	-1.25486
H	-7.94805	-0.32212	-1.42098
H	-6.82771	3.20520	-0.87586
H	-5.08199	2.87927	-0.89461
H	-6.06067	2.38692	0.49383
C	-0.51491	2.17304	3.35738
C	-1.04259	1.66298	4.47335
H	-0.57259	5.84261	0.47836
H	-1.03735	0.59211	4.64691
H	-1.50675	2.28357	5.23548
H	-0.10307	1.48761	2.61829

147
TS-4-ene-major

C	1.21318	3.85410	-0.20955
C	2.19440	3.16290	-0.95043
C	3.46337	3.00577	-0.39501
C	3.78219	3.49061	0.87411
C	2.78354	4.12776	1.60085
C	1.49883	4.31660	1.08611
O	-1.13382	2.52122	0.62730
P	-1.18652	0.94687	0.28681
C	-1.26445	3.43387	-0.40807
O	-0.05457	0.71060	-0.76205
O	-2.51633	0.85841	-0.64035
C	-2.53746	3.68585	-0.92944
C	-0.12679	4.13420	-0.81232
C	-3.67325	1.53561	-0.29685
C	-3.72175	2.92615	-0.46533
C	-0.29636	5.14682	-1.75884
C	-2.65975	4.69520	-1.89031
C	-1.55027	5.42448	-2.29783
C	-4.78766	0.78846	0.09224
C	-4.93619	3.57371	-0.21967
C	-5.98481	1.47310	0.31430
C	-6.06111	2.85483	0.16461
C	-4.70190	-0.70136	0.20225
C	-4.32524	-1.30131	1.42217
C	-4.22976	-2.69012	1.47237
C	-4.48006	-3.49771	0.36080
C	-4.86770	-2.88103	-0.82410
C	-4.98735	-1.49124	-0.92378
O	-1.20207	0.12365	1.50611
H	4.22705	2.48544	-0.96969
H	3.01315	4.49207	2.60065
H	0.56974	5.72992	-2.05689
H	-3.63636	4.89166	-2.32291
H	-1.66044	6.21032	-3.03807
H	-4.98386	4.65368	-0.32458
H	-6.86552	0.90102	0.59232
H	-6.99792	3.37057	0.34875
H	-3.93091	-3.16898	2.40255
H	-5.06573	-3.48704	-1.70385
H	0.32260	-0.24731	-0.73869
C	2.29599	-0.94645	1.37655
C	3.30537	-1.64902	2.14486
C	4.63356	-1.63648	1.84294
O	1.59636	-3.38592	0.62745
B	1.91938	-2.06993	0.16969
O	3.24174	-2.11403	-0.61299
O	0.84823	-1.63334	-0.69183
C	4.18257	-2.80496	-0.10703
C	0.01536	-2.77577	-0.98949
C	5.53568	-2.68298	-0.67094
C	6.57802	-3.53290	-0.24885
C	5.77507	-1.68115	-1.61889
C	7.04131	-1.51593	-2.16012
C	7.84432	-3.35415	-0.81629
C	8.07805	-2.35699	-1.75579
C	0.23846	-3.66434	0.27554
C	0.09158	-5.15741	0.01753
C	-0.65237	-3.24157	1.44243
C	0.56588	-3.41166	-2.26484
C	-1.41482	-2.30353	-1.19788
H	1.35292	-0.78520	1.90756
H	2.64859	-0.01608	0.91855
H	2.94607	-2.39945	2.84904
H	5.04807	-0.84725	1.22366
H	5.34321	-2.26741	2.37123
H	3.90264	-3.68240	0.47402
H	7.22045	-0.74122	-2.89835
H	8.64560	-4.02729	-0.52742
H	9.06958	-2.24273	-2.18262
H	0.25284	-5.70432	0.95126

H	0.82029	-5.50950	-0.71622
H	-0.91731	-5.38979	-0.34305
H	-0.29222	-3.73546	2.35046
H	-1.69537	-3.52909	1.27451
H	-0.62379	-2.15694	1.59134
H	-0.05149	-4.25488	-2.58946
H	1.59107	-3.76273	-2.11209
H	0.57522	-2.66001	-3.05925
H	-1.82518	-1.80664	-0.31280
H	-1.45675	-1.60530	-2.04067
H	-2.06575	-3.15324	-1.43138
C	-5.37324	-0.87039	-2.25882
C	-6.53038	-1.60582	-2.94269
C	-4.15270	-0.80011	-3.18558
H	-5.70674	0.15530	-2.07156
H	-7.38500	-1.71941	-2.26886
H	-6.85851	-1.04697	-3.82494
H	-6.23255	-2.60307	-3.28325
H	-3.34646	-0.21856	-2.72886
H	-3.77183	-1.80875	-3.38732
H	-4.41957	-0.33875	-4.14269
C	-4.09467	-0.46901	2.67503
C	-3.09675	-1.09397	3.65134
C	-5.43166	-0.21815	3.38840
H	-3.68076	0.49596	2.36392
H	-2.85734	-0.37184	4.43805
H	-3.51380	-1.98192	4.14064
H	-2.16821	-1.36133	3.14364
H	-6.14329	0.30901	2.74716
H	-5.88457	-1.17097	3.68596
H	-5.27635	0.38249	4.29093
C	-4.35405	-5.00534	0.50101
C	-4.12753	-5.73344	-0.82400
C	-5.58928	-5.57354	1.21380
H	-3.48081	-5.19542	1.14195
H	-3.29191	-5.30287	-1.38637
H	-3.90898	-6.79002	-0.64116
H	-5.01945	-5.68891	-1.45869
H	-5.73683	-5.09989	2.18870
H	-6.48614	-5.38997	0.61178
H	-5.49173	-6.65392	1.36475
C	1.91270	2.59903	-2.33590
C	2.51966	1.20470	-2.53937
C	2.42870	3.54579	-3.42832
H	0.82812	2.50011	-2.44206
H	3.60999	1.25704	-2.64584
H	2.28682	0.53243	-1.70931
H	2.12617	0.75938	-3.45889
H	3.51019	3.69218	-3.32450
H	1.95103	4.52761	-3.37385
H	2.23563	3.12812	-4.42240
C	0.46539	5.02240	1.95016
C	0.88798	6.46629	2.24646
C	0.20456	4.24373	3.24482
H	-0.47808	5.06598	1.39875
H	1.04475	7.02765	1.31998
H	0.11837	6.97775	2.83397
H	1.82126	6.49483	2.81951
H	-0.10869	3.21950	3.02509
H	1.10404	4.20322	3.86919
H	-0.58410	4.73102	3.82781
C	5.17476	3.31566	1.44792
C	6.22534	4.03974	0.59896
C	5.52485	1.83251	1.60078
H	5.17650	3.76788	2.44797
H	6.26970	3.61301	-0.40923
H	7.21960	3.94419	1.04789
H	5.98888	5.10328	0.50259
H	4.77945	1.31408	2.21176
H	5.55705	1.34339	0.61907
H	6.50723	1.70630	2.06868
C	6.36789	-4.58178	0.77146
C	7.26660	-4.89479	1.70578
H	4.95034	-1.04087	-1.91632
H	7.07958	-5.68593	2.42384
H	8.21007	-4.36224	1.79057
H	5.42584	-5.12531	0.74883

147

TS-5-ene-major

C	-4.380000	-0.784000	0.467000
C	-4.786000	-0.266000	-0.782000
C	-5.260000	1.044000	-0.845000
C	-5.351000	1.854000	0.287000
C	-4.919000	1.328000	1.500000
C	-4.427000	0.026000	1.615000
O	-1.749000	-1.520000	1.201000
P	-0.516000	-0.985000	0.309000
C	-2.596000	-2.537000	0.798000
O	-1.107000	-0.225000	-0.918000
O	-0.023000	-2.353000	-0.396000
C	-2.129000	-3.859000	0.768000
C	-3.930000	-2.207000	0.548000
C	0.319000	-3.428000	0.406000
C	-0.702000	-4.198000	0.978000
C	-4.829000	-3.252000	0.326000
C	-3.061000	-4.872000	0.518000
C	-4.403000	-4.576000	0.316000
C	1.671000	-3.755000	0.517000
C	-0.328000	-5.338000	1.698000
C	1.997000	-4.914000	1.226000
C	1.009000	-5.697000	1.817000
C	2.735000	-2.891000	-0.078000

C	3.639000	-2.221000	0.775000
C	4.671000	-1.476000	0.207000
C	4.844000	-1.371000	-1.172000
C	3.924000	-2.017000	-1.992000
C	2.865000	-2.767000	-1.474000
O	0.463000	-0.286000	1.160000
H	-5.578000	1.440000	-1.808000
H	-4.976000	1.952000	2.390000
H	-5.872000	-3.008000	0.145000
H	-2.714000	-5.900000	0.465000
H	-5.113000	-5.376000	0.131000
H	-1.100000	-5.936000	2.172000
H	3.043000	-5.191000	1.315000
H	1.283000	-6.586000	2.375000
H	5.367000	-0.950000	0.861000
H	4.021000	-1.937000	-3.072000
H	-0.685000	0.710000	-1.078000
C	1.914000	-3.431000	-2.458000
C	1.204000	-2.385000	-3.327000
C	2.648000	-4.460000	-3.327000
H	1.147000	-3.969000	-1.896000
H	0.668000	-1.661000	-2.706000
H	0.480000	-2.869000	-3.991000
H	1.921000	-1.842000	-3.955000
H	3.138000	-5.218000	-2.708000
H	3.417000	-3.982000	-3.944000
H	1.945000	-4.964000	-3.998000
C	3.522000	-2.258000	2.293000
C	3.353000	-0.848000	2.866000
C	4.723000	-2.971000	2.925000
H	2.620000	-2.816000	2.558000
H	2.489000	-0.361000	2.406000
H	4.245000	-0.234000	2.693000
H	3.187000	-0.890000	3.948000
H	4.612000	-3.017000	4.014000
H	4.831000	-3.993000	2.547000
H	5.654000	-2.436000	2.705000
C	6.027000	-0.593000	-1.718000
C	7.310000	-1.427000	-1.588000
C	5.844000	-0.127000	-3.163000
H	6.141000	0.299000	-1.086000
H	7.227000	-2.339000	-2.191000
H	7.485000	-1.725000	-0.551000
H	8.180000	-0.862000	-1.938000
H	6.655000	0.550000	-3.448000
H	4.892000	0.395000	-3.302000
H	5.867000	-0.975000	-3.856000
C	-4.736000	-1.080000	-2.069000
C	-3.838000	-0.418000	-3.120000
C	-6.145000	-1.319000	-2.626000
H	-4.296000	-2.055000	-1.848000
H	-2.827000	-0.295000	-2.722000
H	-3.785000	-1.040000	-4.020000
H	-4.221000	0.565000	-3.417000
H	-6.626000	-0.371000	-2.894000
H	-6.103000	-1.941000	-3.526000
H	-6.785000	-1.819000	-1.892000
C	-3.997000	-0.469000	2.987000
C	-2.853000	0.383000	3.548000
C	-5.185000	-0.505000	3.955000
H	-3.627000	-1.493000	2.886000
H	-2.010000	0.409000	2.852000
H	-2.503000	-0.030000	4.501000
H	-3.179000	1.413000	3.731000
H	-5.992000	-1.134000	3.566000
H	-5.591000	0.499000	4.120000
H	-4.875000	-0.904000	4.927000
C	-5.910000	3.262000	0.202000
C	-4.993000	4.178000	-0.615000
C	-7.333000	3.269000	-0.367000
H	-5.954000	3.657000	1.225000
H	-4.889000	3.807000	-1.642000
H	-3.994000	4.225000	-0.172000
H	-5.400000	5.194000	-0.662000
H	-7.993000	2.619000	0.215000
H	-7.747000	4.283000	-0.357000
H	-7.342000	2.916000	-1.404000
C	2.400000	1.093000	-1.253000
C	3.656000	1.759000	-1.011000
C	4.093000	2.082000	0.245000
O	1.602000	3.332000	-2.295000
B	1.298000	2.387000	-1.262000
O	1.448000	2.963000	0.131000
O	-0.098000	2.014000	-1.428000
C	2.516000	3.618000	0.394000
C	-0.592000	2.623000	-2.636000
C	2.814000	4.065000	1.767000
C	2.329000	3.423000	2.929000
C	3.620000	5.206000	1.870000
C	3.947000	5.742000	3.105000
C	2.694000	3.974000	4.165000
C	3.477000	5.117000	4.259000
C	0.360000	3.852000	-2.773000
C	-0.067000	5.017000	-1.875000
C	0.549000	4.337000	-4.203000
C	-2.060000	2.961000	-2.427000
C	-0.418000	1.621000	-3.777000
H	2.117000	0.386000	-0.467000

H	2.319000	0.647000	-2.248000
H	4.150000	2.229000	-1.863000
H	3.712000	1.535000	1.105000
H	5.000000	2.659000	0.397000
H	2.936000	4.223000	-0.414000
H	4.567000	6.631000	3.170000
H	2.374000	3.473000	5.073000
H	3.736000	5.512000	5.236000
H	-0.257000	4.676000	-0.852000
H	-0.968000	5.511000	-2.253000
H	0.744000	5.751000	-1.850000
H	1.003000	3.561000	-4.823000
H	-0.409000	4.631000	-4.645000
H	1.211000	5.208000	-4.209000
H	-2.637000	2.044000	-2.267000
H	-2.191000	3.593000	-1.547000
H	-2.468000	3.479000	-3.302000
H	0.643000	1.415000	-3.951000
H	-0.860000	1.993000	-4.706000
H	-0.913000	0.681000	-3.513000
C	1.517000	2.194000	2.868000
C	0.726000	1.749000	3.847000
H	3.982000	5.677000	0.959000
H	0.191000	0.815000	3.714000
H	0.566000	2.291000	4.776000
H	1.546000	1.611000	1.954000

147

TS-1-ene-minor

C	-4.30802	0.25802	0.77738
C	-4.10170	-1.04943	1.25901
C	-4.67835	-2.12261	0.57349
C	-5.40636	-1.94450	-0.59897
C	-5.53217	-0.64659	-1.09396
C	-5.00295	0.45972	-0.43149
O	-2.23695	1.98331	-0.11684
P	-0.82706	1.20734	-0.26511
C	-2.74765	2.21045	1.14851
O	-1.01036	-0.18703	0.41247
O	0.05618	1.95831	0.86401
C	-2.22332	3.26420	1.90722
C	-3.82052	1.42661	1.57550
C	0.06060	3.34137	0.88638
C	-1.03455	4.01564	1.43962
C	-4.42754	1.77622	2.78469
C	-2.85060	3.56956	3.11850
C	-3.95376	2.84093	3.54710
C	1.21081	3.99197	0.44089
C	-0.94398	5.40560	1.56202
C	1.26710	5.37852	0.59469
C	0.19916	6.08045	1.15007
C	2.33531	3.21358	-0.16556
C	2.52958	3.23749	-1.55907
C	3.63229	2.56850	-2.09526
C	4.52776	1.86072	-1.29798
C	4.28193	1.80937	0.07328
C	3.19541	2.46068	0.65610
O	-0.33976	1.26611	-1.65052
H	-4.52965	-3.12584	0.96250
H	-6.06931	-0.49434	-2.02957
H	-5.28808	1.20420	3.11819
H	-2.45123	4.37410	3.72930
H	-4.43810	3.09297	4.48495
H	-1.78767	5.95312	1.97222
H	2.16415	5.90317	0.27956
H	0.25705	7.15900	1.25525
H	3.78543	2.59814	-3.17030
H	4.96283	1.23836	0.70437
H	-0.75872	-0.93859	-0.24458
C	2.25339	-0.94418	-1.46755
C	3.56636	-1.56084	-1.40244
C	4.26659	-1.70739	-0.24492
O	1.38318	-3.31385	-2.10988
B	1.20999	-2.23491	-1.18562
O	1.58426	-2.62255	0.25771
O	-0.20113	-1.92355	-1.16964
C	2.66561	-3.26279	0.43937
C	-0.82981	-2.59475	-2.27242
C	3.18560	-3.40484	1.80707
C	4.30699	-4.21493	2.07957
C	2.55860	-2.68835	2.83365
C	3.03559	-2.76572	4.13393
C	4.76157	-4.28730	3.40038
C	4.14098	-3.56832	4.41556
C	0.08551	-3.85160	-2.39622
C	-0.25281	-4.90918	-1.34258
C	0.10844	-4.47343	-3.78376
C	-2.27832	-2.86152	-1.89774
C	-0.74945	-1.68295	-3.49595
H	2.10137	-0.15976	-0.71833
H	1.98003	-0.56800	-2.45694
H	3.89363	-2.12238	-2.27865
H	4.01573	-1.09776	0.61942
H	5.19531	-2.27052	-0.20321
H	2.98664	-3.94163	-0.35041
H	2.54557	-2.20817	4.92535
H	5.60077	-4.93696	3.62914
H	4.51384	-3.64400	5.43226
H	-0.32389	-4.46008	-0.34664
H	-1.19848	-5.41379	-1.56579
H	0.54377	-5.65968	-1.33003
H	0.76197	-5.35089	-3.78336

H	0.48756	-3.76548	-4.52333
H	-0.89572	-4.79447	-4.08180
H	-2.77177	-3.47437	-2.66123
H	-2.82176	-1.91310	-1.81863
H	-2.35179	-3.36818	-0.93144
H	-1.14371	-0.69795	-3.23095
H	0.28841	-1.55608	-3.81751
H	-1.32689	-2.09146	-4.33150
C	2.97404	2.32335	2.15434
C	4.12065	2.95987	2.94786
C	2.77801	0.85349	2.54698
H	2.05580	2.85543	2.41868
H	4.23020	4.01893	2.69484
H	3.93626	2.87963	4.02444
H	5.07229	2.46201	2.73113
H	1.98407	0.39615	1.94652
H	3.70131	0.27846	2.40441
H	2.50278	0.77119	3.60466
C	1.58223	3.97555	-2.49418
C	1.22670	3.15237	-3.73723
C	2.17325	5.33073	-2.90468
H	0.64798	4.15516	-1.95198
H	0.84887	2.16933	-3.44927
H	0.44822	3.66968	-4.30778
H	2.08901	3.03086	-4.40241
H	2.37210	5.96719	-2.03734
H	3.12003	5.18642	-3.43815
H	1.48668	5.86425	-3.57058
C	5.76678	1.19507	-1.86725
C	6.95496	2.16527	-1.81131
C	5.57519	0.66684	-3.28979
H	5.99693	0.33963	-1.21848
H	7.13536	2.50909	-0.78836
H	7.86803	1.68810	-2.18372
H	6.75167	3.04605	-2.43062
H	4.66959	0.05740	-3.37113
H	5.49373	1.48746	-4.01083
H	6.43428	0.05700	-3.58696
C	-3.25957	-1.34175	2.49424
C	-2.26233	-2.48525	2.25991
C	-4.14471	-1.67085	3.70371
H	-2.67507	-0.44494	2.72251
H	-2.77137	-3.45092	2.16163
H	-1.66187	-2.31709	1.36237
H	-1.58307	-2.56365	3.11568
H	-3.53011	-1.88416	4.58494
H	-4.81883	-0.84605	3.95024
H	-4.75907	-2.55492	3.49737
C	-5.20845	1.83851	-1.03958
C	-6.69889	2.19329	-1.10875
C	-4.55271	1.93522	-2.42229
H	-4.72680	2.57835	-0.39457
H	-6.83315	3.20501	-1.50546
H	-7.23977	1.50212	-1.76460
H	-7.16077	2.14715	-0.11758
H	-4.66187	2.94842	-2.82320
H	-3.48597	1.70082	-2.36667
H	-5.02430	1.24449	-3.13049
C	-6.06963	-3.08860	-1.34837
C	-5.58055	-4.47484	-0.93146
C	-7.59490	-3.00189	-1.19234
H	-5.83308	-2.95345	-2.41332
H	-5.87154	-4.70036	0.10063
H	-6.02912	-5.23937	-1.57306
H	-4.49194	-4.56195	-1.00484
H	-8.09139	-3.78918	-1.76939
H	-7.97678	-2.03404	-1.52988
H	-7.87085	-3.12206	-0.13892
C	5.00741	-4.96464	1.01545
C	6.33098	-5.12212	0.96927
H	1.69915	-2.07189	2.58954
H	6.80210	-5.69804	0.18005
H	6.98495	-4.67059	1.71044
H	4.40009	-5.41256	0.23175

147
TS-2-ene-minor

C	4.20770	0.00188	0.84298
C	3.89137	1.29812	1.29810
C	4.38858	2.39703	0.59264
C	5.15780	2.25378	-0.55915
C	5.39283	0.96295	-1.02946
C	4.93047	-0.16698	-0.35361
O	2.24525	-1.86833	-0.00460
P	0.79477	-1.17071	-0.13730
C	2.78232	-2.04388	1.25867
O	0.90498	0.23219	0.52975
O	-0.03548	-1.96492	0.99975
C	2.32904	-3.11447	2.03964
C	3.80754	-1.18707	1.66152
C	0.04363	-3.34538	1.04316
C	1.18119	-3.94280	1.59921
C	4.45121	-1.48351	2.86595
C	2.98770	-3.36208	3.24749
C	4.05166	-2.56348	3.64939
C	-1.06689	-4.07094	0.61190
C	1.17194	-5.33309	1.74961
C	-1.04272	-5.45441	0.79623
C	0.06654	-6.08091	1.36145
C	-2.22484	-3.36043	-0.01592
C	-2.37111	-3.36867	-1.41572
C	-3.47975	-2.73114	-1.97922
C	-4.42367	-2.06679	-1.20067
C	-4.22848	-2.03399	0.17953
C	-3.14583	-2.66477	0.78980

O	0.30045	-1.27008	-1.52071	C	-3.00430	-2.58117	2.30236
H	4.17130	3.40065	0.95295	C	-2.79042	-1.13374	2.76274
H	5.96214	0.82698	-1.94748	C	-4.21464	-3.20859	3.00460
H	5.28126	-0.85773	3.17931	H	-2.12025	-3.15429	2.59904
H	2.64386	-4.17813	3.87647	H	-2.72139	-1.08711	3.85569
H	4.56262	-2.77240	4.58369	H	-1.86673	-0.72676	2.34130
H	2.04867	-5.82285	2.16354	H	-3.62503	-0.49368	2.45144
H	-1.90890	-6.03737	0.49802	H	-4.36097	-4.24457	2.68383
H	0.07133	-7.15841	1.49058	H	-5.13272	-2.65451	2.78042
H	-3.59577	-2.74890	-3.05862	H	-4.07524	-3.19963	4.09072
H	-4.94339	-1.48707	0.79413	C	-1.37331	-4.07254	-2.32469
H	0.61693	0.99360	-0.11440	C	-1.07095	-3.28490	-3.60354
C	-2.21322	0.77505	-0.59873	C	-1.87158	-5.48000	-2.68094
C	-3.60338	1.14677	-0.75046	H	-0.43032	-4.16727	-1.77572
C	-4.32612	1.76697	0.22357	H	-0.77837	-2.26061	-3.36487
O	-1.64723	2.65621	-2.37798	H	-0.24559	-3.76392	-4.14029
B	-1.37209	2.16579	-1.06754	H	-1.93091	-3.26827	-4.28253
O	-1.84004	3.16685	-0.00652	H	-2.02563	-6.09541	-1.79013
O	0.06161	2.01401	-0.95764	H	-2.82666	-5.41870	-3.21562
C	-3.01454	3.64455	-0.08940	H	-1.15141	-5.99057	-3.32916
C	0.69025	2.53780	-2.14374	C	-5.66430	-1.42185	-1.79314
C	-3.59858	4.39857	1.03108	C	-6.86918	-2.35949	-1.63103
C	-3.22943	4.19650	2.38071	C	-5.50653	-1.01266	-3.25829
C	-4.58655	5.33197	0.70210	H	-5.86519	-0.51573	-1.20434
C	-5.20441	6.09508	1.68386	H	-7.02886	-2.61883	-0.58025
C	-3.86486	4.97706	3.35114	H	-6.69822	-3.28953	-2.18435
C	-4.83780	5.91384	3.01444	H	-7.78259	-1.89369	-2.01652
C	-0.47999	2.45941	-3.18203	H	-6.36676	-0.41776	-3.58056
C	-0.43530	3.54675	-4.24652	H	-4.59656	-0.42551	-3.42177
C	-0.57845	1.08106	-3.83939	H	-5.45632	-1.89184	-3.90992
C	1.11639	3.96917	-1.82622	C	3.02982	1.54322	2.52963
C	1.89904	1.66887	-2.46189	C	3.89225	1.90137	3.74775
H	-1.94361	0.52521	0.43238	C	1.98731	2.64655	2.30187
H	-1.88980	-0.01517	-1.28405	H	2.48446	0.61916	2.74550
H	-4.01211	1.12338	-1.76168	H	4.47428	2.80843	3.54793
H	-3.99699	1.72029	1.25946	H	4.59365	1.10193	4.00027
H	-5.33616	2.12477	0.04332	H	3.26130	2.08982	4.62311
H	-3.42250	3.82035	-1.08823	H	2.45316	3.63765	2.26140
H	-5.96063	6.82442	1.41361	H	1.27663	2.65903	3.13568
H	-3.57016	4.85072	4.38837	H	1.42908	2.49268	1.37464
H	-5.30599	6.50613	3.79440	C	5.23420	-1.53777	-0.93777
H	-0.52060	4.54016	-3.80056	C	6.74514	-1.78998	-1.00760
H	-1.26983	3.40951	-4.94029	C	4.58115	-1.70013	-2.31581
H	0.49735	3.49254	-4.81875	H	4.80611	-2.29886	-0.27935
H	-1.53921	1.01647	-4.35960	H	7.20661	-1.69225	-0.02001
H	-0.52234	0.27951	-3.09644	H	6.94699	-2.79791	-1.38475
H	0.22284	0.92648	-4.56952	H	7.23537	-1.07739	-1.68001
H	1.80867	3.94961	-0.97749	H	3.49902	-1.55473	-2.25341
H	0.24952	4.57953	-1.55369	H	4.98769	-0.97610	-3.03125
H	1.62231	4.43556	-2.67761	H	4.77207	-2.70355	-2.71088
H	1.61240	0.61970	-2.56906	C	5.71078	3.46564	-1.28541
H	2.38115	2.00197	-3.38803	C	5.08387	3.62118	-2.67516
H	2.63348	1.74690	-1.65077	C	7.23942	3.40884	-1.38236

H	5.44265	4.35102	-0.69432
H	5.28820	2.74018	-3.29439
H	3.99831	3.73590	-2.60393
H	5.49240	4.49798	-3.18877
H	7.55992	2.55693	-1.99192
H	7.63039	4.31903	-1.84882
H	7.69378	3.30320	-0.39303
C	-2.24559	3.17220	2.80212
C	-2.44952	2.36982	3.84935
H	-4.86603	5.45751	-0.34110
H	-1.70837	1.63225	4.14003
H	-3.36682	2.40788	4.43214
H	-1.33957	3.06976	2.21546

147
TS-3-ene-minor

C	2.16198	3.09237	-0.21519
C	2.89432	2.35112	-1.16122
C	4.17077	1.88816	-0.82042
C	4.72540	2.12443	0.43528
C	3.92983	2.76217	1.38762
C	2.66006	3.25302	1.09292
O	-0.43888	2.39590	0.73513
P	-0.99790	0.93533	0.33565
C	-0.35586	3.40082	-0.21341
O	0.03158	0.35531	-0.68550
O	-2.24190	1.31588	-0.62695
C	-1.52639	4.04859	-0.62755
C	0.91207	3.79535	-0.63899
C	-3.17979	2.22607	-0.16093
C	-2.86030	3.58829	-0.17909
C	0.99551	4.90870	-1.48018
C	-1.39938	5.14744	-1.48232
C	-0.14759	5.58220	-1.89906
C	-4.43872	1.75092	0.20817
C	-3.85539	4.49829	0.19150
C	-5.40978	2.69289	0.55384
C	-5.12172	4.05550	0.55143
C	-4.73931	0.28684	0.18188
C	-4.72060	-0.45797	1.37923
C	-5.04780	-1.81039	1.32040
C	-5.35335	-2.45321	0.11991
C	-5.33792	-1.70079	-1.04997
C	-5.04229	-0.33439	-1.04043
O	-1.32016	0.14417	1.53357
H	4.74571	1.34410	-1.56637
H	4.32888	2.89824	2.39200
H	1.97834	5.24734	-1.79440
H	-2.29896	5.64757	-1.82875
H	-0.06212	6.44111	-2.55666
H	-3.61915	5.55830	0.20312
H	-6.40459	2.34286	0.81239
H	-5.88687	4.77218	0.83158
H	-5.03487	-2.40138	2.23409
H	-5.55795	-2.18045	-2.00088
H	0.20883	-0.66077	-0.56113
C	1.46616	-1.73662	1.92993
C	2.45809	-0.76081	1.48356
C	3.79187	-1.01437	1.48578
O	0.35546	-3.92099	0.95930
B	1.13052	-2.77450	0.66968
O	2.54634	-3.26997	0.24442
O	0.49949	-2.09201	-0.46606
C	3.34467	-2.46511	-0.31615
C	-0.44351	-3.01930	-1.05484
C	4.74970	-2.81917	-0.57170
C	5.49173	-3.74263	0.19963
C	5.34091	-2.18049	-1.66718
C	6.65452	-2.44702	-2.03018
C	6.81178	-3.99585	-0.18634
C	7.39079	-3.35958	-1.28045
C	-0.83408	-3.89924	0.17683
C	-1.94830	-3.26369	1.00454
C	-1.20510	-5.33192	-0.18604
C	-1.59315	-2.23385	-1.67026
C	0.30954	-3.80110	-2.13035
H	1.83539	-2.35681	2.75203
H	0.50482	-1.28325	2.19203
H	2.11151	0.14086	0.96855
H	4.19466	-1.85729	2.04473
H	4.49977	-0.29976	1.08296
H	2.92673	-1.66084	-0.92848
H	7.09673	-1.94901	-2.88659
H	7.38329	-4.72771	0.37591
H	8.41688	-3.58683	-1.55227
H	-1.73337	-2.21274	1.22920
H	-2.03432	-3.80886	1.94990
H	-2.90915	-3.31149	0.48349
H	-1.48423	-5.87160	0.72341
H	-0.36399	-5.85461	-0.64660
H	-2.05919	-5.35517	-0.87247
H	-1.22284	-1.60778	-2.48903
H	-2.09846	-1.59087	-0.94159
H	-2.34307	-2.92028	-2.08040
H	0.73905	-3.09391	-2.84738
H	1.12146	-4.38577	-1.68752
H	-0.35685	-4.48018	-2.67053
C	-5.05605	0.42689	-2.35772
C	-6.42067	0.32398	-3.04919
C	-3.93149	-0.05302	-3.28259
H	-4.87821	1.48582	-2.14595
H	-6.43326	0.93240	-3.95946
H	-7.22282	0.67124	-2.39079
H	-6.64492	-0.70891	-3.33656
H	-4.04381	-1.11866	-3.51530

H	-3.94857	0.50152	-4.22716
H	-2.95641	0.09428	-2.81005
C	-4.38852	0.18481	2.71814
C	-3.54604	-0.71672	3.62508
C	-5.67627	0.60075	3.44295
H	-3.79481	1.08312	2.51842
H	-3.23151	-0.15196	4.50868
H	-4.11680	-1.58213	3.98010
H	-2.65096	-1.06293	3.10514
H	-6.30100	-0.27864	3.63799
H	-5.44136	1.07099	4.40373
H	-6.26678	1.30725	2.85279
C	-5.70781	-3.92939	0.13546
C	-5.31087	-4.66498	-1.14515
C	-7.20570	-4.10970	0.41632
H	-5.15111	-4.38206	0.96756
H	-4.26369	-4.47602	-1.40505
H	-5.44523	-5.74387	-1.02053
H	-5.93107	-4.35387	-1.99284
H	-7.49028	-3.63026	1.35759
H	-7.79624	-3.65297	-0.38577
H	-7.46840	-5.17141	0.47411
C	2.34346	2.04865	-2.54839
C	2.43083	0.55576	-2.88657
C	3.05988	2.87244	-3.62585
H	1.28213	2.31504	-2.55619
H	3.47372	0.23305	-2.98912
H	1.94086	-0.04771	-2.11726
H	1.93377	0.35692	-3.84179
H	2.65047	2.65047	-4.61696
H	2.95571	3.94616	-3.44684
H	4.13063	2.63822	-3.64107
C	1.87103	3.94432	2.19331
C	2.62083	5.16376	2.74262
C	1.53030	2.95201	3.31221
H	0.92817	4.30400	1.77257
H	3.56158	4.87110	3.22151
H	2.85565	5.87460	1.94425
H	2.01184	5.67740	3.49349
H	0.95689	2.10536	2.92375
H	2.44113	2.56533	3.78340
H	0.93327	3.44353	4.08742
C	6.15649	1.76404	0.80441
C	7.00050	3.04490	0.88727
C	6.81955	0.76253	-0.13882
H	6.12882	1.31689	1.80853
H	7.04491	3.52859	-0.09469
H	8.02329	2.81608	1.20438
H	6.57112	3.76052	1.59420
H	6.93505	1.18405	-1.14424
H	6.24749	-0.16610	-0.22522
H	7.81884	0.50681	0.22662
C	4.93838	-4.41695	1.39463
C	5.65968	-4.64407	2.49447
H	4.75264	-1.46393	-2.23556
H	5.22856	-5.15305	3.34993
H	6.69139	-4.31402	2.58524
H	3.89642	-4.71529	1.36138

147
TS-4-ene-minor

C	-2.34792	3.03339	0.09701
C	-3.04679	2.34931	1.10878
C	-4.30205	1.80259	0.81757
C	-4.86880	1.90499	-0.45059
C	-4.10787	2.49901	-1.45800
C	-2.85808	3.06466	-1.21554
O	0.26365	2.33688	-0.79829
P	0.92896	0.93747	-0.34537
C	0.15838	3.41532	0.06152
O	-0.06814	0.28648	0.66722
O	2.11531	1.44011	0.63333
C	1.30761	4.13579	0.41228
C	-1.12119	3.81140	0.45064
C	3.03239	2.34414	0.11566
C	2.66053	3.68833	0.00925
C	-1.24099	4.99275	1.18781
C	1.14435	5.30214	1.16610
C	-0.11997	5.73533	1.54398
C	4.31756	1.88903	-0.18202
C	3.62526	4.60007	-0.43146
C	5.25476	2.83320	-0.60605
C	4.91209	4.17649	-0.73797
C	4.68073	0.45008	-0.00799
C	4.86549	-0.37312	-1.13233
C	5.25753	-1.70188	-0.93573
C	5.43871	-2.23914	0.33478
C	5.23056	-1.40230	1.43268
C	4.86059	-0.06773	1.29105
O	1.34003	0.15016	-1.51838
H	-4.84918	1.29674	1.60998
H	-4.51753	2.53312	-2.46685
H	-2.23465	5.32710	1.47110
H	2.02783	5.85850	1.46490
H	-0.23190	6.64676	2.12208
H	3.34907	5.64460	-0.54169
H	6.26488	2.50023	-0.82546
H	5.65159	4.89382	-1.07872
H	5.40553	-2.33188	-1.80822
H	5.36003	-1.81222	2.43428
H	-0.16458	-0.73637	0.50980
C	-1.42463	-1.84965	-2.02867
C	-2.41154	-0.89139	-1.53414
C	-3.73541	-1.17686	-1.44297
O	-0.21866	-4.01480	-1.12079
B	-0.99701	-2.88061	-0.78720

O	-2.37457	-3.39103	-0.26701
O	-0.30752	-2.18207	0.30344
C	-3.12084	-2.57775	0.35061
C	0.72804	-3.06459	0.79591
C	-4.49836	-2.91242	0.74229
C	-5.32124	-3.84038	0.06485
C	-4.97597	-2.23880	1.87202
C	-6.25388	-2.47516	2.36077
C	-6.60479	-4.06038	0.57502
C	-7.07074	-3.38973	1.70213
C	1.04887	-3.90602	-0.47828
C	2.00227	-3.17320	-1.41928
C	1.57434	-5.30258	-0.17510
C	1.88720	-2.22966	1.31547
C	0.11387	-3.90065	1.91761
H	-1.82256	-2.47881	-2.83025
H	-0.49007	-1.37379	-2.34190
H	-2.05756	0.02939	-1.06061
H	-4.15350	-2.04289	-1.95337
H	-4.43145	-0.47164	-1.00540
H	-2.64620	-1.76462	0.90770
H	-6.60748	-1.95145	3.24267
H	-7.23705	-4.79451	0.08544
H	-8.07119	-3.59228	2.07157
H	1.66556	-2.14691	-1.59440
H	3.01816	-3.12715	-1.01467
H	2.02484	-3.70464	-2.37595
H	1.79848	-5.81647	-1.11445
H	0.83676	-5.89596	0.36984
H	2.49758	-5.24958	0.41449
H	1.56890	-1.64253	2.18297
H	2.28066	-1.54790	0.55342
H	2.70962	-2.88112	1.63236
H	-0.29273	-3.22866	2.68019
H	0.86099	-4.54590	2.38945
H	-0.69784	-4.52598	1.53344
C	4.69507	0.78398	2.54153
C	6.00640	0.85073	3.33454
C	3.54575	0.27843	3.42028
H	4.44909	1.80530	2.23555
H	5.89808	1.51688	4.19680
H	6.29319	-0.13771	3.70979
H	6.82455	1.22335	2.71057
H	3.71968	-0.75559	3.74044
H	3.45332	0.89706	4.31955
H	2.59948	0.31725	2.87426
C	4.70256	0.14455	-2.55472
C	3.83110	-0.76760	-3.42390
C	6.07921	0.34699	-3.20281
H	4.19854	1.11495	-2.50712
H	3.73685	-0.33752	-4.42685
H	2.83260	-0.86296	-2.99431
H	4.26934	-1.76574	-3.53616
H	6.60924	-0.60925	-3.28209
H	5.97271	0.75905	-4.21173
H	6.70718	1.02675	-2.61840
C	5.87514	-3.67591	0.57583
C	7.31504	-3.70528	1.10899
C	5.75480	-4.58223	-0.64887
H	5.21993	-4.08171	1.36099
H	7.41996	-3.10189	2.01534
H	7.62419	-4.73029	1.33912
H	8.00032	-3.30081	0.35601
H	4.74571	-4.57044	-1.07303
H	6.45709	-4.27770	-1.43289
H	5.99638	-5.61376	-0.37503
C	-2.47924	2.19683	2.51347
C	-2.49781	0.73766	2.98213
C	-3.22846	3.08107	3.51804
H	-1.43149	2.51175	2.49119
H	-3.52479	0.38569	3.13369
H	-1.99610	0.09130	2.25553
H	-1.97621	0.64321	3.94001
H	-2.80892	2.96413	4.52278
H	-3.16986	4.13837	3.24499
H	-4.28825	2.80412	3.55852
C	-2.10205	3.69378	-2.37481
C	-2.90339	4.83334	-3.01543
C	-1.72592	2.62881	-3.41257
H	-1.17269	4.12381	-1.99123
H	-3.83275	4.46449	-3.46283
H	-3.16489	5.59596	-2.27523
H	-2.31865	5.30931	-3.80915
H	-1.10407	1.84803	-2.96509
H	-2.62145	2.15788	-3.83382
H	-1.16458	3.08214	-4.23620
C	-6.27999	1.44233	-0.77869
C	-7.20996	2.66218	-0.85870
C	-6.85045	0.40883	0.19094
H	-6.24367	0.98367	-1.77712
H	-7.26460	3.15678	0.11736
H	-8.22216	2.36136	-1.14866
H	-6.84424	3.39347	-1.58531
H	-6.97469	0.83163	1.19463
H	-6.21267	-0.47645	0.27418
H	-7.83741	0.08026	-0.14931
C	-4.88491	-4.55327	-1.15544
C	-5.70494	-4.80966	-2.17682
H	-4.32646	-1.52000	2.36515
H	-5.35586	-5.34669	-3.05229
H	-6.73978	-4.47713	-2.18251
H	-3.84480	-4.85565	-1.20953

147

TS-5-ene-minor

C	4.10474	-0.71323	-0.45454

C	4.39497	0.25448	0.53119	C	-4.45990	2.68888	-3.58828
C	4.77062	1.53522	0.12651	C	-0.35150	3.49289	3.38397
C	4.85240	1.89390	-1.21885	C	-1.36533	4.31413	4.16865
C	4.50839	0.93817	-2.16827	C	1.06281	3.77961	3.89213
C	4.13039	-0.35963	-1.81595	C	-2.15848	1.67773	3.20308
O	1.58671	-1.89031	-0.86744	C	-0.06555	1.15262	4.48534
P	0.40966	-1.19965	-0.00990	H	1.33194	1.89249	-0.35445
C	2.52904	-2.66391	-0.20844	H	2.04790	3.03148	0.84872
O	1.15179	-0.42287	1.12751	H	1.03660	4.95486	-0.26821
O	-0.15414	-2.47950	0.80602	H	-0.05790	2.86093	-2.24421
C	2.19654	-3.96755	0.18088	H	-0.26314	4.70148	-2.33464
C	3.80540	-2.12183	-0.04793	H	-1.63898	4.41765	0.01029
C	-0.30023	-3.71235	0.19961	H	-3.94961	0.61428	-3.32142
C	0.83081	-4.50225	-0.03093	H	-4.78053	4.81665	-3.62070
C	4.79065	-2.95008	0.49361	H	-5.17190	2.49496	-4.38464
C	3.21005	-4.75447	0.73812	H	-2.36251	4.23341	3.73120
C	4.49724	-4.25375	0.88624	H	-1.07038	5.36749	4.15458
C	-1.59876	-4.14455	-0.07762	H	-1.40909	3.98579	5.21304
C	0.62041	-5.80942	-0.48544	H	1.79598	3.15301	3.37430
C	-1.76767	-5.45974	-0.50861	H	1.15328	3.60545	4.96917
C	-0.66531	-6.29166	-0.69876	H	1.29952	4.82768	3.68772
C	-2.70318	-3.14174	0.00060	H	-2.29483	0.64673	2.86137
C	-3.16138	-2.55791	-1.19404	H	-2.61351	2.33893	2.46087
C	-4.11504	-1.54209	-1.11568	H	-2.68096	1.80704	4.15683
C	-4.58900	-1.06202	0.10112	H	1.02504	1.21559	4.48324
C	-4.11689	-1.65716	1.27139	H	-0.43965	1.51389	5.44939
C	-3.17922	-2.68811	1.24382	H	-0.35127	0.10067	4.38339
O	-0.54155	-0.48281	-0.87202	C	-2.69764	-3.29318	2.55281
H	5.01359	2.27540	0.88671	C	-3.83408	-4.05512	3.24574
H	4.54903	1.20894	-3.22188	C	-2.09816	-2.23596	3.48619
H	5.79880	-2.56089	0.59821	H	-1.90621	-4.01408	2.32450
H	2.97196	-5.76214	1.06596	H	-4.23469	-4.83886	2.59551
H	5.27497	-4.87848	1.31341	H	-3.47954	-4.52106	4.17123
H	1.48155	-6.43932	-0.68878	H	-4.65684	-3.37807	3.50158
H	-2.77165	-5.82330	-0.70657	H	-1.29933	-1.68599	2.97900
H	-0.80908	-7.31078	-1.04284	H	-2.85873	-1.51966	3.81810
H	-4.48380	-1.08788	-2.03234	H	-1.67849	-2.71035	4.37994
H	-4.47806	-1.29843	2.23439	C	-2.63342	-2.98668	-2.55569
H	0.62428	0.32855	1.56982	C	-2.35254	-1.80003	-3.48334
C	1.20430	2.83768	0.18061	C	-3.60280	-3.96830	-3.22681
C	0.85253	3.95472	-0.66293	H	-1.68082	-3.50296	-2.40132
C	0.05620	3.83140	-1.76768	H	-1.77222	-1.02968	-2.96626
O	-0.41222	3.86636	2.00600	H	-1.78605	-2.13815	-4.35727
B	-0.14325	2.70185	1.20980	H	-3.28398	-1.36114	-3.85911
O	-1.27352	2.44082	0.23685	H	-3.76092	-4.86147	-2.61525
O	-0.01432	1.58721	2.11938	H	-4.57821	-3.49207	-3.38022
C	-1.67881	3.43494	-0.45951	H	-3.22035	-4.28344	-4.20360
C	-0.66317	1.96274	3.34715	C	-5.56893	0.09412	0.14763
C	-2.65331	3.19157	-1.53638	C	-5.00587	1.26487	0.96098
C	-3.32109	4.27252	-2.14732	C	-6.93077	-0.34682	0.69515
C	-2.87957	1.87428	-1.95669	H	-5.70958	0.44272	-0.88427
C	-3.78161	1.63064	-2.98454	H	-4.01096	1.54766	0.60228
C	-4.23317	3.99439	-3.17000	H	-5.66588	2.13628	0.89031

H	-4.91574	0.99714	2.02043
H	-7.35244	-1.15991	0.09693
H	-6.83343	-0.70448	1.72640
H	-7.63912	0.48842	0.69432
C	4.33035	-0.05335	2.02122
C	3.54784	1.00998	2.80057
C	5.73962	-0.19468	2.61234
H	3.80010	-1.00173	2.15022
H	2.54838	1.15242	2.38126
H	3.44213	0.70115	3.84691
H	4.06565	1.97642	2.79936
H	6.31378	-0.97982	2.11256
H	5.68848	-0.43505	3.67965
H	6.29525	0.74380	2.50227
C	3.78873	-1.33733	-2.93023
C	5.00532	-1.59715	-3.82734
C	2.59285	-0.84145	-3.75253
H	3.50657	-2.29363	-2.48232
H	5.85040	-1.97562	-3.24385
H	4.76051	-2.33487	-4.59870
H	5.32829	-0.67993	-4.33175
H	1.72573	-0.65878	-3.11162
H	2.83663	0.08797	-4.27951
H	2.31591	-1.58720	-4.50538
C	5.30213	3.28126	-1.63715
C	6.68504	3.62078	-1.07061
C	4.27424	4.34563	-1.23974
H	5.37851	3.28145	-2.73217
H	6.65840	3.67244	0.02327
H	7.02457	4.59358	-1.44120
H	7.42352	2.86500	-1.35319
H	3.30121	4.13684	-1.69433
H	4.13912	4.36633	-0.15165
H	4.60250	5.34086	-1.55869
C	-3.07378	5.67548	-1.74873
C	-2.98497	6.68369	-2.61727
H	-2.33216	1.05982	-1.48108
H	-2.82680	7.70359	-2.28325
H	-3.05783	6.51848	-3.68895
H	-2.96814	5.88901	-0.68700